KARADENİZ TECHNICAL UNIVERSITY
THE GRADUATE SCHOOL OF NATURAL AND APPLIED SCIENCES

DEPARTMENT OF CIVIL ENGINEERING

COLLAPSE SIMULATION OF HALF-SCALED UNREINFORCED MASONRY BUILDING AND VALIDATION OF SHAKING TABLE TESTS

MASTER'S THESIS

Ridwan Adebayo BELLO

JULY 2022
TRABZON

KARADENİZ TECHNICAL UNIVERSITY

THE GRADUATE SCHOOL OF NATURAL AND APPLIED SCIENCES

DEPARTMENT OF CIVIL ENGINEERING

COLLAPSE SIMULATION OF HALF-SCALED UNREINFORCED MASONRY BUILDING AND VALIDATION OF SHAKING TABLE TESTS

Ridwan Adebayo BELLO

This thesis is accepted to give the degree of

"MASTER OF SCIENCE"

By

The Graduate School of Natural and Applied Sciences at Karadeniz Technical University

The Date of Submission	:	**10 /06 /2022**
The Date of Examination	:	**04 /07 /2022**

Supervisor : **Assoc. Prof. Murat GÜNAYDIN**

Trabzon 2022

ACKNOWLEDGEMENT

The success of this work is attributed to Almighty God for his love, grace, favour and kindness and for strengthening me throughout this research and also for giving me the knowledge to tackle and overcome the problem of this research work.

First of all, thanks to the Türkiye Scholarship (YTB) for considering me worthy of a scholarship and providing me with the incredible opportunity to study at the prestigious Karadeniz Technical University. Appreciation to my supervisor, Assoc. Prof. Murat GÜNAYDIN for his support, guidance, constructive criticism, patience, full availability and advice concerning this research. You give tutorship a whole new definition. You take it to heights that seem surreal yet real. I would like to show my sincere gratitude to Prof. Dr Ahmet Can ALTUNIŞIK for giving me an opportunity to work with the Dynamic Academy Team and for giving me access to the research facilities of the Structural Health Monitoring Laboratory. His dedication and keen interest to educate has inspired me to seek a career in academia. My thanks are also extended to the department's head in the person of Prof. Dr Şevket ATEŞ as well as Prof. Dr Süleyman ADANUR.

To Research Assistants in persons of Ali Kaya, Ali Fuat GENÇ, Fezayil SUNCA and Fatih OKUR, I want to say a very big thank you for your collective effort in making the experimental campaign a success. Your support in every aspect is sincerely appreciated. *Allah kolaylik versin!*

I would like to express my sincere appreciation to Kai KOSTACK for his aspiring guidance during the learning process of Blender and BCB. I am thankful for his invaluable knowledge shared and readily available to attend to any questions. *Vielen Dank!*

My enormous thanks go to all Dynamic Academy Team, especially my amiable handler Yunus Emrahan AKBULUT. Mustafa, SARIKOÇ, Zafer, Mert, Sara, Fatemeh MOSTAFI, Olguhan, Moussa, Algıhan, Ebru, Esin, Sebahat, Cihat, Yasin, Alihan; you are all appreciated for the support and encouragement I received throughout my studies. *Çok Teşekkür Ederim*

To my friends Khalid, Oloko, Akande, Akanmu, Atom, Ladi, Swagga, Sitanda, Oluwa53un, Diallo, Halidu, Glay, Zeynep, Esma, Merve, Aleyna, Kolee and many others who I am unable to name, thank you all for your support and unconditional love. A special thanks to Zain KALHA for all the salvage, and Seren CAVDAR who donated her hard disk that made the continuation of computational works possible during this study. To a friend turn brother Adil GUJRI, words fail me here.

My utmost appreciation goes to my mother Mrs Rofiah Iyabode TIJANI for taking the role and responsibility of both a father and a mother – you are simply the BEST. To my sister Azeezah, cousin Opeyemi AKINPELUMI and Big Mummy Thanks for the trust and support that I feel wherever I go and whatever I do

Ridwan Adebayo BELLO

DECLARATION

This research thesis, titled "Collapse Simulation of Half-Scaled Unreinforced Masonry Building and Validation of Shaking Table Tests", which I, Ridwan Adebayo BELLO presented as a Master's Thesis, was originally written by me and fully supported by my advisor, Assoc. Prof. Murat GÜNAYDIN, that I have gathered the data presented therein myself, that I have performed the experiments in the appropriate laboratory, that no results in this thesis have been fabricated, that I have fully documented the information I have obtained from other sources both in the text as well as the list of references, that I acted in compliance with scientific research and code of ethics during the research, and that no result from this thesis has been submitted/accepted for a degree at any other institution. In the event that the aforementioned declaration is violated, I accept full responsibility. 04/07/2022

Ridwan Adebayo BELLO

TABLE OF CONTENTS

Yüksek Lisans Tezi

ÖZET

DONATISIZ YIĞMA BİNANIN GÖÇME SİMÜLASYONU VE SARSMA MASASI DENEYLERİ İLE DOĞRULANMASI

Ridwan Adebayo BELLO

Karadeniz Teknik Üniversitesi
Fen Bilimleri Enstitüsü
İnşaat Mühendisliği Anabilim Dalı
Danışman: Doç. Dr. Murat GÜNAYDIN
2022, 119 Sayfa, 11 Sayfa Ek

İnsanların ölümüne depremin değil göçen binaların neden olduğu sıklıkla ifade edilir. İlk uygarlıkların doğuşuna kadar uzanan ve bilinen en eski yapı olan yığma yapılar, halen dünyanın mevcut yapı stokunun önemli bir bölümünü oluşturmaktadır. Düşey yükler etkisinde güvenilir olan yığma yapılar deprem gibi dinamik etkiler altında savunmasız kalabilmektedir. Bu nedenle yığma yapıların deprem gibi dinamik etkiler altında dinamik davranışlarının incelenmesi, olası hasar ve/veya göçme mekanizmalarının irdelenmesi önem arz etmektedir. Bu çalışma kapsamında laboratuvar ortamında inşa edilen donatısız yığma bir binanın farklı dinamik etkiler altında oluşan hasar ve/veya göçme durumlarının sayısal olarak simülasyonunun gerçekleştirilmesi amaçlanmaktadır. Yığma bina yedi farklı dinamik etki altında sarsma masası üzerinde test edilmiştir. Sarsma masası deneyleri sonucunda model üzerinde oluşan ivmeler ve yer değiştirmeler ölçülmüştür. Ayrıca, her bir durum için meydana gelen hasar durumları belirlenerek karşılaştırılmış ve bu hasar durumlarına bağlı hasar indeksleri belirlenmiştir. Sarsma masasında uygulanan son dinamik etkide bina göçmüştür. Sarma masası deneylerinden elde edilen hasar durumlarının sayısal simülasyonları için Bullet Constraints Builder ve Blender yazılımları kullanılmıştır. Gerçekleştirilen sayısal simülasyonlarla, yığma binanın sarsma masası deneylerinden elde edilen hasar ve/veya göçme durumlarının yüksek benzerlikte elde edildiği, çatlak oluşumu ve yayılımının ayrıca elde edilebildiği görülmüştür.

Sonuç olarak yığma binaların yapısal davranışının değerlendirilmesinde veya olası güçlendirme kararının alınmasında ya da güçlendirmenin etkinliğinin belirlenmesinde sayısal simülasyonlarının kullanılabileceği, olası bir göçme durumunda ise enkaz yalımının durumunun ayrıca belirlenebileceği sonucuna varılmıştır.

Anahtar Kelimeler: Blender, Göçme simülasyonu, Sarsma masası, Yığma yapılar

Master's Thesis

SUMMARY

COLLAPSE SIMULATION OF HALF-SCALED UNREINFORCED MASONRY BUILDING AND VALIDATION OF SHAKING TABLE TESTS

Ridwan Adebayo BELLO

Karadeniz Technical University
The Graduate School of Natural and Applied Sciences
Civil Engineering Graduate Program
Supervisor: Assoc. Prof. Murat GÜNAYDIN
2022, 119 Pages, 11 Pages Appendix

It is often stated that earthquakes do not kill people; rather the collapsed structures do. Masonry structures, the oldest known structure dating back to the birth of the first civilizations, still constitute an important part of the existing building stock of the world. Masonry structures, which are reliable under vertical loads, may be vulnerable to dynamic effects such as earthquakes. For this reason, it is important to examine the dynamic behaviour of masonry structures under dynamic effects such as earthquakes and to examine possible damage and/or collapse mechanisms. This study aimed to numerically simulate the damage and/or collapse conditions of an unreinforced masonry building constructed in a laboratory environment under different dynamic effects. The masonry building was tested on shaking tables under seven different dynamic effects. As a result of shaking table experiments, accelerations and displacements on the model were measured. In addition, the damage cases for each case were determined and compared, and the damage indices related to these damage cases were determined. In the last dynamic effect applied on the shaking table, the building collapsed. Bullet Constraints Builder and Blender software were used for numerical simulations of the damage conditions obtained from the wrap table experiments. With the numerical simulations carried out, it was seen that the damage and/or collapse conditions obtained from the shaking table tests of the masonry building were obtained with high similarity, and the crack formation and propagation could also be obtained.

As a result, it has been concluded that numerical simulations can be used to evaluate the structural behaviour of masonry buildings and/or to take a possible reinforcement decision and/or to determine the effectiveness of the reinforcement, and in case of a possible collapse, the formation of the debris insulation can be determined separately.

Key Words: Blender, Collapse Simulation, Shaking table, Masonry structures

LIST OF FIGURES

Page

LIST OF TABLES

Page

LIST OF ABBREVIATIONS

BCB	Bullet Constraints Builder
BC	Before Christ
CoF	Coefficient of Friction
DEM	Discrete Element Method
DI	Damage Index
EQ	Earthquake
FM	Fracture Modifier
G-1D	Grade 1 Damage
G-2D	Grade 2 Damage
G-3D	Grade 3 Damage
G-4D	Grade 4 Damage
G-5D	Grade 5 Damage
G-6D	Grade 6 Damage
GMD	Ground Motion Data
IDR	Interstory Drift Ratio
JRC	Tests performed at the Joint Research Centre Ispra, Italy
PGA	Peak Ground Acceleration
RBD	Rigid Body Dynamics
RC	Reinforced Concrete
SPH	Smoothed Particles Hydrodynamics
ST	Shaking Table
TUE	Masonry shear wall Tested at the University of Eindhoven
UPC	Experiments developed jointly by Universitat Politècnica de Catalunya
URM	Unreinforced Masonry

1. GENERAL INFORMATION

1.1. Introduction

Masonry, the oldest building material known to humanity dating back to the dawn of the first civilizations, represents a significant portion of the world's existing structure. The construction of the most ancient and historical structures (such as artefacts, monuments, cathedrals and cities across a wide range of cultures) was made possible by employing masonry. Most of these primaeval structures are still in use throughout the world and a large portion of them have become the regal and majestic landmarks of their situating country. Acting as a reflection of the culture of civilization as well as the genius of engineering and architectural knowledge of our ancestors. Although there have been significant advancements in masonry materials and applications in recent decades, the processes for assembling bricks and blocks are fundamentally unchanged from those created thousands of years ago. There have been various advancements in masonry materials, processes, and applications throughout history. The primary impacting components were cultural heritage and economic success, material and skill expertise, availability of raw materials, along with architectural philosophy [1, 2].

The most essential feature of masonry construction is its simplicity and aesthetic appealing characteristics (pattern, texture, scale, colour, and long-lasting appearance). Additionally, due to desirable features such as ease of maintenance, durability, stability, fire resistivity, flexibility, protection against daily temperature change, and sound absorption, masonry is still commonly employed to date in the construction industry. Numbers don't lie they say - The multitude of masonry structures that are to this day in operation after dozens or hundreds of years reflect their resilience [3]. Innovative structural masonry applications, on the other hand, are hampered by the fact that design regulations have not managed to keep up with innovations in concrete and steel. In spite of the apparent simplicity of masonry structures' construction, understanding and characterizing their mechanical behaviour, particularly in seismic loading conditions, is a true challenge considering the nature of masonry structures. This is due to the complicated units' behaviour, grout, interconnections, and masonry as a composite structure which are distinguished by a particularly complicated and nonlinear behaviour. Additionally, the said nonlinear behaviour may be ascribed to the occurrence of joints between bricks that could be filled with mortar but do not have to [3].

Structures are safely designed based on an accurate understanding of their collapse condition. The knowledge of ductility is relied upon in the design of a modern structure to signal looming collapse. Also, in the occurrence of overloading, the ductility property enables the absorption of energy. With this in mind, engineers can design and analyze the safety of reinforced concrete and steel structures with confidence in their failure mechanisms. However, engineers are not as confident (compared to RC and steel structures) in evaluating the safety of masonry structures. Masonry (unlike ductile materials such as RC or steel) cannot absorb energy by yielding. The failure modes (Collapse) of masonry structures are poorly understood, especially in the instance of horizontal acceleration i.e. earthquake (EQ). Masonry structures pose a significant challenge to the structural engineer, who frequently lacks expertise with masonry structures. The applied loads (such as snow, wind e.t.c.) for masonry structures are normally minimal in comparison to the structure's weight, and the deformations caused by these applied loads are infinitesimal. Also, as reported by Heyman [4], the safety of masonry structures depends on their stability compared to RC and steel structures which depend on their material’s strength. Due to these reasons, structural engineers frequently struggle to safely evaluate masonry structures. Although, researchers such as Rot, Paulo B Lourenco [1], Bakeer Tamaam [5], Oliviera [6] and Pere Roca, have done a lot of work on masonry structures. However, there is always room for further research, innovation and development.

1.2. Problem Statement

Masonry structures while typically capable of sustaining gravitational loads are inherently prone to collapse. This collapse could be attributed to unfavourable actions such as excessive deflection, uneven settling of the soil beneath foundations, structural loads, deterioration of materials, poor maintenance and deficiency in the initial builder's structural knowledge. The Tower of Pisa with the Mexico City Cathedral are famous instances of masonry structures at the risk owing to soil settlements, whereas the Cathedral of Pavia and the Cathedral of Florence are examples of masonry monuments at risk due to a lack of structural design [7]. By far, the most common cause of masonry construction collapse is an EQ.

It is often stated that earthquakes do not kill people; rather the collapsed structures do. This was self-evident in the Turkish city of Izmit [8] with over 300,000 homes reported as either damaged, partially or totally collapsed resulting in the death of over 17,480 people. Poor building materials (especially masonry) were cited as a contributing reason to the high death toll. Evidently, when likened to other structural types such as steel structures or reinforced concrete, the masonry structural response to EQ action is the development of cracks even for less intense shocks. The crack often subsequently leads to partial and at times total collapse. Hence, the structural health assessment of existing masonry structures is a contemporary and critical topic all over the world. Although masonry structures got extensive investigations a few decades back, attracting a significant amount of research experimentally as well as numerically. Despite significant progress, the performance of large-scale masonry structures under EQ influence continues to be a major challenge. This safety objective in harmony with the need to preserve historical masonry structures for human continuous access necessitates this research.

1.3. Aims & Objectives

This research aims to develop a visual numerical simulation for analyzing EQ related actions on large-scale masonry structures that could not be achieved in the laboratory. The objectives are as follows;

- Experimentally study the effects of various EQs on the behaviour of laboratory scaled unreinforced masonry (URM) structure by means of a shaking table (ST) test.
- Development of a simplified numerical model that could replicate the behaviour of masonry at all stages of collapse.
- Verification and assessment of developed numerical models in relation to experimental ST test results

1.4. Scope of the Thesis

The study deals with masonry structures with a primary focus on EQ related events using an ST test. The obtained result was visually simulated using Blender and BCB.

1.5. Thesis Outline

The content of this thesis is divided into 6 chapters, with appendices detailing the influence of different parameters on the simulation results.

Chapter 1 acts as motivation, providing a brief introduction to masonry, outlining the problem statement, aims and objectives and defining the scope of the thesis.

Chapter 2 presents the historical background of masonry. A comprehensive history of masonry, as well as an overview of the numerical and analytical assessment of masonry structure, was particularly presented. Additionally, strategies for modelling masonry structure were presented. Also presented in the chapter is the synopsis of the dynamic vibration test, ST test, earthquake and its effects as well as previous works that are correlated with the current study.

Chapter 3 introduces the description and characterization of masonry material. Failure pattern and criteria as well as the inelastic masonry’s behaviour such as softening or hardening, dilatancy and shear & tensile coupling failures were discussed.

Chapter 4 deals with a detailed description of the experimental test, instrumentation, methodology and assessment. The results of the experiments are also presented in this chapter.

Chapter 5 introduces the discrete element method as a fundamental numerical tool for visualizing the influence of EQ on masonry buildings. The working principles of Bullet Physics Engine, Blender and BCB script were presented. A displacement visualization script and parametric analysis were also presented in this chapter.

Chapter 6 is dedicated to the observations, conclusions, recommendations as well as future work plans. The application of the findings in this research is also presented. This is followed by an appendices presentation which details the numerical simulation results.

2. LITERATURE REVIEW

2.1. Background

The notion of arranging units (stones or bricks) atop and adjacent to one another to form masonry structures has remained relatively unchanged. It is among the most ancient building materials and it is still utilized today. However, the kind of units utilized (Sand Lime Bricks, Fly Ash Clay Bricks, Concrete Bricks, Stones, Engineering Bricks, Burnt Clay Bricks), the joint interface (Mortar joints or interlocked), and, if a mortar is employed, the type of mortar used (lime or cement-based) have all evolved through the years. This section discusses masonry history and prior masonry-related studies. Figure 2.1. and 2.2. shows the evolution of masonry and the inventory of URM structures respectively.

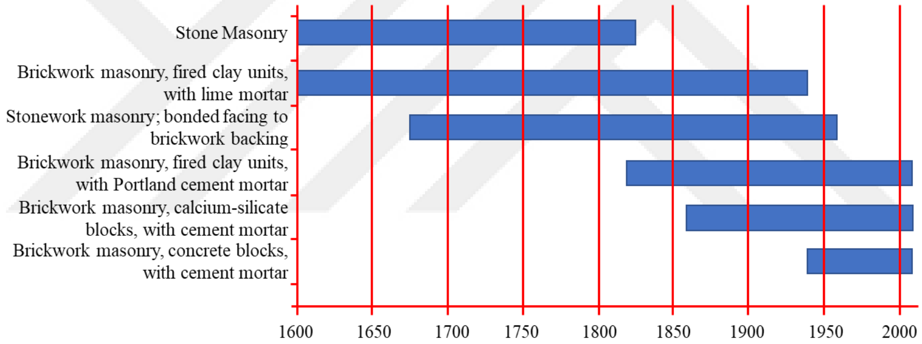

Figure 2.1. The evolution of masonry composition over time [9].

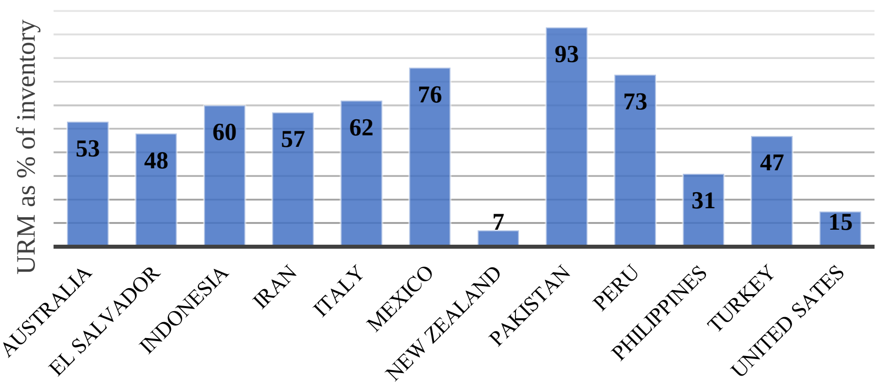

Figure 2.2. Global building inventory of unreinforced masonry structures [10].

2.2. Masonry in History

Human use of tools and materials dated back to when we first cracked open a nut with a rock, razor-sharp a stick to kill a fish, and lit a fire with a flint to produce a spark. We've been building structures since when we had just stacked stones or bound rope (braided long grasses) to form an accommodation. Humans have been developing weapons since we discovered that some rocks split apart to generate sharp blades. Humankind's evolution is deeply connected to our usage of materials and tools. Consequently, the primary ancient stages of human civilisation are not called after human language proficiency, socialization, or economic accomplishments but rather by the engineering materials of the period. The first of the three-stage framework of human evolution is the Stone Age, with Bronze and Iron constituting the other two phases. When one was in school learning about the Stone Age, one was always informed that the first humans were hunter-gatherers who lived off what they could scavenge or capture. Something one wasn't informed of is that it was the dawn of technology when humanity learned to carve stone into hunting tools to defend its territory and build structures and monuments that served as celestial dates and mystical centres [11]. Around the same period, architectural history begins to take shape, and masonry as a construction method emerged. Some of these sorts solidified into stone, mud, clay, or wood buildings, the first most probably being stone. Many wooden bridges were built by the Romans, but none endured the test time, and their legacy is established in their stone bridges [12]. Hence, masonry constructions account for the great bulk of today's architectural legacy owning to the ephemeral and fugacious characteristics of wood [13]. Primitive builders soon invented tholos, see Figure 2.3. – a form of home construction with domed roofs made out of dry-laid stone material. Hence, the tholoi (otherwise known as beehive tomb) are the forerunner of masonry construction. Housing in the ancient Middle East evolved from tent/huts to apsidal homes, and eventually to rectangular structures, see Figure 2.4. Also shown in Figure 2.5. are the Atlas Obscura beehive houses in Turkey. One may form an opinion about the materials employed in ancient structures based on such artefacts, and conclude that they were comparable.

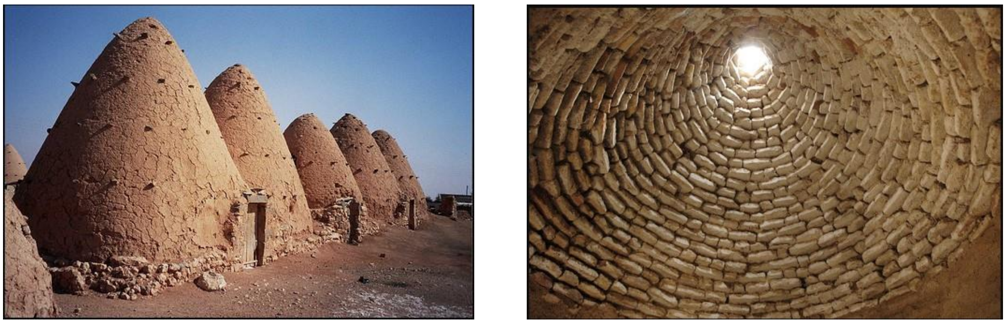

(a) (b)

Figure 2.3. Syrian Beehive Houses (a) External view (b) Internal view [14].

(a)

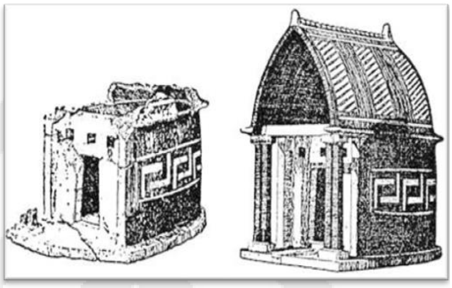

(b)

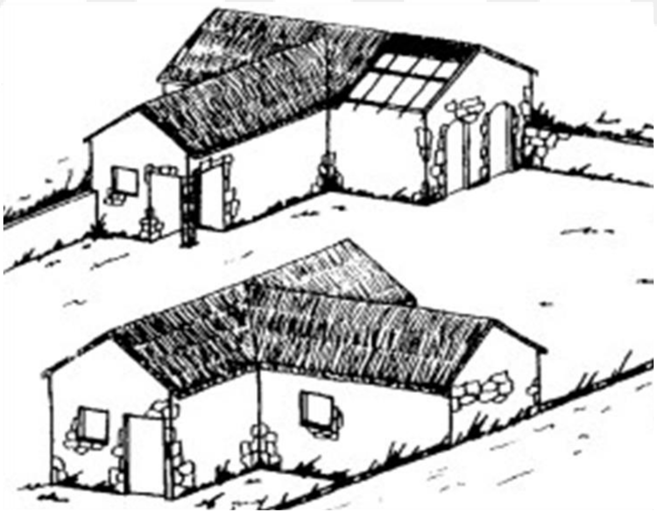

(c)

Figure 2.4. Evolution of houses in the Middle East; (a) Cyprus village beehive dwellings (about 5650 BC); (b) temple house of Hera from Perachora Athens; (c) rectangular houses from an Iraqi village [1].

Figure 2.5. Atlas Obscura- Harran Beehive Houses, Harran, Turkey.

The earliest recorded habitation in the Cyclades is on a low hill at the tip of a tiny headland - Saliagos, near to Antiparos and secluded from the cape of Pounda on Paros only by a tiny channel. Wall remnants from a perimeter fence, a building complex, and other tiny buildings were discovered in a 100 m^2 area. The foundations of the buildings were made of stone, but the superstructures were made of light materials, most likely wood or clay. Although some of the walls seem to be curved, the majority are straight and create roughly rectangular constructions. The walls are made of clean, dry masonry [15].

Dry-stone homes, round and semisubterranean, were discovered at Lake Hullen, Israel (9000 to 8000 B.C.), and are the oldest examples of permanent stone masonry structures [1]. The Walls of Jericho structures (8000 B.C.) are just another early exemplification of masonry structures. Archaeological studies in the same location also discovered more contemporary structures (3000 B.C.) composed of sun-dried mortar and bricks [6]. These fortifications were constructed as military defence and were made of crudely carved limestone with earthen seams [16].

The Assyrians were experts at employing massive labour groups to construct new palaces, temples, and defensive walls, or to restore existing ones: mud bricks could be placed at a pace of one hundred per man per day, according to estimates. Because of its widespread usage, mud-brick is the most significant of ancient Near Eastern construction materials. Many highland sites appear to have been made entirely of stone, but excavation often finds the remnants of a mud-brick superstructure above the masonry, as in the Urartian strongholds. The Canaanites and their Phoenician ancestors in the Levant were accomplished stonemasons, as evidenced by the precisely prepared and finely-jointed masonry built-in uniform, horizontal courses in the thirteenth-century BC palace at Ugarit (Ras Shamra), a flourishing economic city on the coast of Syria. The same high grade of masonry may be found in Samaria's first two stages, under the reigns of Omri and Ahab (c. 880 to 852 BC) [17].

Dating back to pre-historic periods round/spherical stone huts (partially buried into the earth) have been discovered on Ireland's Aran Islands. Egypt had mastered an advanced stonemasonry method by the 4th millennium BCE, eventually resulting in the most spectacular of all ancient constructions, the pyramids [2]. The Egyptian Pyramids, China's Great Wall, Rome's Colosseum, Great Sphinx of Giza, India's Taj Mahal and the magnificent cathedrals of Gothic architecture just to mention a few – stone masonry has been used to construct some of these world's most notable architectural masterpieces and survived to this day serving as evidence of ancient and medieval societies, see Figure 2.6. The skill of stone cutting reached its pinnacle with the Gothic masons. Buttresses, ribbed vaulting, arches, and Piers made up the core of Gothic architecture. The walls encased the structure but did not support it, and they were mostly made up of glass windows [7]. However, problems such as quarrying, cutting, transportation and weight as well as cost make stone a prohibitive material. With these problems comes the advent of mud bricks as masonry materials which subsequently leads to stone becoming mostly a cladding material for aesthetic purposes. Considering the inefficiency and shortage of timber and stone, the high demand for building materials, weight, ease of production as well as the required weather for curing brick justify the shift from stone to brick as a masonry material. The burning of bricks was a natural progression and was considered the first prefabricated component. The bricks' strength and durability significantly improved as a result of this procedure while also necessitating a constant supply of fuel, which was not always accessible. This drawback might attribute to the continuous use of sun-dried bricks. Nonetheless, the mass use of brick was evident in Jericho Palestine, Egypt (The pre-dynastic times 5000 BC), Babylonia (present-day Iraq and parts of Syria), and the Roman empire. The vast, powerful, and unified Roman empire embraced brick which leads to its widespread use. The roman acceptance might have been influenced by the availability of clayey material suited for brick production across the empire. The aftermath of this is the bricks standardization such as uniformed size and the creation of varied shapes for specific purposes. Innovative masonry techniques were also established, such as employing bricks or perfectly polished stones as facings and stuffing the interior space with concrete, see Figure 2.7. The technology of dry-stone block construction was also substantially refined, and notable monuments such as Segovia's aqueduct were constructed, see Figure 2.8.

Another notable structural advancement was the transition to curved/ arched structures from linear structures, such as domes, vaults and arches. The collapse of the Roman Empire resulted in a deviation in western architecture. The adoption of arches, vaults and domes result in structural breakthroughs achieved in the 11th century. The evolution of the arch enabled the substitution of bulky stone and insecure wooden lintels within masonry with brick and/or stone masonry covering larger openings. Masonry towers were used to identify churches, mosques, castles and other structures and it was not long before this method travelled from Europe to the Middle East. Istanbul's Hagia Sophia - 6th century A.D. is shown in Figure 2.9. represent one of the exploitations of arched or curved structures.

Eventually, the prevalent geological formations and circumstances in a specific place have constantly affected the selection of masonry materials. Temples in Egypt, for instance, were built from limestone, sandstone, alabaster, granite, basalt, and porphyry excavated from the Nile River's highlands. The area of western Asia (another prehistoric civilization centre) between the Euphrates and the Tigris, lacked stone rock formations but has abundant deposits of clay. Consequently, the Assyrian and Persian empires' masonry constructions were built of sun-dried bricks with kiln-burned, occasionally glazed, units.

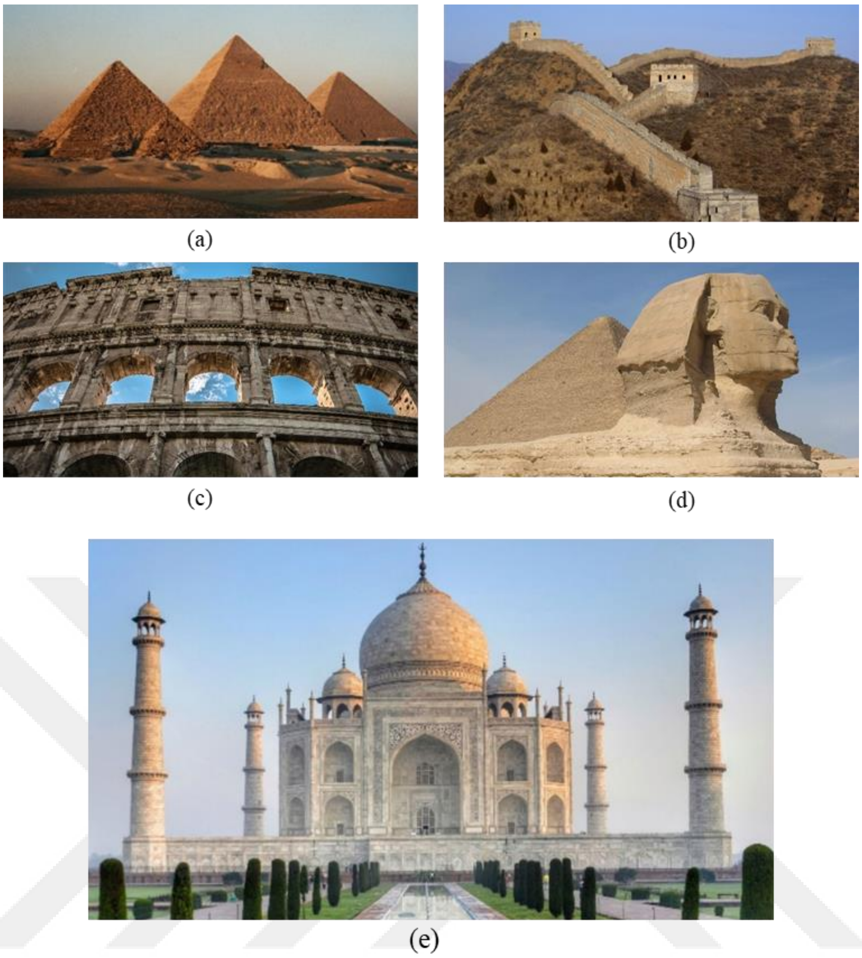

Figure 2.6. Notable architectural masterpieces; (a) The Egyptian Pyramids, (b) China's Great Wall, (c) Rome's Colosseum, (d) Great Sphinx of Giza and (e) India's Taj Mahal

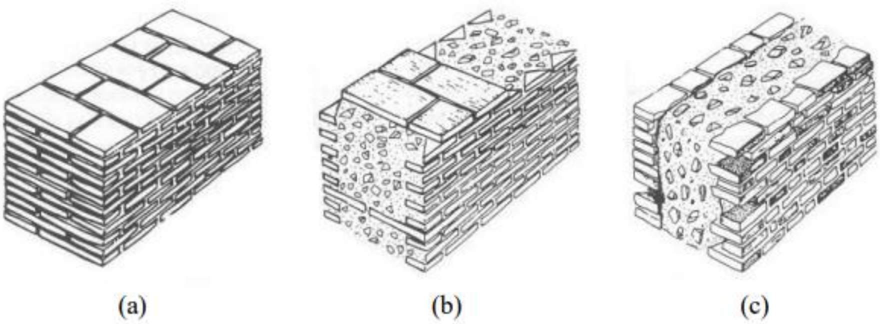

Figure 2.7. The masonry walls invented by the Roman; (a) bonded brick walls, (b) brick-faced walls with header courses and (c) brick-faced walls [6].

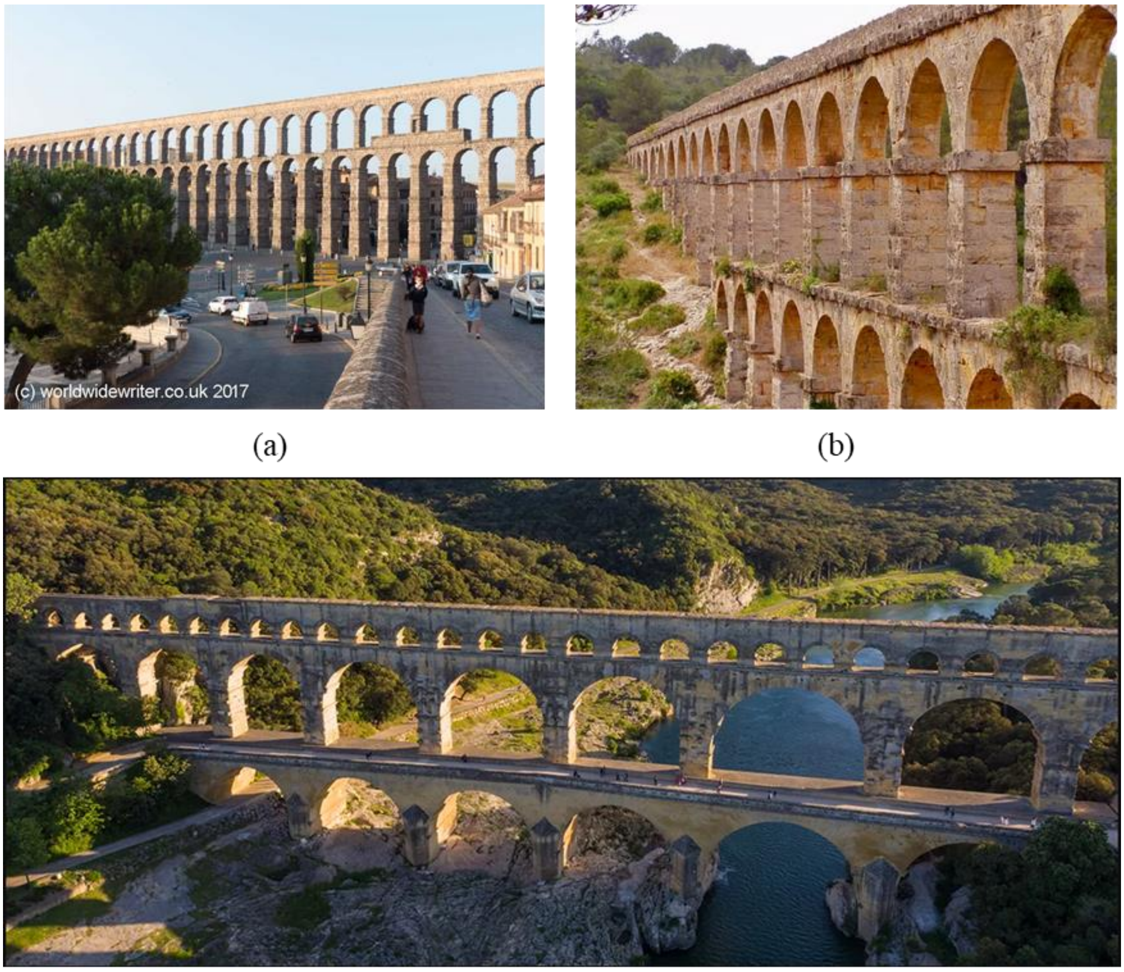

(a) (b)

(c)

Figure 2.8. Notable monumental aqueduct (a) The Roman Aqueduct of Segovia [18], (b) The Tarragona Aqueduct in Spain and (c) The Pont du Gard Roman Aqueduct in France [19].

Figure 2.9. Istanbul's Hagia Sophia

With the passage of time began the role of the structural behaviour of temple and cathedral buildings. Drysdale in his book Masonry structures- Behaviour and Design [20] mentioned the use of support over the opening to support masonry walls above it. Such is that which was employed to create the Lion Gate and the Treasury of Atreus both at Mycenae, Greece, see Figure 2.10. In general, Greek architecture (particularly temples), was aesthetically excellent and founded on precise laws of proportion and equilibrium between the various elements, marking a landmark moment in the building's history. Structural elements such as walls, columns, and beams were constructed using limestone as a block. The Parthenon (Figure 2.11) is by far one of the most iconic Greek architectural structures. The columns are slightly tapered to provide the temple with a symmetrical appearance. The corner columns have a larger diameter than the other columns. The Parthenon is a stunning Greek architectural marvel because it has neither right angles nor straight lines [21].

(a) (b)

Figure 2.10. The use of support over the opening to support masonry walls (a) The Lions Gate and (b) The Treasury of Atreus [22].

Figure 2.11. The Parthenon at Athens [21]

Following Roman architecture is the emergence of Gothic architecture in the 13th century. It marked a step ahead in which both architectural and structural purposes were superbly interwoven. The Roman structures are generally bulky and heavy. Three important modifications were made in an attempt to transform the heavy structures into the lightness and openness of Gothic structures. The insertion of arch ribs, the replacement of the semicircular arch with a pointed arch, and the use of towers and flying buttresses that are better aligned with the thrusts are the three key alterations. These three important modifications resulted in masonry-framed constructions based on linear parts that worked in compression. The columns, flying buttresses, tower, and buttress wall or arch ribs were the framing components (rectilinear and curvilinear). Figure 2.12. illustrate pictures of some of the world's famous Gothic Cathedral. Based on revolutionary conceptions and extraordinary structural performance, Gothic architecture's history is nevertheless defined by failures, cracking, and structural deformations, which indicate the cost of forsaking traditional construction practices.

Sequel to Gothic architecture is the rise of Renaissance architecture originating in Florence in the 15th century. It introduced new ideas of form and proportion, with structures distinguished by mathematical symmetrical both in elevation as well as plan and regular shapes. The late Renaissance (Otherwise known as the Mannerist Movement) style, was distinguished by sophistication, intricacy, and innovation rather than the High Renaissance's harmony, clarity, and repose. Churches, particularly domes, are structurally interesting. Figure 2.13 shows a few of the most notable renaissance architecture. The use of primary ribs and the building of two shells joined by these ribs distinguishes their domes. This approach minimizes construction weight and provides an improved method for modifying the dome's outer and inner contours.

There were no noteworthy or unique structural solutions established during the Baroque period. In reality, the hunt for new forms of expression affected structural notions more than the refining of structural function [16]. In Europe, notable examples include seventeenth-century London situated St. Paul's Cathedral as well as the Panthéon in Paris (eighteenth century). Another significant turning point in the history of the building business was the English industrial revolution of the seventeenth and nineteenth centuries. The introduction of novel construction materials like reinforced concrete and steel resulted in a drastic shift in construction practices. Huge steel bridges, like Scotland's Firth of Forth Bridge, are one of the most iconic constructions of this era.

Because of the gradual acceptance of other construction materials, mainly concrete and steel, the usage of masonry has declined in most parts of the world. Its application has been limited mostly to non-structural components such as infill panels, cladding and facade systems.

Significant advancements in masonry materials and manufacture, design methodologies, and construction processes, on the other hand, have significantly aided the rise of masonry as a competitive building material in a number of developed countries, particularly the Netherlands, Turkey, England, Canada, Germany, Portugal, and the United States [23]

(a) (b) (c) (d) (e) (f) (g) (h)

Figure 2.12. Pictures of the world's famous Gothic Cathedral (a) Amiens Cathedral, France, (b) Notre-Dame de Reims, France, (c) Basilica of Saint-Denis, France, (d) Chartres Cathedral, France, (e) Santa Maria del Fiore, Italy, (f) Westminster Abbey, London, (g) Canterbury, U.K. and (h) Milan Cathedral

(a) (b) (c) (d) (e) (f)

Figure 2.13. Pictures of a few of the most notable renaissance architecture (a) St. Peter's Basilica in Rome, Italy, (b) St. Maria del Fiore, (c) Piazza San Marco – Venice, Veneto, Italy, (d) El Escorial – San Lorenzo de El Escorial, Madrid, Spain, (e) Château de Chambord, France and (f) Basilica Palladiana – Vicenza, Veneto, Italy

2.3. Shaking Table Test – Review

Among the most extensively employed methods for evaluating the structural performance seismically is the ST test. It is frequently used to evaluate the elastic, inelastic, linear and nonlinear structural response dynamically. The nonlinear dynamic response of a full-scale 7-story RC shear wall structure was demonstrated by Martinelli et al. [24]. The excitation was provided by four simulated seismic recordings of amplifying strength. The inelastic behaviour of a bolt-connected two-story portal frame was investigated by Saranik [25] using an ST test. A shaking table test was also utilized by Caballero González [26], Shujin Li et al. [27] and Carydis [28] (just to mention a few) to assess the masonry structure performance under EQ action, which was then used to validate and calibrate numerical models. In addition to the testing of structural dynamics, the application of the ST test has also been extended to the study of geotechnical behaviour as well as outside the scope of civil engineering such as mechanical and aerospace engineering. In an attempt to investigate the seismic behaviour of the embankment slope with various strengthening schemes Lin et al. [29] used a slope model of three embankments to conduct ST experiments. Chen et al. [30] used a plaster model of a three-level, three-span subway station to conduct a series of ST experiments to examine the seismic-induced failure mode and behaviour of the structure on the liquefiable ground. In an attempt to investigate the efficiency of the ST test, Srilatha et al. [31] used a series of ST tests to explore the influence of base shaking frequency on the reinforced and/or unreinforced soil slope's dynamic response.

The structure's dynamic features, seismic reactions, and collapse cause were researched, and weak spots were discovered during rare EQs. However, due to technical issues and outrageous expenses, research on full-size models remains difficult. Consequently, the majority of the studies employed scaled models. For instance, ST experiments were conducted by Liu et al. [32] to examine the performance of a remote museum construction in an extremely active seismic zone. The model was constructed with and without isolation bearings in the base and scaled down by one-thirtieth. The high-rise Shanghai World Financial Centre Tower was scaled down to one-fiftieth for an ST TEST by Lu et al. [33]. Some researchers do, however, employ prototype structures. A full-scale high-rise structure was examined by Lignos et al. [34] on an ST to prove the efficiency of the numerical models utilized. During the experimental phases, Graziotti et al. [35] conducted an ST test on a two-storey full-scale unreinforced masonry structure to investigate its reaction, features, damage mechanism, and progression. According to the above literature study, the ST test is an important technique for evaluating and verifying the structures' dynamic behaviour. It is especially important for constructions that surpass the boundaries of design guidelines and standards. In this context, the current research study is appropriate.

2.4. Numerical and Analytical Evaluation of Masonry Structure – Overview

The practicalities of masonry construction techniques and the scientific knowledge of structural engineering must be harmonized in structural design. Unfortunately, most existing masonry structures were built based on the thumb rules. The geometrical procedures necessary to set out plans and produce the templates and moulds from which masonry would be carved were taught to medieval masons during their apprenticeship. As part of the mason's lodge's mysteries, they were taught the conventional practices and rules of thumb of their profession, and all guild members were pledged to secrecy.

The analysis (both analytical and numerical) of masonry structure has gone unmentioned for a pretty extended time in the historical record. The skill of building masonry structures was learned through practice, experience, and expertise and subsequently handed down from generation to generation. In the book Ten Books on Architecture, Vitruvius [36] examines the characteristics and qualities of wood and stone from several sites and discusses the proportionalities of a number of building materials and structures nonetheless he makes no mention of calculations. During the medieval era, a structure with correct proportions was deemed structurally appropriate, and this belief system was maintained. This period is distinguished by the careful preservation of established proportions that are transmitted down from generation to generation. This practice continues up till the middle ages when little attention was given to the mechanics of arches since the majority of the arches created had withstood the test of time. In fact, there was an unconfirmed report of using the method of "test elephant" to confirm the stability of masonry-built arch bridges. Elephants are used because they are cautiously smart and the largest land creatures and people believed they had a sixth sense that prohibits them from crossing unsafe structures unless stable. How much credence could be attached to this? Can't say for sure, however, the use and credibility of this method were confirmed by Andrew Carnegie in May 1874. It was used to prove to the people of Chicago that the Eads's Bridge (The world's first all-steel bridge to be ever built but with giant masonry granite-faced piers that support the arches and decks as suggested by Billington *et al* [12]) is safe and sound [37]. Several spectacular structures built during the medieval era which are still relatively intact prove that expertise and understanding regarding masonry structure stability and force distribution were not lacking. During the Renaissance in the 1500s, many of the structures created were more slender. This necessitated a solid theoretical foundation for their creation.

In 1675, in the book, A Description of Helioscopes and Some Other Instruments [38] Robert Hooke described the “true mathematical and mechanical form......” for the shape of an ideal arch shape. Hooke, on the other hand, wrote the hypothesis as an anagram – “*abcccddeeeeefggiiiiiiiillmmmmnnnnnooprrsssttttttuuuuuuuux*” (Figure 2.14. highlighted in green). The unencrypted solution to the anagram of Robert Hookes reads "*Ut pendet continuum flexile, sic stabit contiguum rigidum inversum*" which translates to "As hangs a flexible cable so, inverted, stand the touching pieces of an arch". It suggested that Robert Hooke found the portions of stone arches to be fashioned like a reverse catenary. To put that in perspective, the optimum arch shape is the same as that of a freely dangling cable/rope but turned upside down. In contrast to a cable/rope that could endure tension but fail in compression, Hooke knew that the construction materials (masonry) could only survive compressive loads but not tensile ones. With the exception of a negative sign, the mathematics defining the arch and the cable are remarkably similar. As a result, one could use a piece of string to simulate an arch in real-time [39]. On the same page, amongst many other topics, Hooke wrote the anagram "*ceiiinosssttuu*" in relation to "the true theory of elasticity," which would later become the framework upon which contemporary structural analysis is developed, see figure 2.14 highlighted in yellow. About twenty years after Hooke's discovery, David Gregory mathematically characterized the shape of a catenary. Gregory autonomously worked on Hooke's hypothesis and then extended it such that it could be used for arches of eventual thickness. Based on Gregory's letter, whenever a catenary is set within its thickness, stability of the arch is achieved [40]. Stone bridges and domes were designed and analyzed using the catenary analogy during the 18th and 19th centuries. Polonius's examination of the dome of Saint Peter in the Vatican is one of the most famous instances, see Figure 2.15 [41]. During the seventeenth century, a new perspective evolved on the same subject in France. The arch was depicted by LaHaire, Couple, and Coulomb as a succession of rigid bricks that may move relative to one another. Couple suggested that a failure emerges when a substantial amount of joints to trigger a process emerge within an arch [42]. Coulomb presented his memoir Sur une application des règles de Maximis & Minimis à quelques Problemes de Statique., relatifs à l’Architecture to the Royal Academy of Science in Paris in 1773 [43]. It was subsequently published in their Memoires de Mathematique & de Physique in 1776. This memoir is regarded as the first comprehensive theory regarding the stability of arches. Coulomb devised a mathematical theory for characterizing different forms of arch collapse, accounting for the block sliding and relative rotations. Coulomb argued that since sliding between blocks occurs seldom, only the geometries of fracture induced by the block’s relative rotations should be addressed. With the development of graphic statics and thrust line theory in the 19th century, more advance in the study of arches was made. Till the start of the 20th century, graphic statics was used to examine a wide range of stone bridges and structures.

To discuss the computation and modelling of masonry buildings, it is important to understand their core element, namely, their composite nature, which is attributable to the reality that they are built up of blocks connected by mortar-filled joints. The existence of joints, which are the weakest link in masonry buildings, is the reason for their nonlinear and complicated behaviour, which makes numerical modelling challenging. Consequently, a number of approaches and numerical models for masonry structure analysis currently exist. It all depends on the extent of complexities, size of data input, and desired precision. The optimal approach relies on the structure one wants to examine, the data input that is accessible, and the findings that one wants to achieve, all of which are combined with the researcher's expertise and degree of skill. The optimum approach is the one that efficiently gives essential information with an acceptable amount of inaccuracy [13]. In numerical modelling of masonry buildings, two methodologies are used: continuum and discontinuum idealization.

The continuum hypothesis proposes that the observable structure's deformations and strains are represented by continuous functions. The constitutive law of material behaviour outlines the relationships between deformations and strains. Differential equations can be obtained by combining the constitutive law of material behaviour with the equilibrium equation. The analytical solution to differential equations is seldom known; these equations, together with boundary conditions, are often transformed into a variation problem utilising the balancing principles. This is a delicate formulation, hence method like FE is the most frequent method. Although the approximate numerical approaches could also be used.

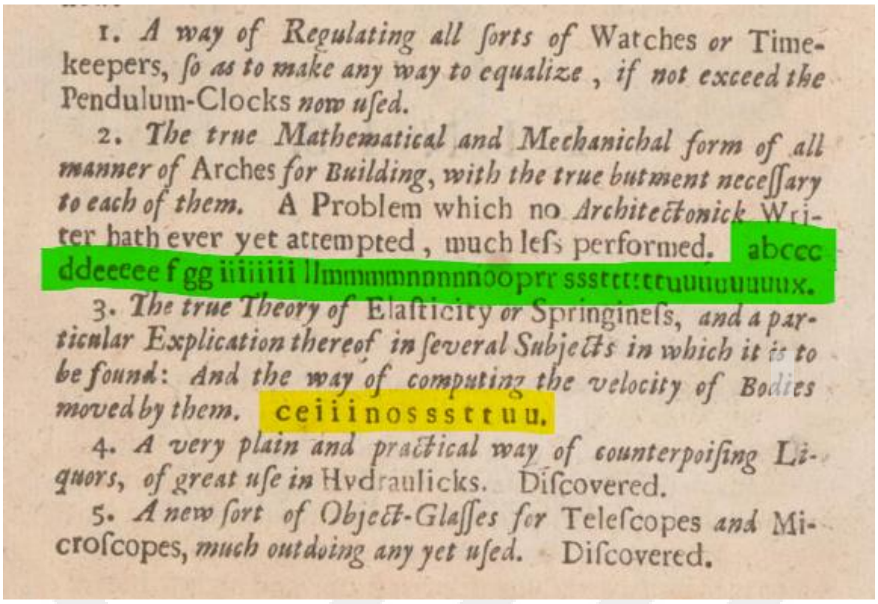

1. *A way of Regulating all ſorts of* Watches *or* Time-keepers, *ſo as to make any way to equalize, if not exceed the* Pendulum-Clocks *now uſed.*

2. *The true Mathematical and Mechanichal form of all manner of* Arches *for Building, with the true butment neceſſary to each of them.* A Problem which no *Architectonick* Writer hath ever yet attempted, much leſs performed. abccc ddeeeee f gg iiiiiii llmmmmnnnnnooprr sssttttttuuuuuuuux.

3. *The true Theory of* Elaſticity *or* Springineſs, *and a particular Explication thereof in ſeveral Subjects in which it is to be found: And the way of computing the velocity of Bodies moved by them.* ceiiinosssttuu.

4. *A very plain and practical way of counterpoiſing Liquors, of great uſe in* Hydraulicks. Diſcovered.

5. *A new ſort of Object-Glaſſes for* Teleſcopes *and* Microſcopes, *much outdoing any yet uſed.* Diſcovered.

Figure 2.14. Robert Hooke’s Anagram [38].

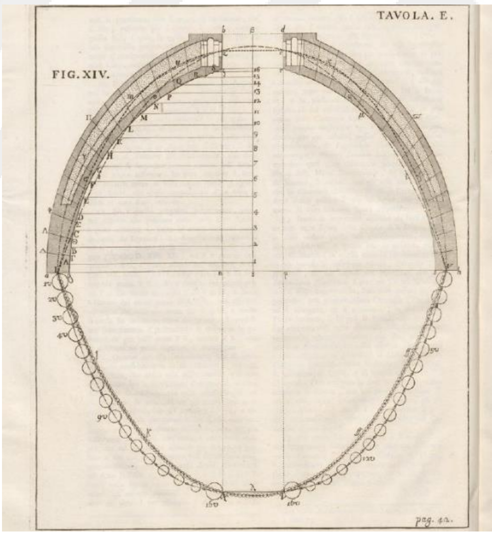

Figure 2.15. Polenius' examination of the Saint Peter's Dome in Rome [41].

The discontinuum concept however depicts the structure as a collection of discrete elements that may be detached during analysis, moved freely, and then reassembled in dynamic interaction that is mutual. Discrete components are typically assumed to be perfectly rigid in this technique, and numerical incorporation of equations of motion of units in time is frequently performed explicitly. DEM is an example of a numerical model that employs this methodology.

Increasingly numerical models are being developed recently that blend the benefits of conceptualization of structures utilizing the discontinuum and continuum techniques. A few of these techniques are based on FEM, whereas others are based on DEM. The ones that have evolved from FEM rely on the discontinuum benefits of implementing contact elements as an interface between the mesh of finite elements. When a crack occurs contact interfaces are employed to define the movement discontinuity in the joint. On the contrary, models that emanate from the DEM, usually explore the effectiveness of continuum idealization in that each discretized element has its own mesh, allowing for the consideration of element deformability (to be discussed further in section 3.1.3).

Methods for analyzing masonry structures seismically are classified into linear or nonlinear. Linear methods include basic modal and static analysis. Nonlinear methods include static approaches of slow but steady pushing otherwise known as pushover analysis and techniques for evaluating structure response over time. In the case of basic static analysis, the seismic loading is simulated with an equivalent static charge using two approaches. The first method involves subjecting the structure to continuous lateral acceleration. This method ignores the fact that the steady acceleration of the base occurs only for a brief amount of time during EQ. Elastic properties of materials cause vibrational effects on the structure which are also ignored during an EQ. This technique is effective for the stability analysis of some historic stone structures, like arches when elastic properties of materials play a little role. The second method is to apply a distributed lateral load along with the height of a structure, increasing from bottom to top, while taking into account the distribution of horizontal forces induced by the structure's dynamic response. A finite element approach is used to calculate eigenvectors and eigenvalues in the seismic computation of a structure utilizing a modal analysis. A laterally distributed load is transmitted to the height of the structure, which is afterwards integrated using various processes, taking into account the form of eigenvectors and their relevance to the structure’s dynamic response [3]. The pushover analysis is premised on the steady increase of the lateral force magnitude while the structure's response is observed [44]. The response over time approach involves calculating the response of the structure in time while taking into account deformations, strain shape, and displacements for a specific input of acceleration at the base.

➢ Analytic Methods

The goal of these approaches is to utilise an analytical approach to anticipate the reaction of the structure during a dynamic impulse, or to estimate the minimum rate of horizontal acceleration of the base that will trigger the structure to collapse. Because structural elements are supposed to be totally rigid in these approaches, it is anticipated that the structure will collapse not because the strength of the material is surpassed, but instead because of a loss of stability. Since analytic equations are sophisticated, these approaches are limited to analysing basic structures such as blocks on a horizontal basis, doorway frames, and arches.

➢ Limit Analysis Method

The method of limit analysis is founded on hypotheses stated in 1730 by Couple [3]: (1) masonry buildings have no tensile strength, (2) masonry structures have unlimited compression strength, and (3) sliding cannot occur between joints. Heyman [4] was one of the first to apply these principles to analyse the stability of stone arch. Adherence to these hypotheses allows the application of cinematic and static plasticity theorems, which are used to compute the factor of charge α required to raise external load until the structure collapses for a given vector of outside loading F.

The static theorem, often known as the low boundary theorem, states that provided a statically acceptable field of internal force for outside loads can be identified, a structure is stable and will not collapse. The lowest degree of safety factor is represented by the largest charge value for which the structure is still in the balance. The structure is unstable if the mechanism for which the work of external forces is larger than or equal to zero can be determined, according to the cinematic theorem. The bottom higher level of safety factor for a structure is represented by a bottom level of load factor in which virtual work of outside forces is zero. Finally, the safety coefficient of a structure must be the same whether calculated using a static or cinematic technique.

➢ Finite Element Method

Because of its lengthy history, the finite element approach is the most often used method for calculating not only masonry buildings but also structures in general. So far, a variety of numerical models based on finite element methods have been created, and they are characterised by the type of finite elements used to discretize the structure, as well as by the constitutive law of materials, which can be linear or nonlinear.

When it comes to computation, the skeleton system and linear finite elements are the simplest approaches to modelling masonry buildings using the finite-element method. Molins and Roca [45] created a numerical model for analysing space structures composed of linear space components with varying cross sections. The model incorporates material and geometric nonlinearity, as well as the Mohr-Coulomb criteria of failure in shear. For the study of masonry buildings, many simplified models that resemble a structure with an analogous frame system have been created [46] [47].

- Discrete Element Method

Cundall and Hart [48] define the discrete element technique as a computational strategy that: (1) allows finite displacements and rotations of discrete bodies, including their total separation, and (2) automatically identifies new contacts among bodies as the calculation advances. Cundall [49] also created the Distinct Element Method, which was designed to mimic the sliding and separation of related rock masses along previously identified fissures or discontinuities. The approach is based on explicit numerical integration of rigid block equations of motion across time. The approach involves reciprocal contact of blocks and allows for arbitrary movement of blocks. In addition to dynamic computations, the approach, like dynamic relaxation methods, allows for the generation of static solutions by viscous damping.

One of the primary goals of the collapse simulation is to allow for the emergence of discontinuities in a continuous material. Because the positions of genuine fissures can be accurately established, the accuracy of collapse simulation may be improved. After cracking and separation, the correct simulation of post-failure behaviour is also very important. The contact and collision of the pieces cause kinetic energy to be dissipated in the post-failure behaviour. The finite element approach is based on continuum mechanics assumptions, and it may accurately simulate pre-failure behaviour. However, it is not appropriate for common fracture propagation and fragmentation problems. The discrete element technique, on the other hand, is designed to address situations with significant discontinuities. It is capable of simulating post-failure behaviour. Combining the finite element approach with the discrete element method yields an effective tool for simulating pre-failure and post-failure behaviour. A transition from continuum to discontinuum is required for a complete simulation of the behaviour using coupled FEM-DEM. The finite element transition from continuum to discontinuum is fraught with difficulties. Various strategies have been developed in the literature for this purpose, and various finite element programmes have incorporated them. Each approach, however, has inherent flaws.

2.5. Previous Related Works

Tamaam Bakeer [5] investigated the collapse mechanism of large-scale masonry structures under the influence of seismic actions. The study involves the development of numerical techniques to replicate the actual masonry behaviour from point of linear elastic to damage progression till eventual collapse. An open-source application – LsDyna was utilized for the development of the numerical models. LS-DYNA is an explicit finite-discrete element code (can also be used implicitly) with the capability to handle huge deformations and discontinuities, making it suitable for the analysis of progressive collapse. The mesh-free approach capability such as smoothed particles hydrodynamic (SPH) was tested to simulate masonry's fragmentation and mode of failure. The essential contextual details regarding the constituent of masonry were also provided in the work. Provided also are the major characteristics, flaws, and demanding problems. The study presented and tested an interface cohesive model based on the smoothness of the yield surface. Two full-scale masonry constructions were tested dynamically and the results were used to validate the proposed models. The proposed technique was subsequently utilized to investigate the performance of historical masonry structures with components of various geometries against basic EQ features. The collapse analysis of whole vintage masonry structures investigated the effects of EQ features on collapse vulnerability. Also developed in the study was a theory for the behaviour of shear failure of masonry shear walls strengthened vertically. It idealizes the behaviour of composite materials with elevated inhomogeneity (such as masonry) following initial failure. Furthermore, collapse analysis was used to establish and validate the seismic retrofitting of renovated vintage structures. The developed technique was tested on a research study of a collapsed terracotta masonry edifice from the Bam citadel during the 6.5 Richter scale 2003 Bam EQ.

Paulo Lourenço [1] in his PhD thesis studied the unreinforced masonry structures nonlinearly. Short-term static loads are applied to the structures under examination, which are not always proportional but are, in essence, monotonous. He developed and evaluated reliable and accurate numerical tools at both the micro and macro levels. The research examines the characteristics of masonry and modelling methodologies for masonry constructions. It addresses the necessity for a detailed material description in order to construct accurate numerical models in particular. Although deformation controlled testing is typically absent, particularly when it comes to masonry composite behaviour. The testing apparatus is described, as well as the results that are useful for numerical reasons. The process for solving a body's equilibrium was also discussed, as well as a review of the general formulation of a plasticity-based constitutive model. An incremental-iterative globally convergent Newton-Raphson approach with line search methodology and control of arclength was used to solve the equations of a nonlinear system that results from finite element discretization. An implicit Euler backward return mapping solved using a regular Newton-Raphson technique and consistent tangential operators for all modes of the composite yield surface were proposed as a general formulation for the numerical application of the theory of multisurface plasticity. A micro-modelling of the masonry interface failure criterion was also presented. An elliptical cap, the Coulomb friction law, as well as a straight tension cut-off, are all part of the multisurface plasticity model presented.

Inelastic behaviour such as coupling between shear and tensile failure, tensile strength softening, dilatancy softening, cohesion softening, friction hardening and/or softening as well as compressive strength softening and hardening were all discussed in the study. The model is validated by comparing the computed numerical results to experimental data published in the literature. Two viewpoints on homogenization procedures are also discussed in the study. The first method seeks to simplify the description of masonry composite behaviour. The method relies on the masonry components' constitutive rules as well as the geometrical arrangement of units and mortar, but it does not discretize the geometry. A unique matrix formulation for elastoplastic behaviour is proposed for this simplified homogenization process, which is based on the assumption of layered materials. The masonry components' discretization is used in a second approach to predict macro-properties of masonry. The computation of the composite elastic constants and the composite tensile fracture energy in the direction parallel to the bed joints are two examples offered. An anisotropic continuum model for masonry macro-modelling was also presented in the study. A Rankine-type yield surface for tension and a Hill-type yield surface for compression are included in the multisurface plasticity model. Anisotropic elasticity and anisotropic plasticity are combined in a manner that permits the prediction of total diverse behaviour in tension and compression along the material axis. The model is validated by comparing the calculated numerical results to experimental data published in the literature. The research was also extended to include a review of engineering applications of the models generated. A few relevances involve the movement-joints spacing in masonry, an illustration of how the generated models might be utilized to get readily available design guidelines. Another usage involves the forecast of damage in existing masonry structures owing to settlements induced as a result of tunnelling, an instance of the evaluation of complicated structures under new loading circumstances. The final application relates to the safety of historic buildings that have been damaged, as an example of evaluating existing structures under contemporary loading circumstances. It should also be highlighted that the models generated and the discussions held in this study apply to much more than brick constructions. The proposed micro-model is predicted to have applications in various fields such as adhesives, joints in rock and stone works, body contact difficulties, and, in general, any sort of interface interaction where bonding, cohesion, and friction between components compose the fundamental mechanical activities. Most anisotropic materials, such as glass, plastics, or wood, as well as any composite, can be used with the macro-model.

Dolatshahi and Aref [50] in their report named Computational, Analytical, and Experimental Modeling of Masonry Structures addressed the knowledge gaps in the modelling of masonry structures subjected to high loadings. A solid and reliable material constitutive model and three-dimensional numerical techniques were developed and validated against results collected by the authors from the experiment data. The development of novel material models and numerical methodologies for simulation of masonry structures within the framework of mesoscale analysis is the emphasis of this report. The development of macro-yield surfaces for the macro-scale study of masonry walls is also covered in this report. Finally, thorough experimental research on masonry walls was conducted using varieties of brick as well as various boundary circumstances. Each test was validated numerically, and the proposed numerical procedure's robustness was confirmed. The constitutive material models postulated are implicit and explicit formulations based as well as seamlessly work with commercially available finite element software like ABAQUS, TNO DIANA and LS-DYNA.

Massart [51] in this study, aimed to fill the gap between macroscopic and mesoscopic presentations and offer a computer technique for plane masonry wall analysis. To address the shortcomings of previous techniques, a multi-scale framework is employed, which permits mesoscopic behaviour characteristics to be included in macroscopic formulations without the necessity for a prior assumed macroscopic fundamental law. Initially, a mesoscopic constitutive formulation for the quasi-brittle elements of the brickwork material is defined, with stiffness degradation as the primary mode of failure. As a result, the description of the mesoscopic is founded on a model of scalar damage. At the mesoscopic scale, plane stress and plane state generalization assumptions are utilized, resulting in the descriptions of the macroscopic continuum in two-dimension. It was shown that by using unit cell computing and periodic homogenization approaches the settings of the identified mesoscopic constituent permit mimicking the typical form of (anisotropic) failure envelopes experimentally observed. The failure mechanisms associated with different macroscopic directional loadings are likewise appropriately represented. The plane-stress descriptions accurately represent the in-plane failure mechanism, whereas the plane state generalization assumption, which introduces reduced three-dimensional effects, is required to model biaxial compressive loading induced failure specifically out-of-plane failure. Damage-induced anisotropy originating from the stacking pattern of the constituent material, which has proven to be difficult to model effectively using equations of macroscopic phenomenological constitutive, is accomplished here in a conventional manner. To predict the macroscopic reaction of the material, the description of identified mesoscopic is used in a scale transition technique. For the extraction of this reaction from unit cells, the first-order computational homogenization procedure is adopted. Damage localization finally emerges as a natural result of the constituents' quasi-brittle character. The commencement of macroscopic localization is considered a phenomenon of material divergence and is identified using eigenvalue analysis of the homogenized acoustic tensor generated from the scale transition process combined with a limit point criterion. The failure mechanisms of the underlying mesostructure in the unit cells are revealed to be significantly connected to the orientations of the macroscopic localization acquired with this form of detection. By integrating localization bands at the commencement of the macroscopic localization, including a width explicitly determined from the material's initial periodicity, a well-posed description of macroscopic is preserved. This enables the description of macroscopic to account for the fracture zone's finite size. The response of the material computed from unit cells might display a snap-back behaviour on the basis of localization of mesoscopic damage in the order of a mortar joint tiny zones. This implies that such a response cannot be used in the conventional strain-driven multi-scale approach. The multi-scale framework necessary to treat the snap-back mesostructure reaction is proposed with modifications. Finally, the multi-scale framework is tested on a basic restricted shear wall problem, demonstrating its capacity to describe complicated structural failure mechanisms.

Oliveira [6] in his work focused on improving the understanding of the behaviour of blocky masonry constructions when subjected to cyclic loading. Uni-axial monotonic and cyclic deformation-controlled experiments were carried out on brick, stone and prisms specimens in order to characterize these materials’ cyclic behaviour completely. The cyclic behaviour of masonry structures was analyzed numerically using the micro-modelling technique. Commencing from an already in existence model of monotonic constitutive that was created for interface elements and totally founded on the theory of plasticity. A novel constitutive model is proposed that is capable of describing the cyclic loading of interface components. The new model was entirely based on the plasticity theory and an existing monotonic constitutive model built for interface components. This new model, too, is based solely on the incremental plasticity theory. Only the shear component is assumed to have elastic unloading. The normal component is described non-linearly. Thus, during unloading/reloading, two additional auxiliary yield surfaces, dubbed unloading surfaces, are provided, which are comparable to monotonic ones. A mixed hardening law governs the motion of the unloading surfaces. In a prototype version of the DIANA finite element code, the suggested constitutive model has been implemented. Following that, the constructed model is used to simulate certain tests from the literature. There is good agreement between numerical and experimental results. The derived constitutive model's performance was evaluated against three types of masonry constructions. The numerical findings reveal that the model can recreate the primary aspects that define cyclic behaviour, including compressive collapse, frictional sliding along joints, and cracking of joints of the masonry. During the investigation of the TUE wall, various structural reactions in opposing directions of horizontal force were discovered. The uneven geometry of the brick shear wall is to blame for such variations. The wall's cyclic analysis revealed the key structural cyclic features, such as dissipation of energy and stiffness deterioration. Based on the findings, it was advised that structures suited for cyclic analysis have symmetrical geometric configurations. Furthermore, the constitutive model was validated against experimental data. The simulation of the UPC prisms was successful, with numerical findings nearly matching the real ones. The JRC wall analysis was only partially successful. The modelling of the high wall was completely satisfied, with the mode accurately capturing the dominating joint opening-closure mode. Significant variations in dissipated energy, failure mode, and structural behaviour were discovered between the TUE wall and the JRC wall (high wall). Such good outcomes were not achievable with the low wall. Although the acquired failure mode was identical to the experimental one, failure began earlier than in the experiment. The significance of precise modelling of the boundary conditions has been stressed, as has the challenge of defining the model parameters appropriately. This challenge comes mostly owing to a lack of sufficient experimental data. A definition based solely on average values has been addressed, apart from any additional information. Lastly, a more precise finite element mesh (rather than 2'1 elements, 4'2 elements was used to model every unit) would most certainly improve understanding of the wall's reaction, particularly in the softening phase, because less energy would be released during the probable collapse of a specified integration point, resulting in a more soft post-peak diagram.

Bustamante [52] investigated the possibilities of rigid block assembly limit analysis in the structural evaluation of historical masonry buildings. A review of the fundamental ideas of limit analysis and prior publications on the subject is conducted. To depict the non-dilatant friction failure mode in brickwork, a limit analysis formulation for materials with non-associated flow rules is used. Two computer tools for two- and three-dimensional models are created. The suggested yield functions can account for restricted compressive pressures. To model standard strengthening procedures, a tie element is included in the formulations. The torsion failure mechanism on frictional joints in the three-dimensional model has not been thoroughly investigated. Theoretical advances to the subject are made, including relationships between torsion strength and other generalised stresses on rectangular joints. Both two-dimensional and three-dimensional models are verified by comparison with experimental and/or numerical evidence, yielding positive outcomes. The proposed unique solution approach allows the user to follow the structure's behaviour roughly throughout the loading history till failure. The same technique can produce superior results in circumstances when earlier recommended procedures underestimate the safety factor. The computer programmes created are used to analyse the behaviour of structural components found in historical masonry constructions. Finally, the benefits and drawbacks of the technique proposed for assessing ancient masonry buildings were discussed. The structural model used in this study was thought to be a good depiction of ancient masonry constructions, consisting of an assembly of stiff blocks interacting through frictional joints. The no-crushing condition was traditionally incorporated in formulations by assuming infinite compressive strength; nevertheless, it has been proved that this hypothesis leads to potentially dangerous outcomes.

The inclusion of restricted compressive stress in the two- and three-dimensional formulations allows for the consideration of stress distributions on the joints at the time of structural collapse and the absence of hinges at the joint edges. The effective compressive stress calculation methods were adapted from the reinforced concrete limit analysis literature, and it is probable that similar calculations need to be altered for ancient masonry buildings. Nevertheless, the validation of two- and three-dimensional models using experimental and numerical data was adequate.

Seyedrezai [53] in his research, studied the behaviour of unreinforced one-way arching walls subjected to blast loading and LS-DYNA (freely available FE program) was used for the simulation. The model is built using data collected earlier during a physical explosion experiment. The created model was validated by the close agreement between numerical and experimental findings. The effect of varying various input factors such as the effect of two-way arching action on the wall's reaction, coefficients of friction, mortar strength, wall height, border condition, and scaled distance were then investigated in a sensitivity analysis. The two-way arching motion, wall height and scaled distance were discovered to be the most relevant characteristics in this investigation. Larger scaled distances result in less deflection, whereas smaller scaled distances result in greater deflection. The height of the wall also has a considerable impact on its reaction to blast loads; the higher the wall, the greater the maximum displacement. Lastly, the impact of two-way vs one-way arching was investigated. To replicate two-way arching, equivalent boundary conditions to the top and bottom of the wall (translational restrictions) were put to the left and right sides of the wall. The findings demonstrated that two-way arching movement can greatly minimise deflection. The two-way arching mechanism allowed the wall to withstand the imposed blast load nearly fully. It is also determined that two-way arching movement can greatly minimise the maximum deflection of the wall.

Van Noort [9] investigated the masonry panels loaded under biaxial and uniaxial loads. It was accomplished by repeating the tests conducted by Page and Dhanasekar using a detailed micro model. In the numerical simulation, three variants per influence variable were chosen. Hence, it was feasible to get numerical findings that could be used to estimate the material behaviour of various masonry kinds. The variables are bond, mortar & mortar- brick interface, and brick types. Analyses were performed on all feasible combinations, yielding a total of 27 masonry types. The possibility to devise a relatively simple process for calculating the smeared material properties of the brickwork using the material properties and dimensions of its components was also investigated.

Aaron Orr [54] conducted research with the goal of developing a holistic examination of the susceptibility of structures vulnerable to landslide impacts using analytical tools and historical analysis of landslide-damaged buildings. The study focused on the shared structural typology of Dominica's Commonwealth. In Dominica, 10 structures were assessed as a result of strong wind speeds, floods, debris flows, and debris slides. One of the 10 buildings was studied using analytical models of its response to simulated landslide impacts, and the results are provided in this dissertation. The analytical simulations begin with the numerical programme RAMMS, followed by the derivation of landslide parameters, such as total landslide volume, for structural reaction analysis with the software Blender, as well as the add-ons Bullet Constraint Builder and Impulse. After calibrating the run-out kinematics and impact dynamics in Blender, the examination of a building's response to simulated landslide impacts was done. Finally, further simulations were run to examine the simulated damage to a typical Dominican structure typology from single collisions with a regulated velocity. Back-analysis was used to evaluate the provided research utilising gathered data of literature values of mortar engineering qualities, landslide-induced damage, deposited landslide types, and in-situ structure typologies. The simulated damage from the analysis, however, was consistently greater than the observed damage during data collection. The simulation is done while exploring the susceptibility of structures vulnerable to landslide effects identifying the simulated particle size of the landslide and assigned breaking thresholds of the mortar walls, particularly the mortar.

Fita *et al* [55] created a programme that makes it simple to set up and recreate EQs. They combined an EQ simulator with a physics-based structural model adapted to brick structures, resulting in simulations with a high degree of realism. They ran a series of experiments on historic stone buildings including walls and cathedrals to confirm the concept. They demonstrate the potential of using EQ simulations and structural vulnerability, a building property that limits the damage caused by seismic movements, in historical research to assist experts in understanding previous events when an EQ occurred. They demonstrated an approach based on off-the-shelf software aimed at users with no prior knowledge of EQ modellings, such as historians, art historians, and curators. The approach was created primarily for aesthetic results, allowing one to quickly duplicate the impacts of EQs on historic stone buildings for the reproduction of past events or the avoidance of future ones at a minimal cost but with high realism. It was stressed that this approach was designed with ease of use and low precision in mind. Nonetheless, it can assist stakeholders in predicting the impact of seismic shifts and their potential repercussions.

Furukawa *et al* [56] investigated the collapse of adobe houses during EQs with varying EQ strengths utilising the original author's 3-dimensional distinct element technique code. They began by assessing structural damage using the damage index, interior-space damage using the w score, and human casualties in falling structures using three casualty criteria. Second, they examined the links between EQ intensity, structure damage, interior-space damage, and casualties. It is discovered that casualties have a larger link with interior-space damage than structural damage, and three vulnerability functions are proposed namely structural, interior-space, and casualty vulnerability functions. The effects of various reinforcement approaches on these functions are also investigated. Finally, a number of analytical approaches are provided for developing vulnerability functions and estimating fatalities using the functions. The adobe constructions without non-structural features are solved in this study. Conversely, in real life, damage to interior space is a mixture of non-structural and structural features that can exist at varying levels of exterior damage. As a result, neglecting this element is seen as a shortcoming of this study. More reliable models would be developed in the next study to elucidate this problematic element. Actual EQ casualty epidemiology research has yielded significant results. The simulation in this study has the ability to compensate for the lack of real-world data, but it is only accepted if its conclusions are validated by real-world data.

Köseoğlu [57] in his research looked at a severely damaged single domed mosque from the 16th century Classical Ottoman architecture. Serious damage to several features of the structure, including the structural brick walls and dome, has lately resulted in the structure's closure to service. Hence, the primary goal of the research was to determine the various causes of the harm. The mosque was built on silty-clay soil, and the water table has shifted significantly as a result of the recent drought, producing soil displacements. The structure is modelled using a linear finite element method. Masonry walls are represented as homogenised macro shell components.

The displacement at foundation joints is caused by a shift in the water table. The analysis findings were compared to the measured damage, and the finite element model was calibrated based on the observed damage. Some ways of rehabilitation were also proposed. To minimise soil movement, Mini-piles up to hard soil (rock) was proposed. To prevent future crack propagation, a steel ring was proposed around the damaged dome base. Additionally, cracks in the masonry walls were recommended to be fixed with an appropriate substance that complements the historic texture.

Gregor Beattie [58] investigated the reliability and applicability of discrete finite element analysis tool (Ls-Dyna) to masonry analysis. Prior to Gregor’s work, vehicle impacts on various types of masonry parapets were modelled using an LS-DYNA. The findings were promising, with a high qualitative agreement between testing and analyses.

This technique was subsequently used to establish masonry barrier evaluation guides namely County Surveyors' Society Guidance Note [59] as well as the new British Standard [60]. The original study's findings showed that unreinforced masonry may perform pretty well in terms of preventing vehicle penetration and managing the rebound of impacted vehicles. However, in order to avoid a premature failure, the analytical technique necessitated the use of artificial parameters. This topic was addressed in Gregor’s work through the use of both experimental testing and FE analysis. The testing work consists of a variety of small and medium size experiments that supply data for the numerical work. To analyse both quasi-static and dynamic material properties, a range of conventional tests and tests devised specifically for this purpose were used. These experiments examine the apparent dynamic improvement of masonry shear and tensile strength. Furthermore, the influence of fracture energy and dilatancy at high strain rates is taken into account. Methods for evaluating the interaction between masonry and reinforcement under varied strain rates have also been devised. The present LS-DYNA interfaces were also rigorously analysed in the numerical models, and improvements that have been applied elsewhere are reviewed and recommendations are given. This has enabled the integration of fracture energy and dilatancy effects. Eventually, a case study was conducted to illustrate the efficacy of the created approach.

Abide Aşıkoğlu et al. [10] investigated the seismic performance of a half-scale two-story unreinforced masonry (URM) structure with plan and elevation structural irregularities. The primary goals are to comprehend the seismic response of URM buildings with torsional effects and assess the reliability of applying simpler methodologies for irregular masonry structures. Nonlinear static assessments are carried out for this purpose utilising three distinct modelling approaches: a continuum model, beam-based macro-element models, and spring-based macro-element models. On the basis of capacity curves and global damage patterns, the performance of each strategy was compared. The numerical predictions and experimental data were found to be in reasonable agreement. Validation of simplified ways was traditionally done with regard to regular structures but based on the variations in base shear capacity revealed in this research. While torsion is present, Structural imperfections appear to be significant to consider when using simplified methods.

3. MECHANICAL BEHAVIOR AND FAILURE OF MASONRY STRUCTURES

3.1. General Description of Masonry

3.1.1. Properties and Behaviour of Unit and Mortar

Brick, a common building material, is often rectangular in shape and made of clay, cement, or other geomaterials. They are typically solid, although they can also be hollow or perforated. In masonry buildings, many types of bricks are employed depending on the quality, manufacturing process, material, and function. The classification types are presented in table 3.1.

Table 3.1. Brick Classification

Process	Quality	Material	Purpose
Unburnt Bricks	First class bricks	Fly ash Clay Brick	Common Bricks
Burnt Bricks	Second class bricks	Concrete Brick	Engineering Bricks
Over Burnt	Third class bricks	Sand-lime Brick	
	Fourth class bricks	Firebrick	
		Burnt Clay Brick	

The term "mortar" refers to a paste made by mixing a binding substance such as cement and/or lime with a fine aggregate such as sand and adding the needed amount of water. The adulterant and matrix are terms used to describe the aforementioned two components of mortar, namely the fine aggregate and binding substance respectively. The matrix binds the adulterant particles, hence the quantity and quality of the matrix will determine the longevity, quality, and strength of the mortar. The mass can securely bond the bricks or stones due to the combined impact of the two components of mortar. The following criteria are used to classify mortars: binding material kind, bulk density, application's nature and special mortars.

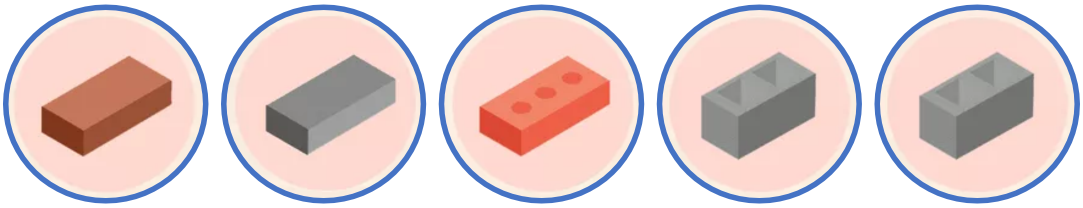

(a) (b) (c) (d) (e)

Figure 3.1. Types of Brick (a) Burnt Clay Brick (b) Sand-lime Brick (c) Engineering Bricks (d) Concrete Brick (e) Fly ash clay Brick.

There are four primary varieties of mortar mix: N, O, S, and M, as well as some technologically modified cement, mixes like K-type. To achieve certain performance qualities like flexibility, bonding properties, and compressive strength, each kind is combined with a distinct amount of cement, lime, and sand. The appropriate mortar mix type for every project is determined by the application and numerous masonry building design parameters. The features and recommended uses of each type of mortar are detailed in ASTM C 270 [61] but are briefly discussed in this thesis next. Table 3.2 presents some of the mortar classifications.

The most prevalent form of mortar is Type N, which is often used on external, above-grade walls. This all-purpose mortar has a strong bonding ability. Because the cement is not overloaded with Portland, it cures gradually and is easier to work with. The compressive strength of Type N mortar is around 750 PSI, making it excellent for usage with masonry or semi-soft stone applications. It's more elastic than a high-strength mortar, which helps to prevent neighbouring masonry units from cracking and spalling. Even though Type N is most typically used for laying bricks, it may also be employed to repoint relatively new brickwork.

The weakest compressive strength is Type O mortar, which has a compressive strength of 350 PSI. It is relatively easy to work with Type O, and the blend's uniformity makes it an ideal choice for repointing a structurally sound wall. Because of its low compressive strength, it's ideal for soft stone applications like laying brownstone or sandstone. More flexing is possible with Type O mortar, which can assist avoid spalls and cracks in masonry units.

Table 3.2. Mortar classification

Binding material kind	Bulk density	Application's nature	Special mortar	Type
Lime mortar (Fat and hydrated)	Heavyweight mortar	Brick-laying mortar	Sound absorbing mortar	N-type
Surkhi mortar	Lightweight mortar	Finishing mortar	Lightweight mortar	O-type
Cement mortar			Fire resistant mortar	S-type
Gauged mortar			X-ray shielding mortar	M-type
Gypsum mortar				K-type

Type S mortar has a compressive strength of around 1800 PSI, making it a medium-strength mortar. Type S mortar may be used to hard coat typical stucco systems and can be utilized on at/or below grade external walls. Type S mortar has better strength and bonding qualities than Type N, and the additional quantity of lime in Type S allows the mortar to resist more moisture while also improving its elastic and bonding properties.

The Type M mortar has the highest compressive strength of the four, at 2500 PSI. When a building might resist excessive lateral stresses and/or gravity, Type M mortar should be utilized. Type M mortar is also a viable choice for projects involving hard stones with compressive strengths of more than 2500 PSI. Type M mortar's properties make it appropriate for below-grade applications including foundations and retaining walls.

Although Type K mortar is seldom employed in novel construction, it is sometimes recommended for restoration or other particular purposes. It has a compressive strength of just approximately 75 pounds per square inch. Type K is typically used to restore the masonry part of historical structures that require a specific mix that is not much stronger than the previous masonry due to its softness. Figure 3.2. presents some brickworks based on the binding material kind.

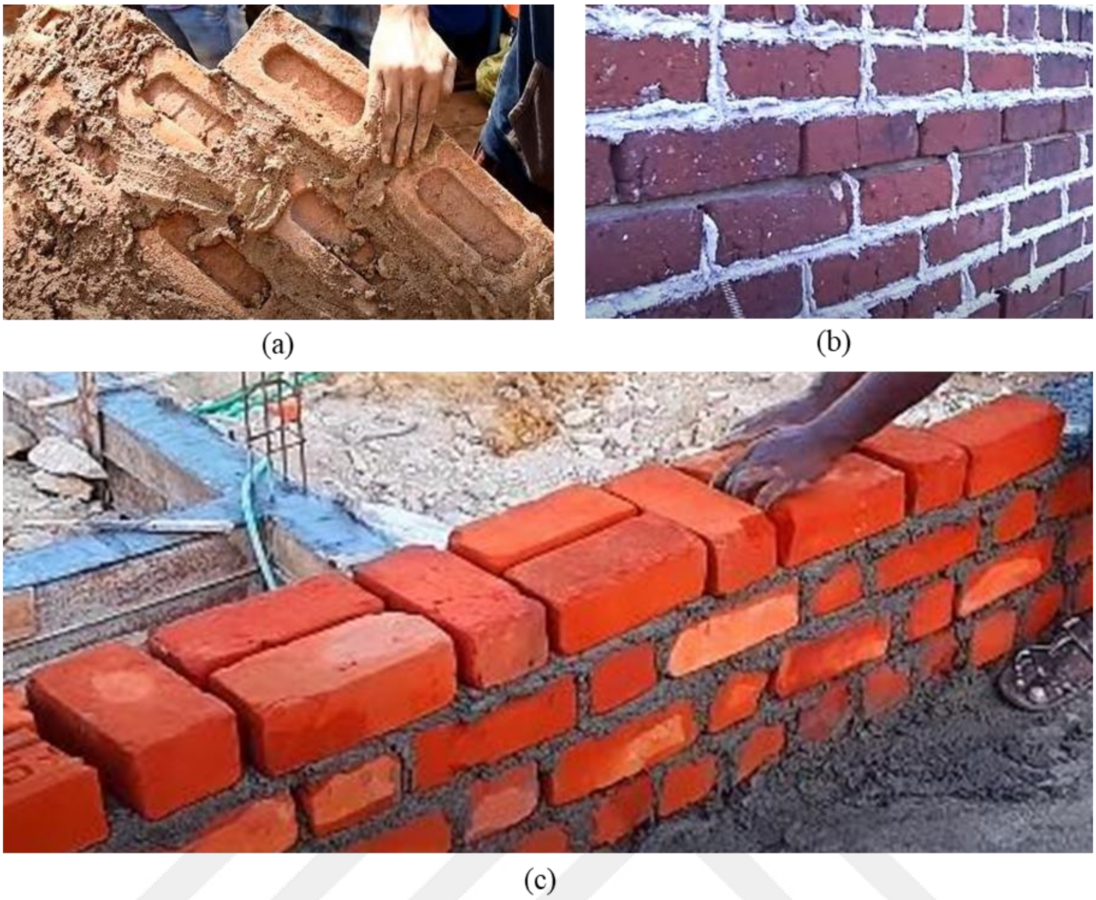

Figure 3.2. Brickwork classification based on mortar (a) Mud mortar (b) Lime mortar (c) Cement mortar [62]

3.1.2. Arrangements and Connection Brick Masonry

The pattern or framework in which bricks are set is known as masonry brick arrangements. In brick masonry, there are many different types of bonding, each with its own appearance, installation challenges, and, in the case of walls, structural problems. The laying and bonding pattern of bricks in walls is used to classify bonds in masonry wall building. When bricks are set close to each other and in layers in walls, mortar fills in between layers of bricks and in grooves. The strength of brick masonry is determined by the type of bond and the materials used in its construction. They play a significant part in the brick masonry's strength, stability, and longevity. Some of the most popular brick bonds are shown in Figure 3.3. The texture of the connection at corners between adjacent and/or orthogonal walls can be categorized as toothing or non-toothing (see Figure 3.4.).

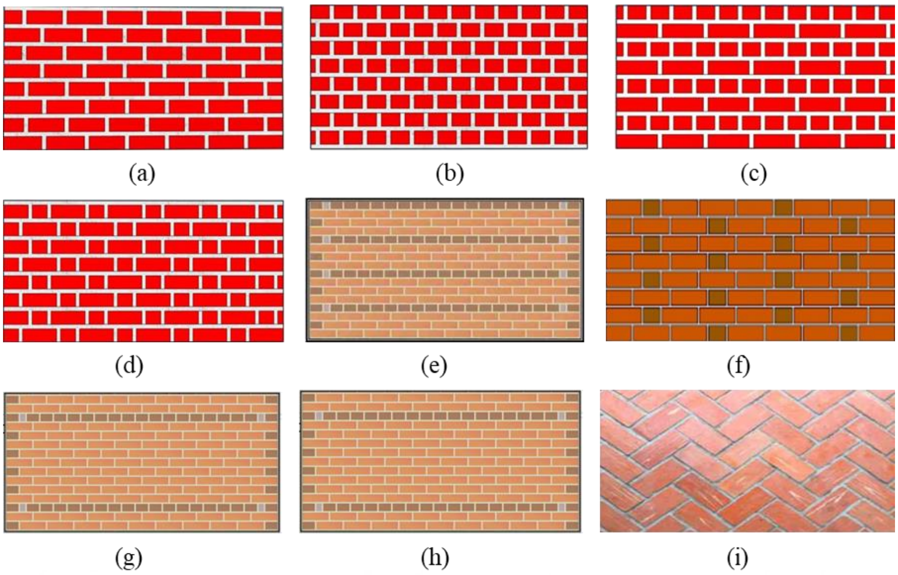

Figure 3.3. Some of the most popular brick bonds (a) stretcher bond, (b) Header bond, (c) English bond, (d) Flemish Bond, (e) English Garden Wall, (f) Flemish Garden Wall Bond, (g) Scottish Bond, (h) American Bond and (i) zig-zag.

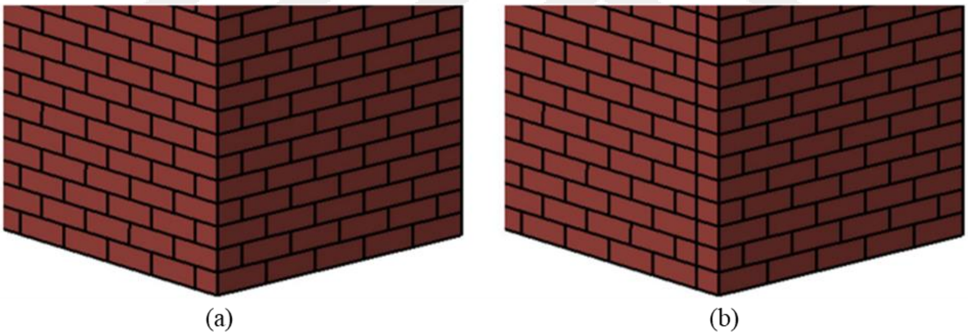

Figure 3.4. Type of corners between two adjacent walls (a) toothing corners and (b) non-toothing corner

3.1.3. Modelling Strategies

Masonry is in its own composite material and the numerical representation of its general behaviour is entirely reliant on the arrangement and characteristics of its elements as well as the execution of the continuum-to-discontinuum transition (see Section 2.4). On this premise, Massart [51] proposed two numerical methodologies namely; the Mesoscopic models and the Macroscopic model. Masonry is described as a heterogeneous configuration with distinct representations for each component in the mesoscopic model. However, computational costs and time consumption limit the extent to which this description could be applicable. At the other end of the spectrum, the overall net behaviour of the elements is assumed to be homogenous, represented by phenomenological constitutive rules. Consequently, failure mode forecasts are often inaccurate and visualization is as well challenging in macroscopic models. Hence, taking into consideration the level of simplicity and accuracy desired, the three most prevalent masonry modelling methodologies are listed below [1].

- Detailed micro-modelling; Units and mortar are depicted by continuous elements, whilst the contact interface between unit and mortar is represented by discontinuous elements such as crack, shear, and crushing potential planes.
- Simplified micro-modelling; Using "geometrically enlarged" masonry units with a unitary "averaged" interface for the two-contact interface and the mortar. The behaviour of the contact interface between unit and mortar is aggregated in discontinuous components, whilst continuum elements are utilized to describe the enlarged units. The material parameters of the enlarged unit as well as that of the masonry joints are required. Owing to the non-incorporation of mortar's Poisson ratio which has a significant influence on compressive strength, this technique is perceived to produce a reduced accuracy.
- Macro-modelling; Every masonry element (units, mortar and contact interface) are smeared out into a unitary homogenized continuum. Masonry's quasi-periodic character has stimulated appropriately to explore the usage of these homogenization strategies. It entails considering masonry as a homogeneous material hypothetically with its constitutive equations distinct from the elements.

The decision about the suitable technique depends on the required accuracy and the size of the model. Micro modelling gives a more realistic representation of the structural behaviour, but it is relatively prohibitive to be used due to the great number of degrees of freedom, requires more input data and also their failure criterion which has an elaborated form owing to the unit mortar interaction. The constitutive equations of the components have normally a simple form, and they are appropriate for the study of the local behaviour of masonry. The constitutive models on the macro-level are relatively simple to use, require fewer input data, and the failure criterion has normally a simple form. It requires prior definitions of constitutive prescriptions. The constitutive equations are relatively complicated and are suitable for the study of the overall behaviour of the entire masonry structure to reduce the numerical calculation. Figure 3.5. shows the masonry modelling methodologies discussed above.

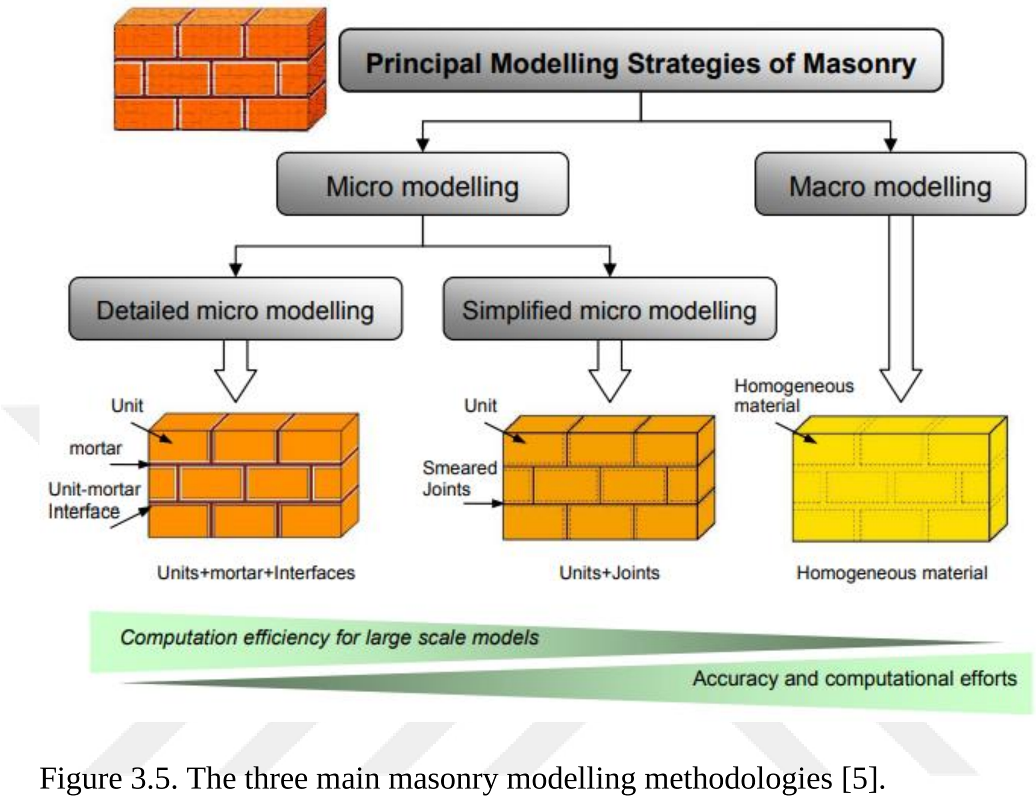

Figure 3.5. The three main masonry modelling methodologies [5].

3.1.4. Damage Classification

European Macroseismic Scale (EMS-98) [63] is the criterion for assessing seismic intensity in European countries, as well as a handful of countries outside of Europe. The EMS-98 scale was released in 1998 as an upgrade to the test version from 1992. The EMS-98 seismic intensity scale is the first to facilitate cooperation between engineers and seismologists instead of being intended solely for seismologists. It includes a comprehensive handbook with instructions, images, and application examples. EMS-98 intensity describes how severely an earthquake impacts a certain location, as opposed to earthquake magnitude scales, which represent the seismic energy delivered by an earthquake. EMS-98 is generally divided into 12 categories, see Figure 3.6. However, a broad and simplified categorization was made for masonry buildings type see Figure 3.7.

I	**Not felt**	Not felt by anyone.
II	**Scarcely felt**	Vibration is felt only by individual people at rest in houses, especially on upper floors of buildings.
III	**Weak**	The vibration is weak and is felt indoors by a few people. People at rest feel swaying or light trembling. Noticeable shaking of many objects.
IV	**Largely observed**	The earthquake is felt indoors by many people, outdoors by few. A few people are awakened. The level of vibration is possibly frightening. Windows, doors and dishes rattle. Hanging objects swing. No damage to buildings.
V	**Strong**	The earthquake is felt indoors by most, outdoors by many. Many sleeping people awake. A few run outdoors. Entire sections of all buildings tremble. Most objects swing considerably. China and glasses clatter together. The vibration is strong. Top-heavy objects topple over. Doors and windows swing open or shut.
VI	**Slightly damaging**	Felt by everyone indoors and by many to most outdoors. Many people in buildings are frightened and run outdoors. Objects on walls fall. Slight damage to buildings; for example, fine cracks in plaster and small pieces of plaster fall.
VII	**Damaging**	Most people are frightened and run outdoors. Furniture is shifted and many objects fall from shelves. Many buildings suffer slight to moderate damage. Cracks in walls; partial collapse of chimneys.
VIII	**Heavily damaging**	Furniture may be overturned. Many to most buildings suffer damage: chimneys fall; large cracks appear in walls and a few buildings may partially collapse. Can be noticed by people driving cars.
IX	**Destructive**	Monuments and columns fall or are twisted. Many ordinary buildings partially collapse and a few collapse completely. Windows shatter.
X	**Very destructive**	Many buildings collapse. Cracks and landslides can be seen.
XI	**Devastating**	Most buildings collapse.
XII	**Completely devastating**	Almost all structures are destroyed. The ground changes.

Figure 3.6. The 12 divisions of the European Macroseismic Scale [63].

Grade 1: Negligible to slight damage (no structural damage, slight non-structural damage) Hair-line cracks in very few walls.Fall of small pieces of plaster only.
Fall of loose stones from upper parts of buildings in very few cases.

G-1D

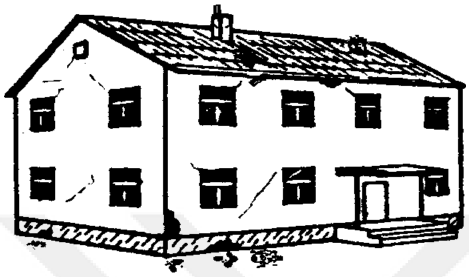

Grade 2: Moderate damage (slight structural damage, moderate non-structural damage)
Cracks in many walls.
Fall of fairly large pieces of plaster.
Partial collapse of chimneys.

G-2D

Grade 3: Substantial to heavy damage(moderate structural damage, heavy non-structural damage)
Large and extensive cracks in most walls. Roof tiles detach. Chimneys fracture at theroof line; failure of individual non-struc- tural elements (partitions, gable walls).

G-3D

Grade 4: Very heavy damage(heavy structural damage, very heavy non-structural damage)
Serious failure of walls; partial structural failure of roofs and floors.

G-4D

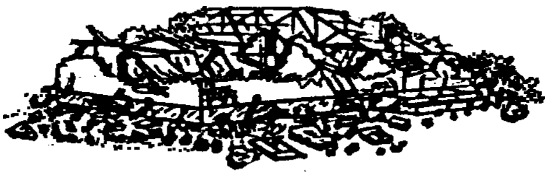

Grade 5: Destruction (very heavy structural damage)
Total or near total collapse.

G-5D

Figure 3.7. Damage classification of masonry buildings [63].

3.2. Softening and Dilatancy

The formation and growth of cracks in masonry materials cause a decrease in elastic modulus alongside inelastic deformation being increased, leaving fewer solid materials per unit of total surface in position to resist an increase in the average stress. A critical stage will be reached sooner or later, beyond which there will be a continuous decline in load in a structural element or an increase in average stress or deformation of a material. The structural element evidently cannot maintain its macroscopically homogenous condition at this post-peak loading stage. And, due to the rising deformation's concentration at the most overstressed or weakest parts, growing inhomogeneity of deformation is indeed emergent. As a result, the material's stress-strain curve softens. Softening is the progressive loss of mechanical resistance that occurs when a material specimen or structure is subjected to a continual increase in deformation. The localization and strain softening phenomenon occurs when the development of deformation concentration on a small volume conforms to strain increase with stress decrease. It is a prominent property of quasi-brittle materials such as concrete, mortar, clay brick, ceramics, rock, and ceramics that collapse owing to a gradual internal crack propagation process [64]. The heterogeneity of the material, which is caused by the existence of multiple phases and material defects such as faults and voids, is usually blamed for such mechanical behaviour. Because of shrinkage during curing and the presence of aggregate, mortar has microcracks even before it is loaded. Due to shrinkage during the burning process, the clay brick has inclusions and microcracks. When a material is exposed to progressive deformation, the cracks, initial stresses, strength and internal stiffness variation promote progressive crack development. The microcracks are initially stable, meaning that they only expand when the stress is raised. Around the time of peak load, crack development accelerates and macrocrack formation begins. Because the macrocracks are unstable, the load must be reduced to prevent uncontrolled development. In a deformation-controlled test, macrocrack development causes softening and cracking to be localised in a small area while the remainder of the specimen unloads. Due to this physical process, Belytschko and Bazant [65] recommend specifying a minimum thickness of the cracking zone to give computational stability as well as a comprehensive characterization of the physical behaviour of masonry materials. The softening behaviour of compressive failure is strongly reliant on the boundary conditions in the experiments as well as the specimen size. Hordijk's work [66] went into great depth into the tensile failure phenomena. In Coulomb friction models, a softening process is exhibited as a decrease of the cohesion for shear failure. Figure 3.8 displays the typical stress-displacement diagrams in the uniaxial state.

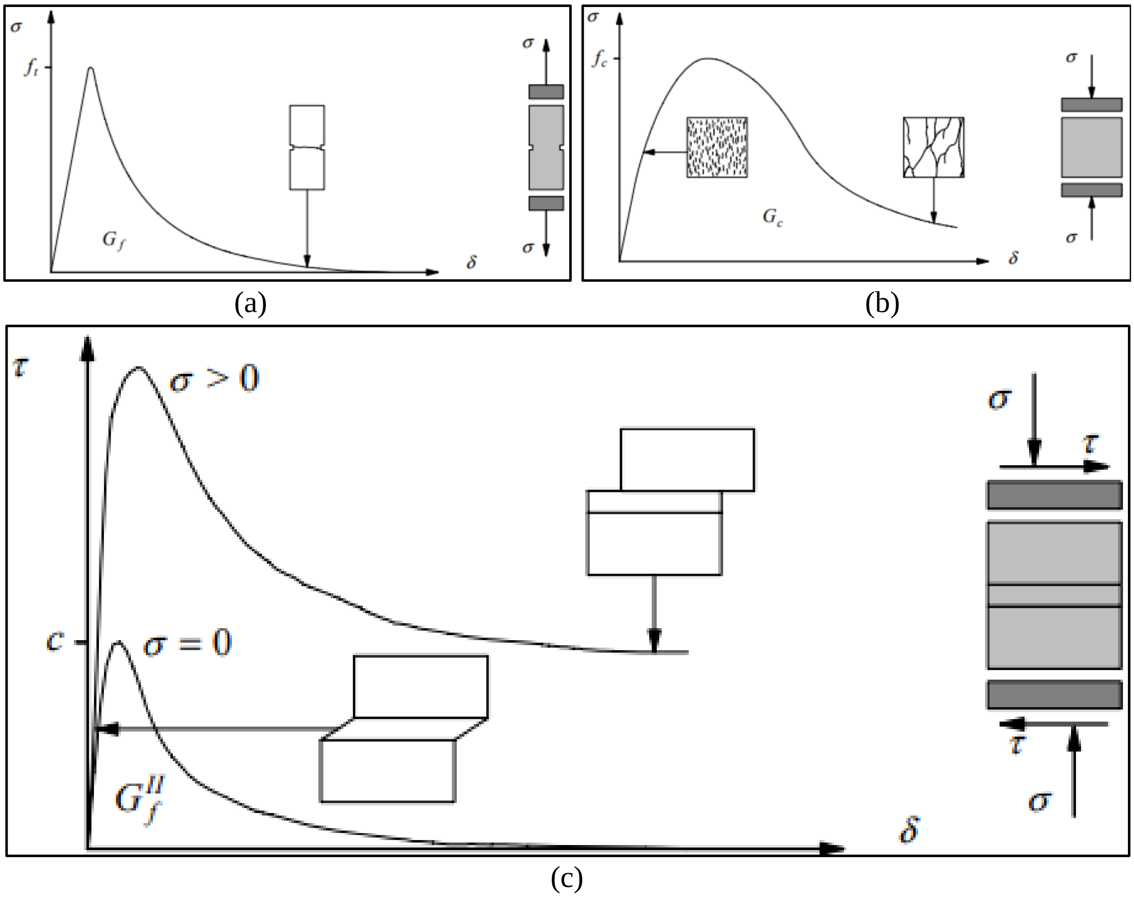

Figure 3.8. Typical stress-displacement diagrams for quasi-brittle materials in uniaxial state (a) Compression state, (b) Tensile state and (c) Shear State [1].

As demonstrated in Figure 3.9a, the dilatancy angle quantifies the elevation of one unit above the other during shearing. Masonry joints have very low dilatancy, and the dilatancy angle varies depending on the intensity of confining force (see Figure 3.9b). The average value of tan for low confining pressures ranges from 0.2 to 0.7, depending on the roughness of the unit surface. Tan approaches zero at high confining pressures. Due to the smoothing of the sheared surfaces as slip increases, tan drops to zero, as shown in Figure 3.9c. The dilatancy angle is crucial when using a micro-model to predict the behaviour of masonry constructions. Masonry crushing, for example, is defined as the breaking of units under tension as a result of mortar dilatancy at high normal stress levels. Hence it is advised that one choose a value of tan equal to zero for practical purposes.

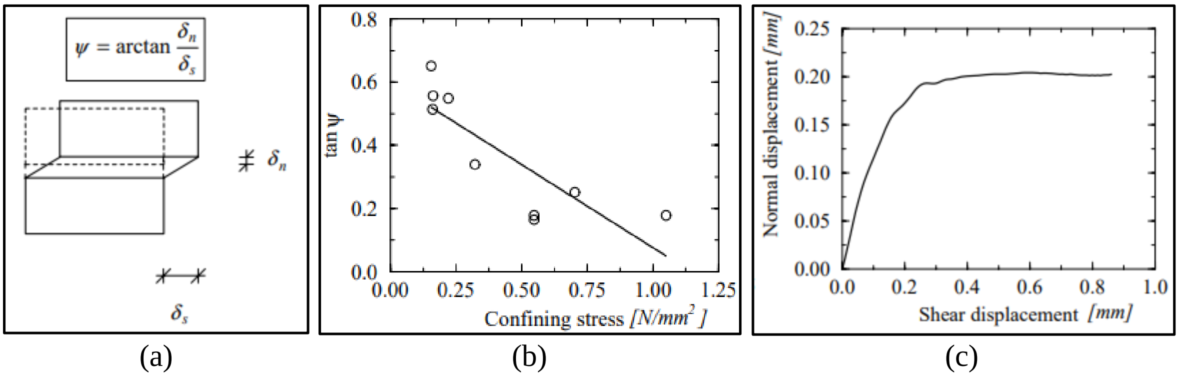

Figure 3.9. Dilatancy angles and typical joint shear bond behaviour for solid clay units; (a)dilatancy angle as a result of adjoining units being uplifted during shearing, (b) dilatancy angle ψ tangent as a function of the normal stress level and (c) The normal and shear displacements relation during loading [1].

3.3. Mortar – Unit Interface Behaviour

The weakest link in masonry construction, particularly in historical masonry, is the unit-mortar contact. The poor connection between the unit and the mortar has a big impact on the overall performance of masonry constructions. One of the most important aspects of masonry behaviour is the nonlinear response of the joints, which is governed by the unit-mortar contact. The absorbency of the units, the water retention capacity of the mortar, the porosity of the mortar, the quantity of binder, and the curing conditions all contribute to the strength of the bonding at the unit-mortar interface. According to Van der Pluijm [67], at the unit-mortar interface, two distinct phenomena occur, one associated with tensile failure (mode I - attributed with stresses acting normal to joints and leading to interface separation) and the other associated with shear failure (mode II - corresponds to a sliding mechanism of the units or shear failure of the mortar joint).

3.3.1. Mode I Failure – Tensile-related Phenomena

Van der Pluijm [67] conducted an experiment that resulted in an exponential decay tension softening curve due to the coalescence of microcracks into a macroscopic crack, see Figure 3.10. Although there is no obvious relationship between bond strength and fracture energy, it has been discovered that increasing bond strength is always related to increased fracture energy. The failure of the interfaces between units and mortar, as well as the bulk failure of mortar, affect the tensile strength. The quality of the mortar, the quality of the bonding between the two materials, and the actual bonding area between the brick and mortar all have a role in the failure mode. The bond area in the inner region of the fractured specimens was less than the cross-sectional area of the specimen. The shrinkage of the mortar and the process of setting the units in the mortar bed have combined to produce this. The shaded area in figure 3.10 which is the area under the stress-displacement curve, corresponds to the mode I fracture energy.

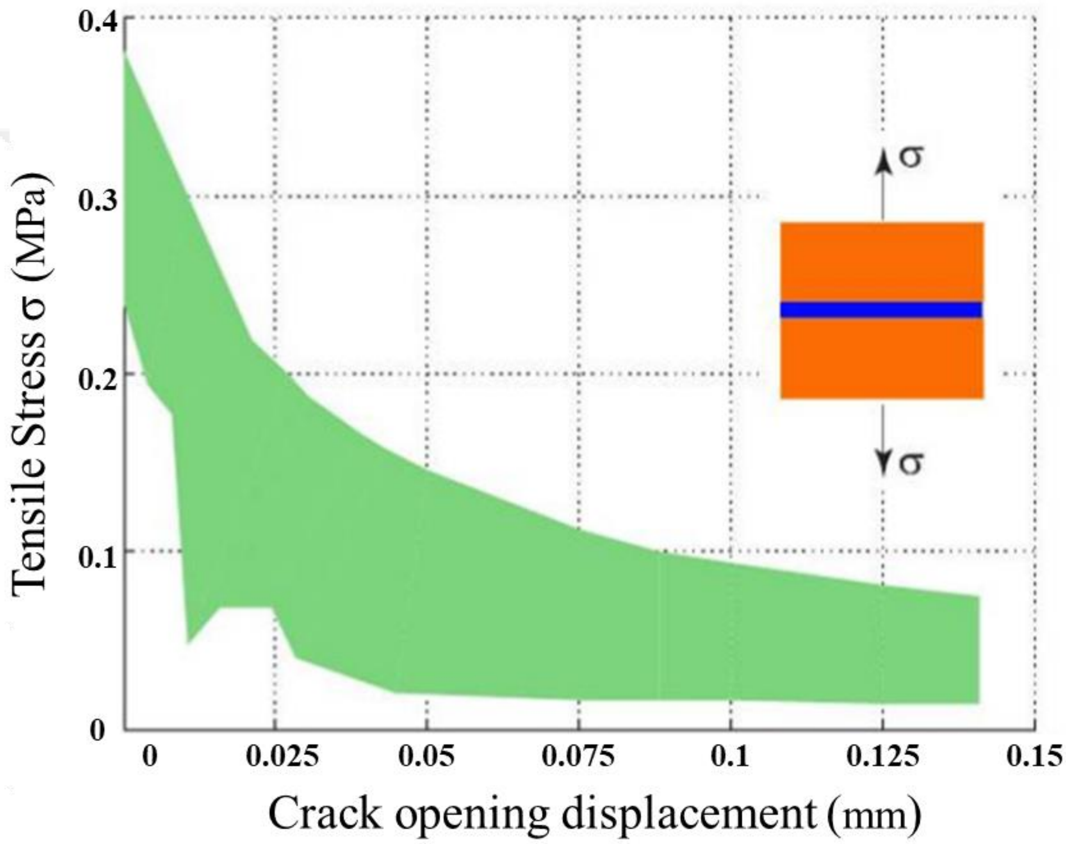

Figure 3.10. Failure Mode I: Stress-crack displacement behaviour at the unit mortar contact [5, 67].

3.3.2. Mode II Failure – Shear-related Phenomena

The shear behaviour of masonry joints is largely determined by the stress of confinement. According to Tammam [5], an increase in compression normal to the bed joint leads to a rise in shear strength has been documented by numerous academics. Shear strength reduces when pre-compression stresses exceed a particular threshold, and a combination of shear-splitting failure or unit splitting can occur. The shear test findings reported by Van der Pluijm [67] were very comparable to the behaviour under tension (Figure 3.11), with the exception that the softening tail does not go back to zero, but rather becomes stable at a specific shear stress level. This level represents the dry friction between two surfaces that do not have any cohesion.

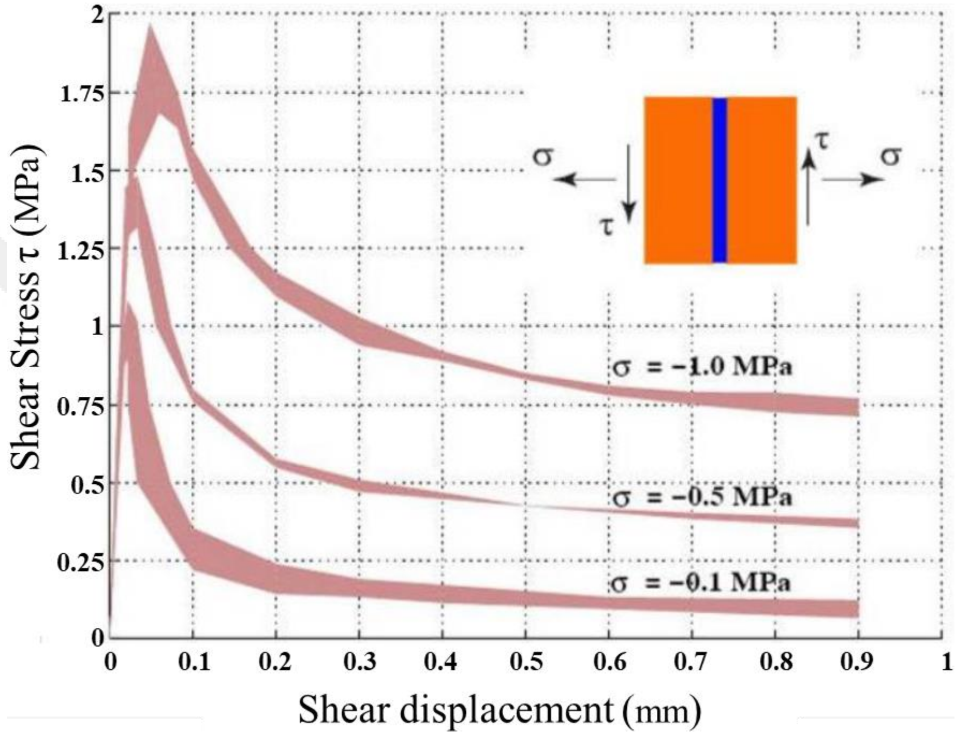

Figure 3.11. Failure mode II: Stress-displacement behaviour for various typical stress levels [5, 67].

3.4. Properties and Failure Behaviour of Masonry

The qualities of masonry's components, as well as the arrangement and interaction of units, have a major role in its failure behaviour. As a result, understanding the mechanical behaviour of individual masonry components, units, and mortar is critical. When investigating the behaviour of masonry components, the first thought is to study the elements separately. However, because the characteristics of mortar are greatly impacted by the interaction between mortar and unit during hardening, this is only achievable for masonry units.

3.4.1. Uniaxial Failure Behaviour of Masonry

According to Vasconcelos [68] in general, a variety of elements impact the mechanical qualities of ancient masonry units formed from natural rocks. The factors include;

- The internal structure of minerals, as well as the degree of anisotropy associated with their organisation and preferred orientation (foliation, flow structures and rift plane)
- Rocks' mechanical characteristics, such as compressive strength and elastic modulus, are highly influenced by physical parameters like porosity and density.
- The weather situation
- Grain size, petrography, and mineralogical properties
- The presence of water has a significant impact on the mechanical behaviour of rocks.

The loss in strength of saturated rocks can be attributed to a chemical or physical modification of their intrinsic qualities on the one hand, and an increase in pore and fissure water pressure on the other. In the case of concrete and other geo-materials, several experimental procedures, primarily compression and tensile tests, are required to characterize the material law of masonry units.

3.4.1.1. Uniaxial Compressive Behaviour of Masonry

In general, masonry unit materials, such as stones and bricks, can withstand compressive loads better than tensile stresses. This is the most important property of geo-materials. Compressive strength tests provide a strong indicator of the materials' overall quality. Many investigations have been carried out to better understand the fracture processes that govern the compressive behaviour of quasi-brittle materials. Coulomb [69] developed his well-known criteria by investigating the fracture of compressed stones. Brittle fracture, according to Griffith [70], is caused by tensile stress concentration at the points of tiny fractures that are randomly dispersed in the isotropic material. All investigations into quasi-brittle fracture should start with the Griffith theory, or at the very least the basic premise from whence the fracture begins. As demonstrated in Figures 3.12 and 3.13, the general behaviour of quasi-brittle materials under compression may be characterized in the following stages:

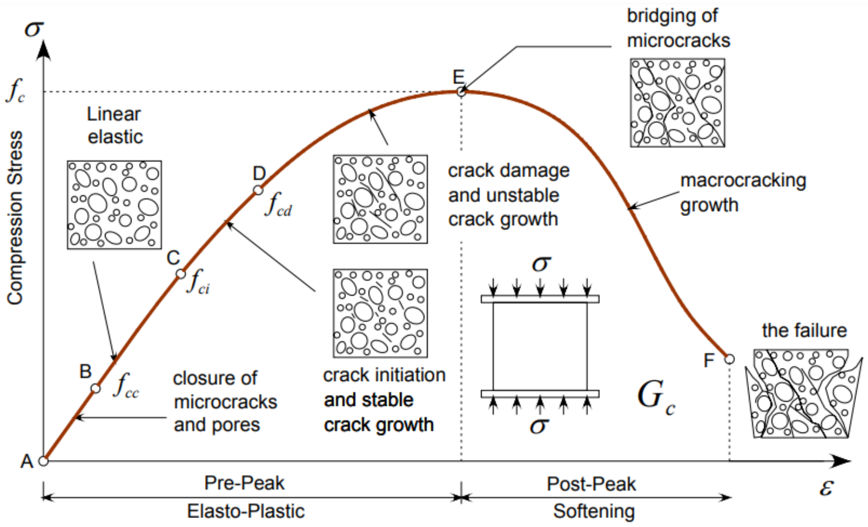

Figure 3.12. Typical behaviour of quasi-brittle materials under uniaxial compression [5].

Phase A – B denotes the closing of existing pores and microcracks. The stress-axial strain curve exhibits nonlinear behaviour during this phase, which is accompanied by an increase in material stiffness.

The linear elastic behaviour follows the closure of pre-existing microcracks: B – C. It has linear elastic behaviour up to a stress level of roughly 30-40% of its conventional strength. Both the axial and lateral stress-strain graphs are linearly connected at this point.

The fracture initiation and steady crack development are the next steps (C to D). This stage begins with microcracking at f_{ci} stress. The nonlinear rise in lateral strain and volumetric strain is caused by the creation and growth of microcracks in the axial direction.

Then there's the crack damage and unpredictably growing cracks (D to E). At the crack damage stress level f_{cd}, unstable microcracking develops. Because the volumetric increase generated by the cracking process is greater than the standard volumetric decrease due to the axial load, it is associated with the point of reversal in the total volumetric strain diagram V_r, which refers to the maximum compaction of the specimen and the beginning of dilation. As a result of the volume increase, a quick and considerable rise in lateral stresses has been seen at this stage. The spread of microcracking is no longer independent. It begins bridging to create fracture surfaces parallel to the maximal primary stresses until the compressive strength reaches its maximum.

The weakening and development of macrocracks will eventually occur (E to F). As strain localization occurs, it causes the material to gradually weaken owing to macrocracking development. Examples of failure patterns that demonstrate strain localization is evident in the compressional failure of Granite specimens. When the peak load is achieved, microcracks are bridged, resulting in macrocracks. The brittleness of the material is shown by the inclination of the stress-strain curve at this point. At this point, macrocracks become unstable, and compression crushing occurs at a constant amount of tension.

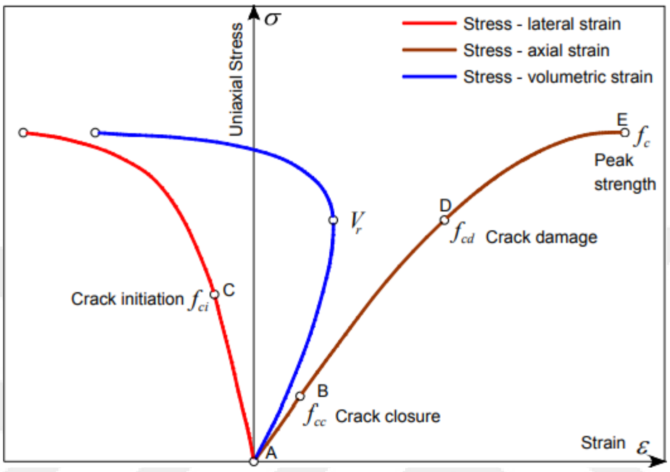

Figure 3.13. A typical stress-strain diagram showing the facture process under compression up to peak load [5, 71].

3.4.1.2. Uniaxial Tensile Behaviour of Masonry

Tensile failure of quasi-brittle materials used to make masonry units leads to the localisation and micro-crack proliferation. The cohesive fracture model presented by Hillerborg et al. [72] accurately describes the tensile behaviour of such materials. It incorporates the tension softening process zone via a fictional crack ahead of the preexisting fracture. There are two zones in the Hillerborg crack: a true crack where no more stresses are communicated and a damaged zone expanded in the fracture process zone where stresses are still transferred. Tensile behaviour is defined by two constitutive laws connected with distinct stages of the material throughout the loading process according to the cohesive crack model as shown in Figure 3.14.

The Pre-peak stage is defined by an elaso-plastic stress relationship that is valid until the peak load is reached. The nonlinearity before the peak is caused by the micro-cracking process. The tiny cracks are stable and only expand as the load increases.

The Post-peak stage is defined by softening behaviour in the fracture process zone (C to F). In this stage, the tension progressively decreases from its highest value to near zero. This refers to extending the distance between the crack's two lips to the critical value of opening w_c, indicating failure. The acceleration of fracture development near the peak load is the cause of such behaviour. The tiny fractures begin to bridge, resulting in obvious macro fissures. The macro fractures are unstable, which means that the load must be reduced to prevent uncontrolled expansion. The extended tail of the softening stage is caused by the stress-transfer process due to the bridging effect. The softening diagram represents the stress displacement relationship that defines this stage. The softening diagram, which is defined by the tensile strength t_f and the fracture energy I_{Gf}, which is represented by the area under the softening diagram, play an important role in the description of the fracture process.

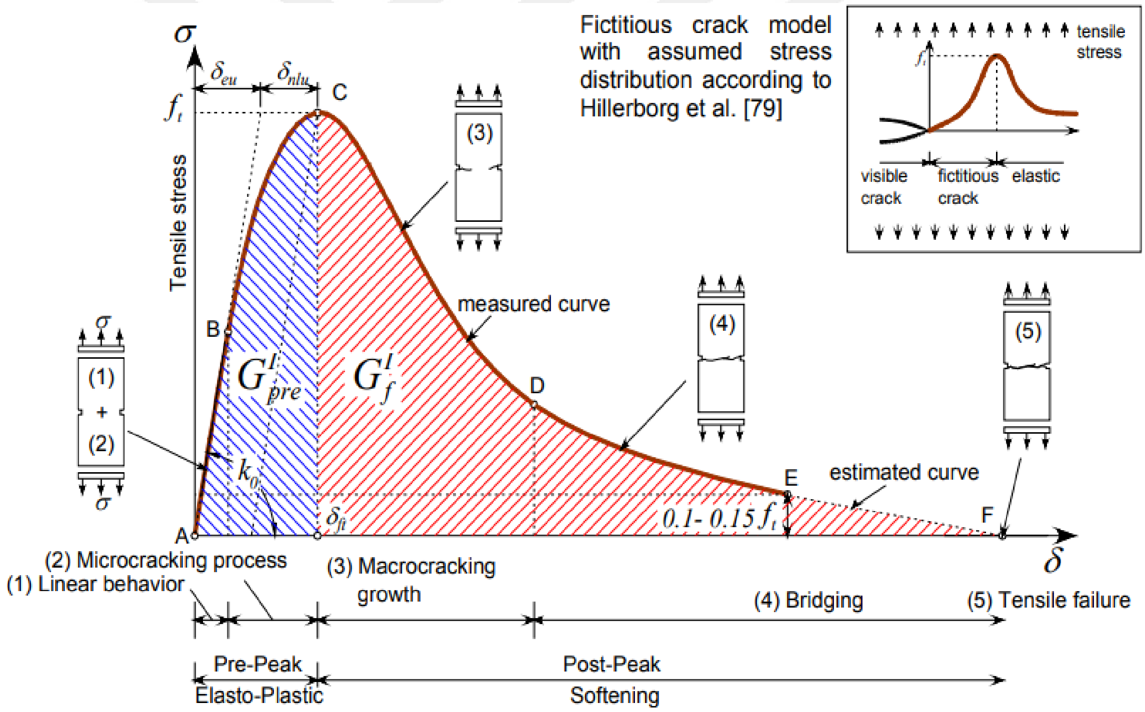

Figure 3.14. Typical behaviour of quasi-brittle materials under uniaxial tension [5].

3.4.2. Biaxial Failure Behaviour of Masonry

The constitutive behaviour of masonry under biaxial loads cannot be fully characterised by the constitutive behaviour under uniaxial loading circumstances. Because masonry is an anisotropic material, the effect of the biaxial stress state has been examined up to peak stress to offer a biaxial strength envelope that cannot be characterised merely in terms of primary stresses. As a result, the masonry biaxial strength envelope must be characterised either in terms of the entire stress vector in a given set of material axes or in terms of primary stresses and the rotation angle between the principal stresses and the material axes. Figure 3.15 depicts the most comprehensive collection of experimental data for brickwork exposed to proportionate biaxial force. The experiments were carried out by Page [73]. The experiments were conducted using half-scale solid clay components. The direction of the primary stresses with respect to the material axes, as well as the principal stress ratio, have a significant impact on the failure mode and strength. Figure 3.16 also depicts the many forms of failure.

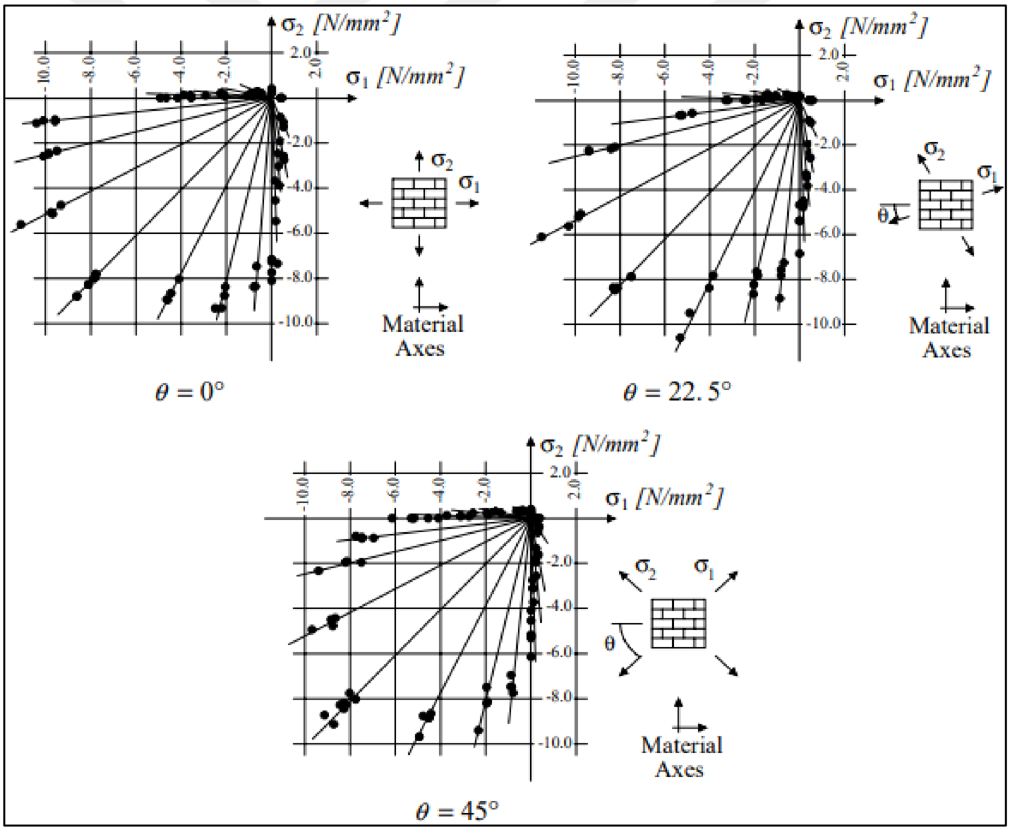

Figure 3.15. Biaxial strength of solid clay units' masonry [1, 73].

Cracking and sliding of the head and bed joints caused failure in uniaxial stress. Because no experimental findings are available, the impact of lateral tensile stress on tensile strength is unknown. The tensile strength is reduced by lateral compressive stress, which may be explained by the damage caused to the composite material by micro-slip of the joints and microcracking of the units. A failure occurred in compression-tension loading scenarios either by cracking and sliding of the joints alone or by a combination process involving both units and joints. Similar forms of failure occurred in uniaxial compression, however, in biaxial compression, a seamless transition to another type of failure mode was discovered. Regardless of the direction of the major loads, biaxial compression failure often occurred by splitting the specimen at mid-thickness in a plane parallel to its free surface. For principal stress ratios that are less than and greater than 1, orientation was important, and failure occurred through a composite mechanism combining joint failure and lateral splitting. Friction in the joints and internal friction in the units and mortar can explain the increase in compressive strength during biaxial compression.

According to Nelissen [74], the failure envelope of concrete appears to be substantially independent of the loading route. This indicates the presence of a single failure mechanism, namely continual microcrack development. As a result, there is some concern about the validity of Page's [73] masonry failure envelope for nonproportional loads. Especially given the possibility of multiple failure modes being triggered. Another topic to consider is the scarcity of experimental data on the softening of masonry under biaxial loading, even though the softening of masonry is undoubtedly impacted by the biaxial stress condition. It should also be noted that the strength envelope depicted in Figure 3.15 has limited relevance for various forms of brickwork. Distinct materials, unit forms, and geometry are likely to have different strength envelopes and failure mechanisms. Dhanasekar et al in their work – The Failure Of Brick Masonry Under Biaxial Stresses [75] investigated the failure modes of a solid clay unit's masonry under biaxial loading at varying angles, see Figure 3.16.

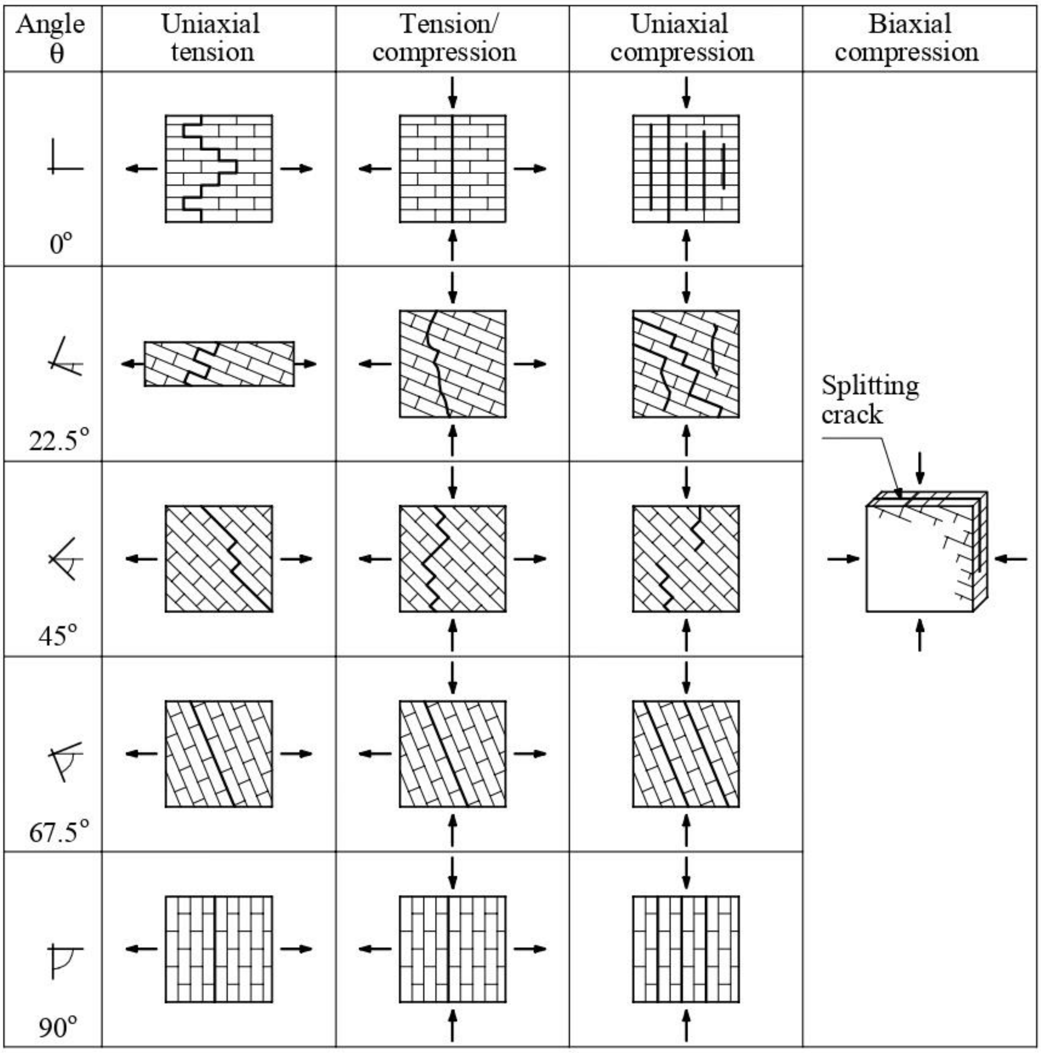

Figure 3.16. Modes of failure of solid clay units masonry under biaxial loading [1, 75].

3.4.3. Triaxial Failure Behaviour of Masonry

While uniaxial tests are the most fundamental tests for determining damage behaviour and strength of the material, they fall short when a general material failure model is required, which is especially true for geo-materials such as masonry elements. Consequently, to define the failure behaviour of such materials the standard triaxial laboratory tests are utilised.

Triaxial tests are performed on a cylinder sample with axial stress σ_1 and lateral stress σ_3. The triaxial testing can provide the failure curve that defines the relationship between hydrostatic pressure $P = (\sigma_1 + 2\sigma_3)/3$ and von Mieses stress $\sqrt{3J'_2} = \sigma_1 - \sigma_3$. This curve is the most significant piece of information for characterising the material failure behaviour of various geomaterials. When hydrostatic compression is used, another crucial relationship,

$\sigma_1 = \sigma_3 = \sigma$, may be found from triaxial testing. The nonlinear relationship between volumetric strain and hydrostatic pressure is described by this curve. According to Schwer [76], the following stages characterise this relationship for typical geomaterials as presented in Figure 3.17.

- In the first phase (p0 < p < p1) the slope matches the bulk modulus K and the material remains elastic.
- The second phase is as follows: (p1 < p < p2) the material's pores are compressed
- The third phase is as follows: (p2 < p) There exists no more pores and the material is entirely crushed.
- The fourth phase is pressure removal.

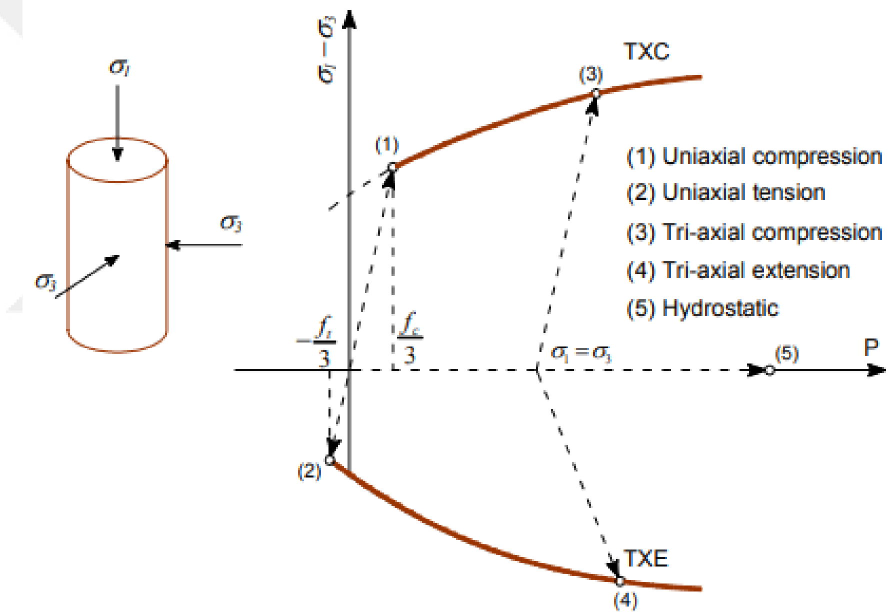

Figure 3.17. The relation between von Mises stress and the hydrostatic pressure obtained from the triaxial tests [5].

3.5. Masonry as a Composite Failure

In order to understand the composite behaviour of masonry, all plausible failure mechanisms of the mortar and units must be examined. Many research efforts have been made to develop masonry failure theories based on the fundamental features of the component materials. The failure of masonry is governed by the strength and interaction of the masonry components, as well as their varying deformation properties. Based on diverse assumptions, several scholars have created failure theory. Among the assumptions are (but are not limited to);

- Failure theory is based on elastic analysis and takes into account the interaction of masonry components.
- Based on a nonuniformity factor compounded by an assumed linear connection between local compressive stress and lateral biaxial tensile strength.
- Based on a unit's equilibrium and strength concerns within a wall
- Based on the balance and strength concerns of a unit within a wall, but incorporates the stresses occurring on the head joints
- The equations that characterise the masonry surface failure but were lacking the influence of unit dimensions.

Figure 3.18 shows the commonly observed basic masonry failure mechanisms in various experiments.

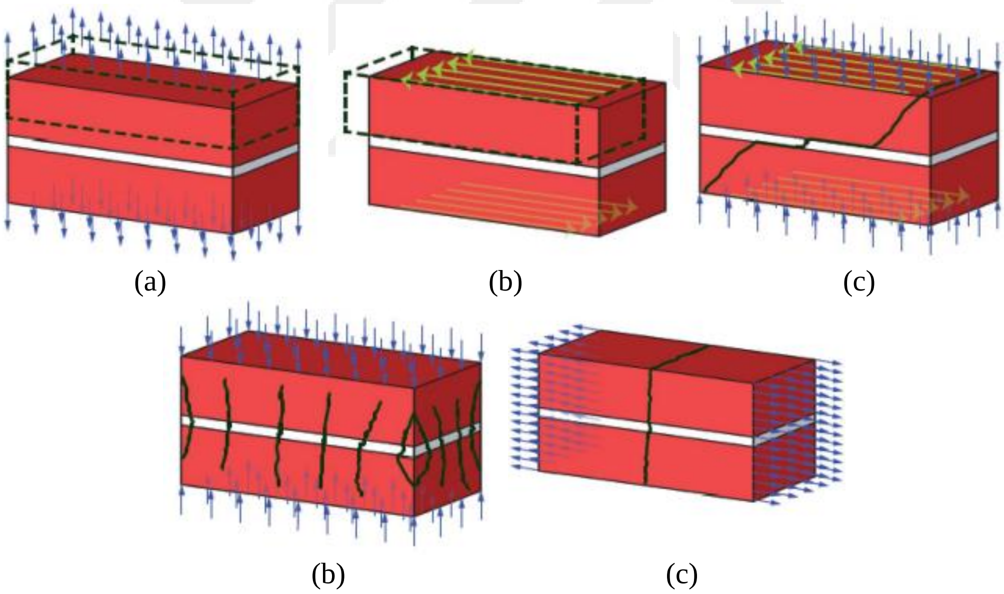

Figure 3.18. Commonly observed basic masonry failure mechanisms; (a) block-mortar bond tensile failure, (b) block-mortar bond shear sliding, (c) diagonal masonry cracking, (d) masonry crushing and (e) block and mortar tensile cracking

4. EXPERIMENTAL CAMPAIGN

The demand for enhanced and more controllable experiments to enable research on the performance of the structure under EQ action is constantly growing. Even with testing methodologies and computer modelling, experimental research on full-size brick buildings remains difficult. Dynamic testing techniques nowadays range from actual dynamic loading tests to faux dynamic tests in real-time or expanded time. When the structure is loaded by random EQ action, the complexity increases. Due to technical issues and expensive expenses, it is not always possible to conduct experimental tests that accurately reflect the actual behaviour of a physical problem in the real world. In the event of an EQ, the execution of the experiment under strong motion will most probably destroy the equipment, rendering the measurement operation useless. Moreover, the cost of constructing a large number of full-scale structures to be evaluated under various loading circumstances is exorbitant and impractical. In an attempt to circumvent the aforementioned difficulty, the model is usually scaled down to a laboratory-size model and the same model is frequently utilized under various loading conditions, resulting in severe structural damage at the last phase of loading. Within the scope of this research, a variety of experimental trials were conducted to evaluate the performance of a half-scaled masonry construction subjected to seismic action.

4.1. Model Description and Construction

The half-scaled masonry model was constructed using a perforated engineering brick. The length, width and height of the brick correspond to 102mm, 215mm and 65mm respectively. Figure 4.1 presents the geometrical details and views of the masonry model and units. The percentage ratio of hollow to solid for brick is approximately 23% which is in compliance with the Turkish Building Earthquake Code [77]. The stretcher bond method with toothing texture was employed for the construction. The mortar thickness is approximately 7.5mm and the mortar mix ratio is 1 to 3 (cement: sand). The masonry is approximately 1800mm square and 1600mm tall. The masonry is equipped with openings on the north and south side with an RC support over the openings. The door (south side) measures 100mm in height and 45 mm in length. It is 65 mm above the notch level, directly from the first brick level. The window (north side) measures 55mm in height and 45 mm in length. The supports over the openings are 650mm long and 75mm tall and are reinforced with an 8mm steel bar. An 1800mm RC square slab was used as the overhead surface. It is 25-grade concrete 100mm thick and reinforced with 8mm steel in both directions. The masonry was constructed on an RC square base. The base is 35-grade concrete with a 14mm rebar at the compression and tension side. The base measures 2100mm square and 200mm high. Bricks at the bottom of a building are tempted to slide, shear or even bounce away from the base. To prevent such occurrence the base was equipped with a 100mm wide and 30mm deep notch that serves as a place-in for the masonry. Figure 4.2 presents the pre and post-construction images. The base is also equipped with 16-24mm (approximately) vertical holes. The holes permit the fixation of the RC base to the ST. To ensure a perfectly fixed model, the model was further guided with two angle plates of steel each on both East & west side of the model, see figure 4.3. The complete model was placed on the ST using a flat polyester lifting sling and a single girder overhead crane. The flat polyester lifting sling was attached to the base of the model using a lifting hook. The other end of the lifting sling was attached to the single girder overhead crane.

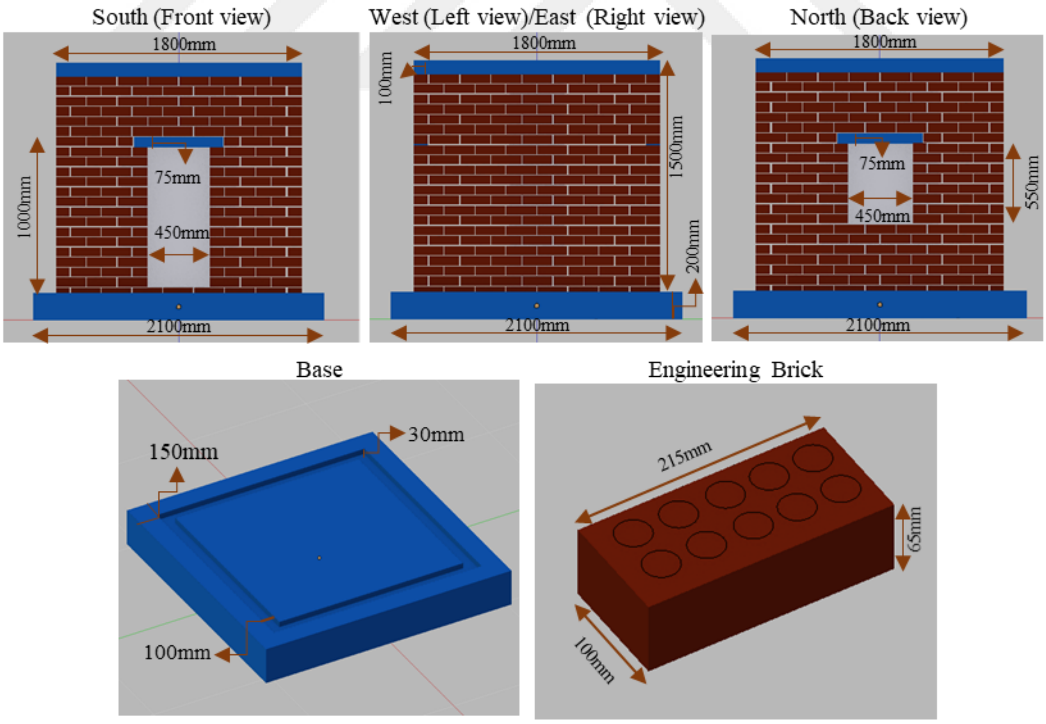

Figure 4.1. The geometry details and views of the masonry model and units

Figure 4.2. The pre-and post-construction photos

Figure 4.3. Steel angle installation

4.2. Instrumentation, Tests Description and Ground Motion Data Imputation

4.2.1. Instrumentation

Linear variable differential transformer (LVDT) and Accelerometers (Uniaxial and Triaxial) were used to collect data regarding the local and global behaviour of the model during the experimental campaign. A total of four LVDTs were used to monitor the displacement of the models. All are placed on the east side of the masonry which corresponds with the direction of movement. One LVDT is placed in the middle of the RC base, another one in the middle of the masonry and the last two were placed at the opposite edges of the slab. Placement of the LVDTs at different locations and heights allows the observation of data such as nodal displacement, relative displacement and drift ratios of the model. A total of 10 accelerometers (three uniaxial accelerometers and seven triaxial accelerometers in specific) were used. A biaxial accelerometer was also mounted to the ST (fixed platform). It was used as a reference point for comparing the applied and observed seismic excitations. Jumps and phase changes in accelerometer data connote the start point for softening and formation of cracks. The uniaxial accelerometers were used to measure only out-of-plane response at the east and west side of the masonry. Whilst the triaxial accelerometers were used to measure both in and out-of-plane responses the masonry model at different elevations.

Figure 4.4. Accelerometer and LVDTs positioning and arrangement

4.2.2. Shaking Table Description

ST is an experimental platform for verifying the seismic performance of building structures by simulating EQ motion. The ST works by imposing dynamic movement on the ST's actuators. The dynamic movement data are created by the computer in real-time. The influence of actual seismic acceleration records on the model’s performance could be replicated. These tests can identify the internal stresses and deformations induced by genuine earthquakes on building systems or building parts as closely as possible. Also, issues regarding structural assembly and inertial effects may be clearly shown and assessed. The size of the tested model is restricted by the ST's capacities such as dimension and weight limit. Hence the model's size is often reduced to fit the available capacity, or the test can be done on only a portion of the structure. The constructed half-scaled masonry model was tested within the scope of this research using the 35-ton payload capacity uniaxial ST facility at the Department of Civil Engineering, Karadeniz Technical University, Trabzon. The test was carried out on the 2nd day of September 2021.

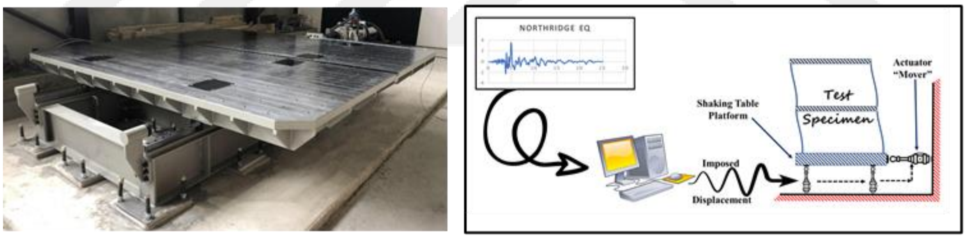

(a) (b)

Figure 4.5. Shaking table Description; (a) front view of a typical uniaxial shaking table and (b) the working mechanism.

4.2.3. Ground Motion Data Imputation

The acceleration components of EQ data and sine wave functions were used as the ground motion data. The data were subsequently used to impose dynamic movement on the actuator of the ST. The peak ground accelerations (PGA) were used in this technique. The accelerations were incremental in such a way that permits observation of various damage conditions. Within the scope of this research, the ground motion data (GMD) consists of a total of 6 seismic excitations (3 EQ data and 3 sine wave functions). The ground motions are Northridge, Coyote Lake, Parkfield, 4-Cycles Sine Wave, 6-Cycles Sine Wave, and 10-

Cycles Sine Wave. Detailed data on the GMDs are presented in Table 4.1. The EQ data were acquired from the website of the Pacific Earthquake Engineering Research Centre Database [78].

Table 4.1. Earthquake Details (*Based on Modified Mercalli Intensity Scale)

ID	Name	City	Year	Station	PGA	Magnitude	Intensity *
GMD-1	Northridge	Los Angeles	1994	W Pico Canyon Rd	0.35	6.7	IX (Violent)
GMD-2	Coyote Lake	California	1979	Gilroy Array #6	0.42	5.7	VII (Very strong)
GMD-3	Parkfield	California	2004	Parkfield - Fault Zone 1	0.6	6	VII (Very strong)
GMD-4	4-Cycles Sine Wave	-	-	-	0.8	-	-
GMD-5	6-Cycles Sine Wave	-	-	-	0.8	-	-
GMD-6	10-Cycles Sine Wave	-	-	-	0.8	-	-

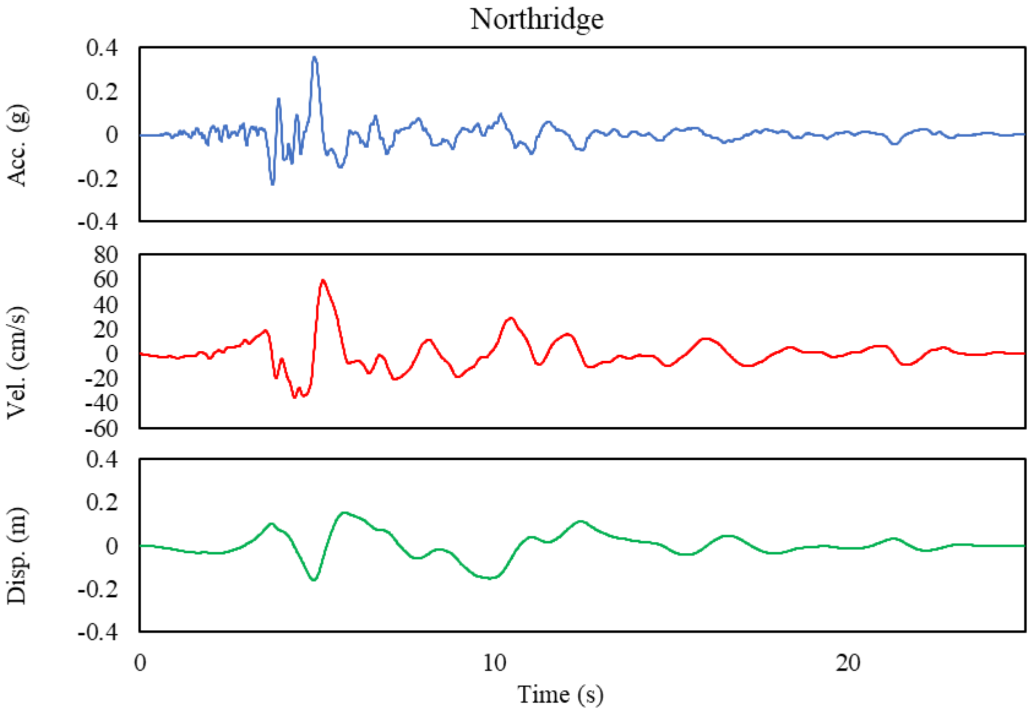

Figure 4.6. Northridge EQ record

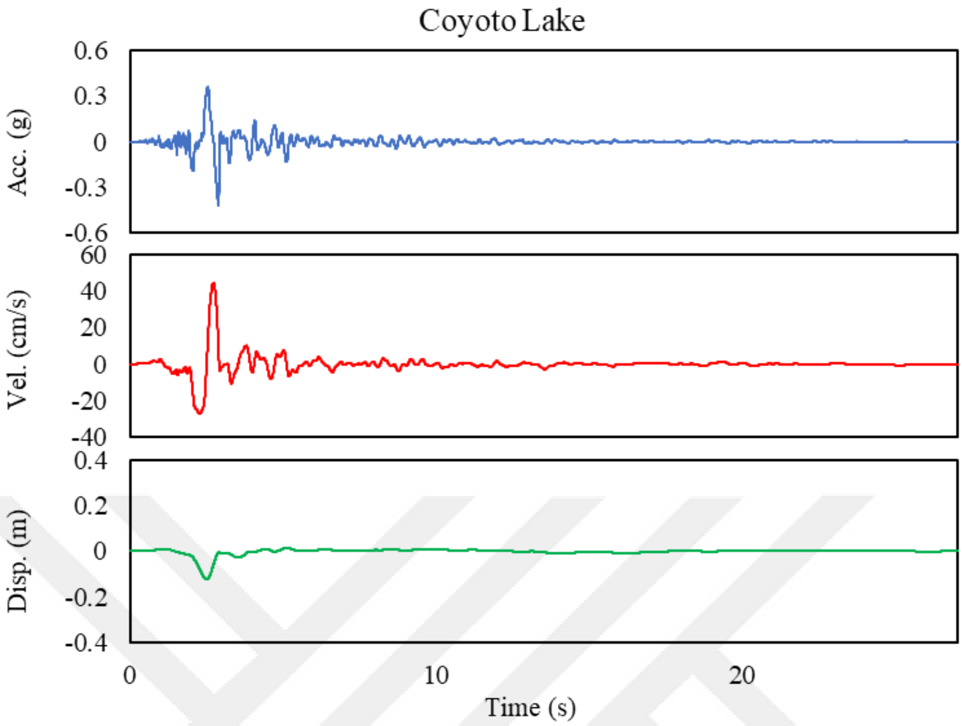

Figure 4.7. Coyote Lake EQ record

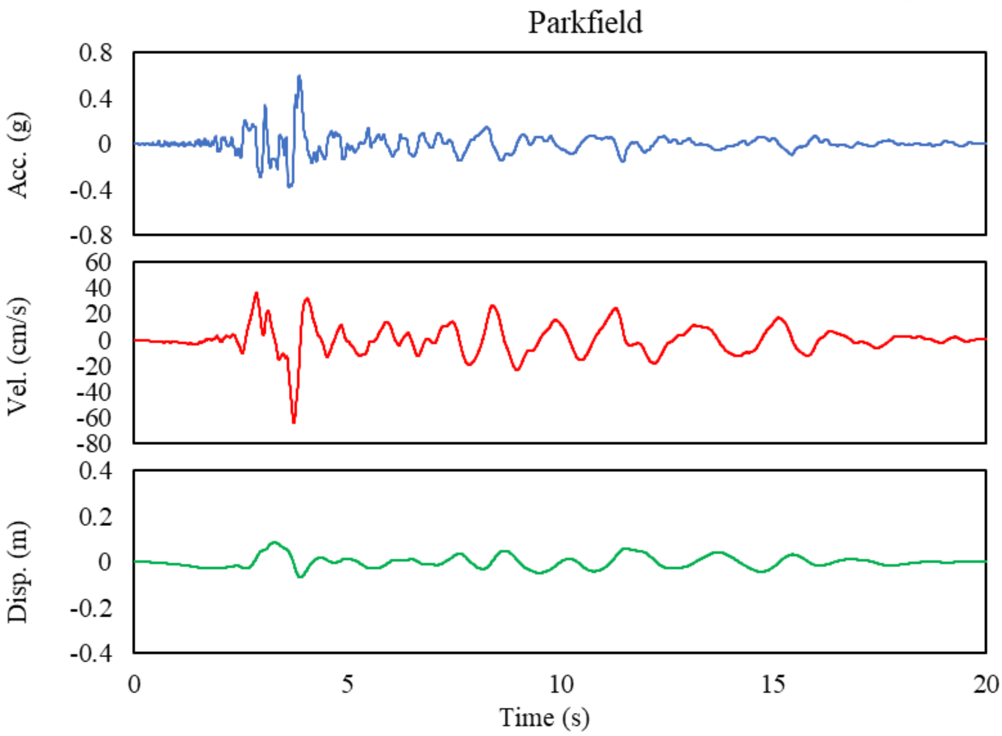

Figure 4.8. Parkfield EQ record

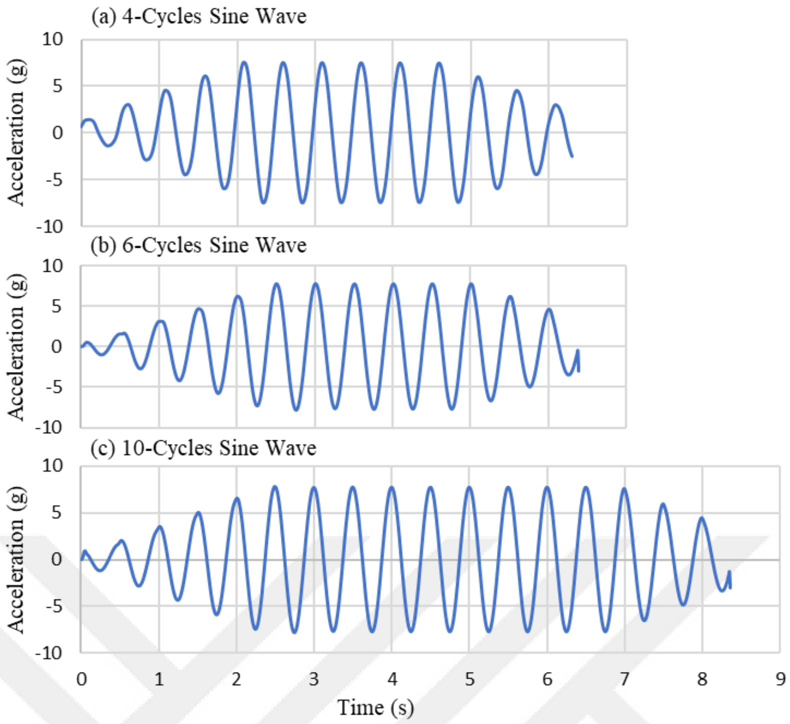

Figure 4.9. Sine Waves; (a) 4-Cycles, (b) 6-Cycles and (c) 10-Cycles.

4.3. Testing Methodology

The tests were conducted in a sequential and consecutive manner. The tests were carried out by applying EQs on the model along the in-plane direction (X- direction). The base acceleration was gradually raised starting from 0.35g to 0.60g and then sine functions until the model collapsed. Table 4.2. presents the sequence of the experiment.

Table 4.2. - Sequence of the experiment

ID	Test	Utilized Data
1_EQ1	ST Test	Northridge
2_EQ2	ST Test	Coyote Lake
3_EQ3	ST Test	Parkfield
4_EQ4	ST Test	4-Cycles Sine Wave
5_EQ5	ST Test	6-Cycles Sine Wave
6_EQ6	ST Test	10-Cycles Sine Wave
7_EQ7	ST Test	10-Cycles Sine Wave

4.4. Post-Test Visual Damage Assessments

Visual investigation of the model was carried out in the sequel to every dynamic movement imposed on the ST. The development and propagation of cracks were carefully observed and noted. This aid in the evaluation of damage progression. Ambient vibration measurements before and after each ST TEST established the modal parameters for the initial and current damage status of the model. These parameters were compared to evaluate the damage experimentally. The damage categorization specified in EMS-98 (discussed in section 3.1.4.) was used to provide a qualitative description of the damage found in the test model. The visual observation as viewed externally is presented in Figure 4.10. Existing cracks from the previous testing are shown by black markings, whereas cracks found during testing are represented by blue. There were no obvious cracks in the first two (2_EQ1 and 4_EQ2) ST tests. The first micro-crack in the masonry was observed after the application of GMD-3 EQ. It was not fully built and located in close proximity to the slab on the southern side of the model with no noticeable cracks on the other sides. As a result, the structural damage was classified as G-1D at this point.

The subsequent ST tests (8_EQ4 and 10_EQ5) revealed that existing micro-cracks had significantly expanded and many new ones had developed on all external sides. A huge percentage of the cracks were almost horizontal at this point. They were caused by sliding motion at the first two layers of brick slightly below the slab. Previous experimental research conducted by Chellappa and Dubey [79] on unreinforced masonry buildings found similar crack propagation as presented in Table 4.3. A diagonal crack (staircase-shaped shear failure described by Ganz [80]) which is attributed to in-plane deformation was also observed on the southern side of the masonry. The diagonal cracks were formed along the mortar bed joints. It stretched from the right top corner of the opening towards the right edge of the slab. The width of diagonal and nearly horizontal cracks was less than 1mm. Additional the observed damages were mild consequently the structural damage was classed as G-2D type. The last but one ST test (12_EQ6) results in the further expansion of the already existing cracks. Shear-sliding cracks were also discovered at the first two layers of brick, slightly above the foundation level and around the support over openings. As of the conclusion of the test, the residual widths of existing diagonal cracks and near-horizontal had not considerably expanded at the end of the shaking test. Conversely, the videos recorded during the ST test revealed otherwise. It was observed that the breadth of the shear-stepped diagonal fracture at the top corner of the door had significantly increased. The crack widths were discovered to be in the centimetre range. As a result, the structural damage was classified as G-4D type. Afterwards, the measuring systems (accelerometers and LVDTs) were removed from the test setup for security reasons. The damage pattern of the G-4D model as seen from the exterior is shown in Figure 4.11. In the last ST test (14_EQ7), a 10-cycles sine function wave was reapplied to the G-4D model. This resulted in the complete collapse of the masonry model. The structural damage classification at this stage is obviously G-5D type. The failure was triggered by the out-of-plane deformations in the eastern side of the masonry. The out-of-plane deformations were perpendicular to the direction of seismic excitations. As a result, the model's static stability diminished. The width of the staircase-shaped diagonal crack at the right top corner of the door also widened, and the masonry model eventually collapsed.

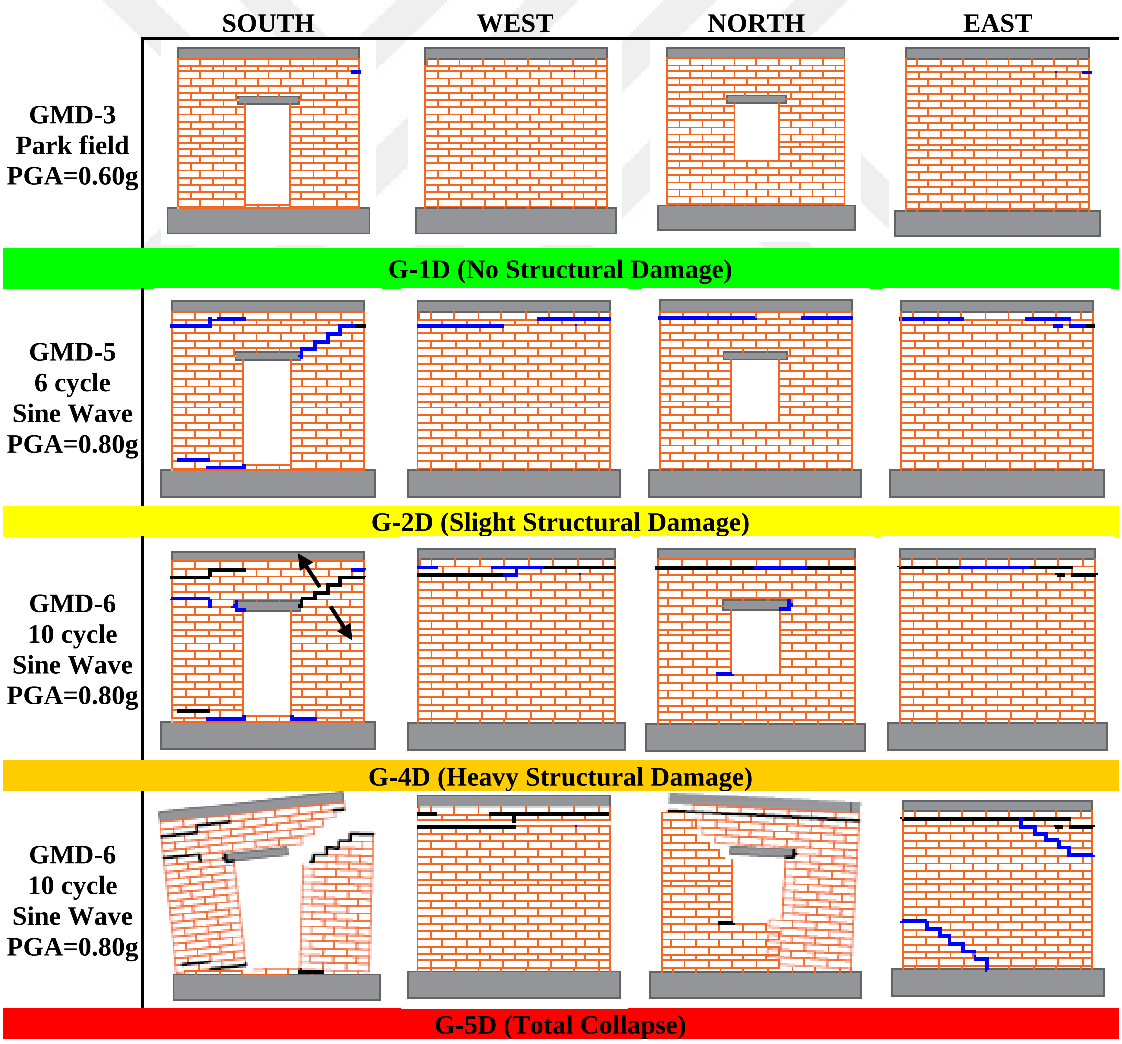

Figure 4.10. The pattern of cumulative damage on the model's external surface

Table 4.3. Similarities between current research and the test conducted by Chellappa and Dubey *[79]*.

Current Research	Test conducted by Chellappa and Dubey
	
	
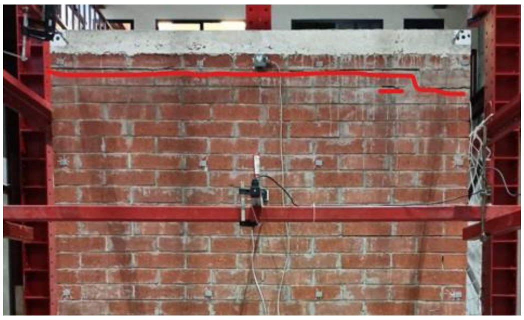	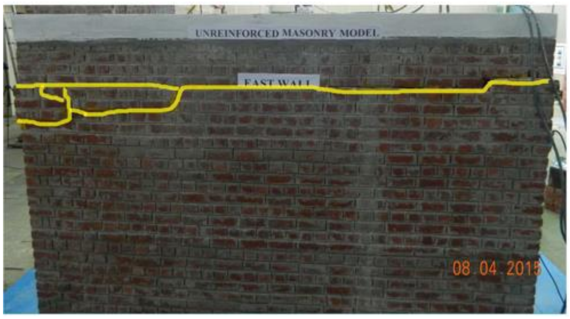

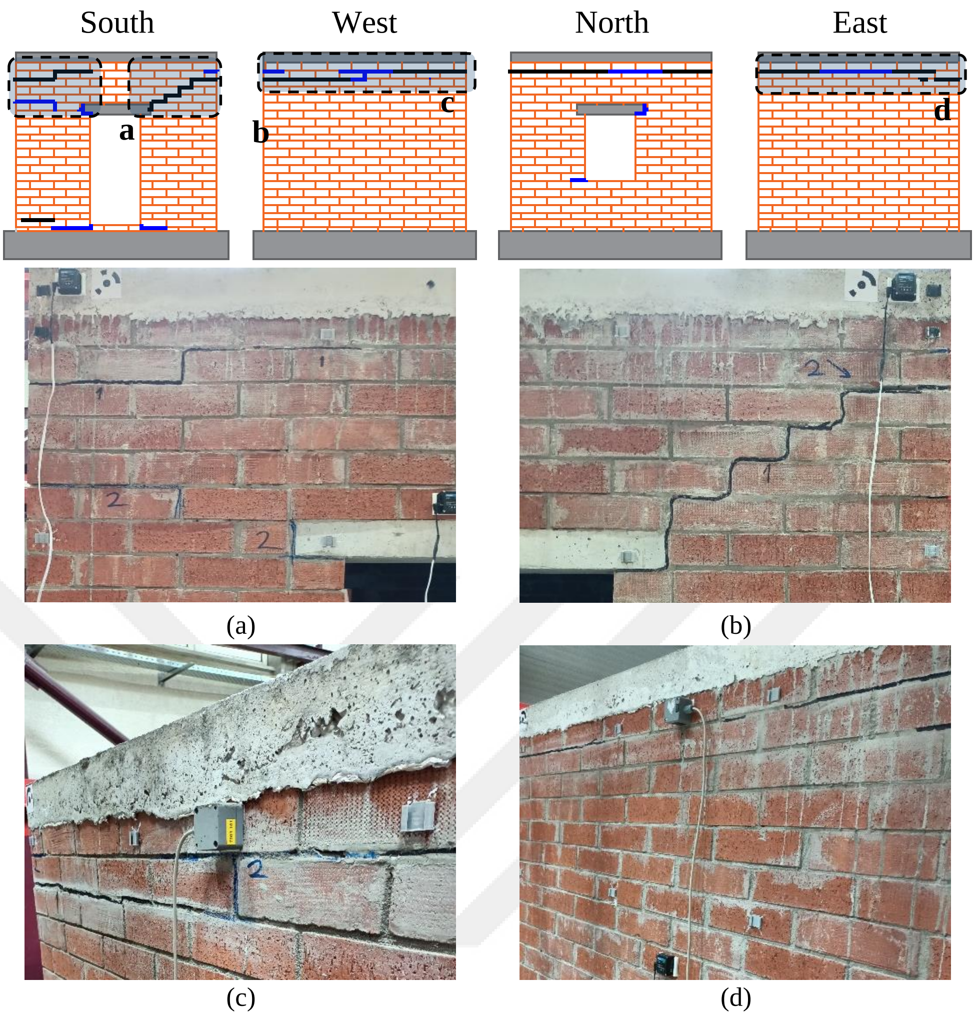

Figure 4.11. The pattern of damage on the model's external surface for the G-4D type; (a, b) shear-sliding and shear-stepped diagonal cracks and (c, d) near-horizontal sliding cracks at the tops of eastern and western walls.

4.5. Shaking Table Test Results and Evaluation

In this part, experimental structural responses are given by processing the measurement system outputs. Seven triaxial and three uniaxial accelerometers were employed for the ST tests. In addition, four LVDTs were mounted to record the shifting displacement response along the height of the masonry model. The relative displacements, Interstory Drift Ratios (IDRs), and absolute accelerations for each seismic stimulation were compared using the experimental results. The relation between observed damage and structural reactions was also explored.

4.5.1. Relative Displacements

Figure 4.12. represents the variations in maximum relative displacements caused by each seismic shock. The relative displacements measured at the test specimen's roof and mid-height were compared for this purpose. Figure 4.12. shows that relative displacements increase as PGAs increase, with the exception of the GMD-2 Coyote Lake Earthquake (PGA=0.42g) and the GMD-3 Parkfield Earthquake (PGA=0.60g). On the other hand, because the northern and southern walls had differing opening ratios, there were substantial disparities in the relative displacements collected at the roof corners. The differences were estimated as follows: 56.88 % for the GMD-3 Parkfield Earthquake (PGA=0.60g), 73.97 % for the GMD-5 six-cycle Sine Wave (PGA=0.80g), and 79.37 % for the GMD-6 ten-cycle Sine Wave (PGA=0.80g). The opening areas for the northern and southern walls were $0.45m^2$ and $0.25m^2$ respectively. This had an effect on the walls' in-plane rigidity. It was therefore concluded that torsion exists at the roof level during the ST test. Figure 4.13. depicts the time history of relative displacements recorded from roof corners during the ST test when damage conditions of G-1D and G-4D types were observed. Torsion reactions were considerably activated as the breadth of the shear-stepped diagonal fracture in the southern wall increased.

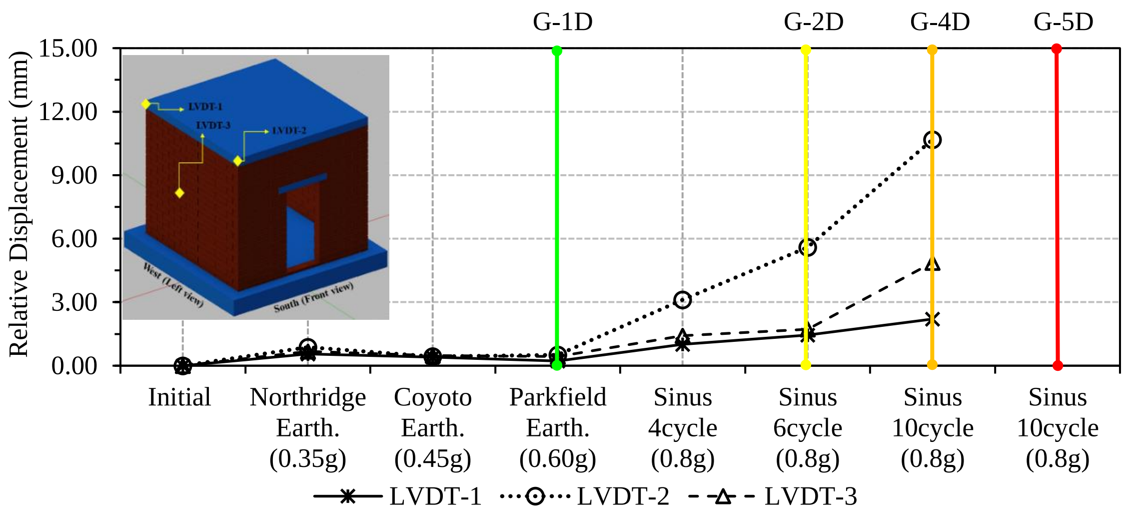

Figure 4.12. Variation in the maximum relative displacements observed during the ST tests

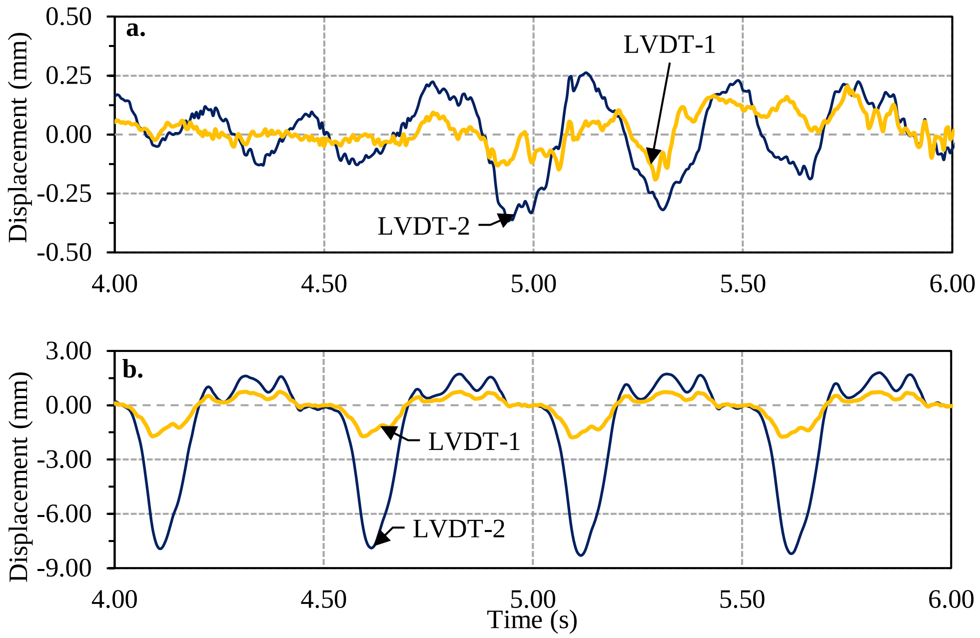

Figure 4.13. The time history of relative displacements derived from eastern roof corners; (a) GMD-3 and (b) GMD-6.

4.5.2. Interstory Drift Ratios

Figure 4.14. depicts the fluctuation of IDRs determined employing maximum relative displacements following ST tests. Calvi in his work – “A Displacement-Based Approach for Vulnerability Evaluation of Classes of Buildings” [81] recommended drift limitations for masonry buildings based on deterioration states. Calvi’s postulation is founded on clay bricks masonry and subassemblies. As a result, its application to other masonry materials is irrational, albeit being a reasonable initial trial attempt. The masonry constructions' threshold drift ratios were established as less than 0.1% for G-1D, 0.1% for G-2D, 0.1 -0.3 % for G-3D, 0.3 percent -0.5 % for G-4D, and higher than 0.5 percent for G-5D.

The greatest IDR observed in the model was 0.05% during the ST test conducted under GMD-3 Parkfield Earthquake (PGA=0.60g), in which the damages were classed as G-1D type. Maximum IDRs were determined as 0.35% and 0.68% for seismic excitations creating damage conditions of G-2D and G-4D kinds, respectively, see Figure 4.14. These values were only partially consistent with the suggested threshold values. One explanation for this condition might be that the link between engineering parameters (displacement, IDR, etc.) and damage in ST testing cannot be continually monitored. According to Graziotti et al. [82]

and Tomassetti et al. [83], this condition permits merely a sequence of deformations to be associated with a given damage state, rather than a precise threshold value.

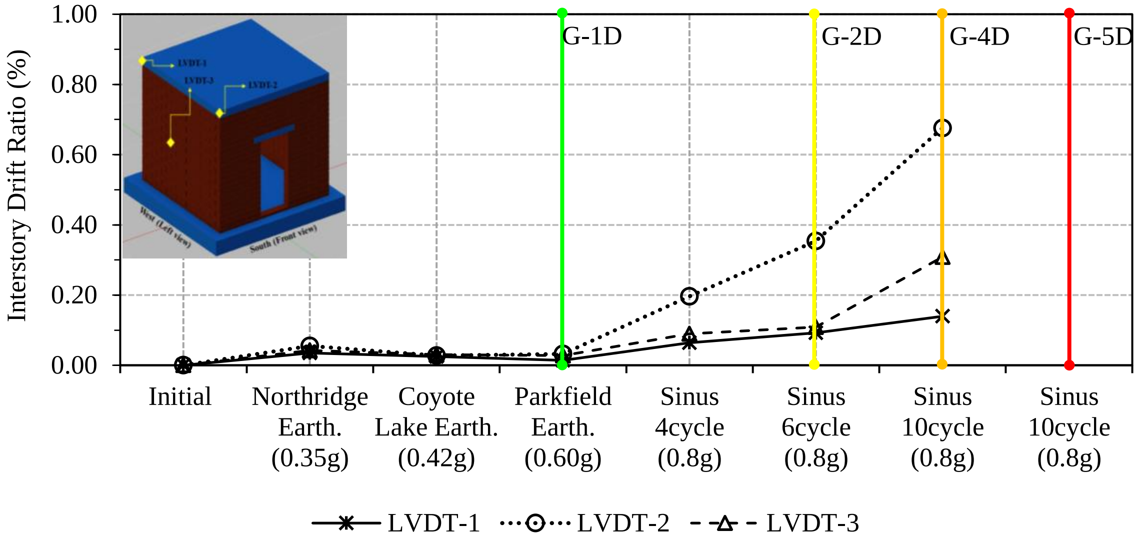

Figure 4.14. Variation in the maximum IDRs obtained during the ST test

4.5.3. Absolute Accelerations

Jumps and phase shifts between signal data acquired from the accelerometers during ST testing can be utilized as indications for the start of softening and crack formation. Researchers such as Bothara *et al.* [84] and Ghezelbash *et al.* [85] linked the damage to disparities between obtained data. For this objective, the acceleration responses at mid-height and roof altitudes for ST testing with damage circumstances of G-1D, G-2D, and G-4D types were compared see Figure 4.15. In the GMD-3 Parkfield Earthquake (PGA=0.60g), when hairline cracks were noticed, the time histories of accelerations were found to be in harmony, with no phase shift or jump between signal data.

Figure 4.14 showed that, as damage increased, there were notable differences in acceleration responses at mid-height and roof heights. However, notable phase changes were not observed for the DS-2 type damage state. As illustrated in Figure 4.15c, phase shifts and jumps were observed between accelerometer outputs in a DS-4 damage situation where severe damage was detected, and crack widths approached the order of centimetres. Figure 4.16 compares the peak acceleration values of the test specimen recorded at the mid-height and roof heights. As previously indicated, the discrepancies between the obtained values in the undamaged condition were insignificant, but the peak accelerations became inconsistent with the increased damage.

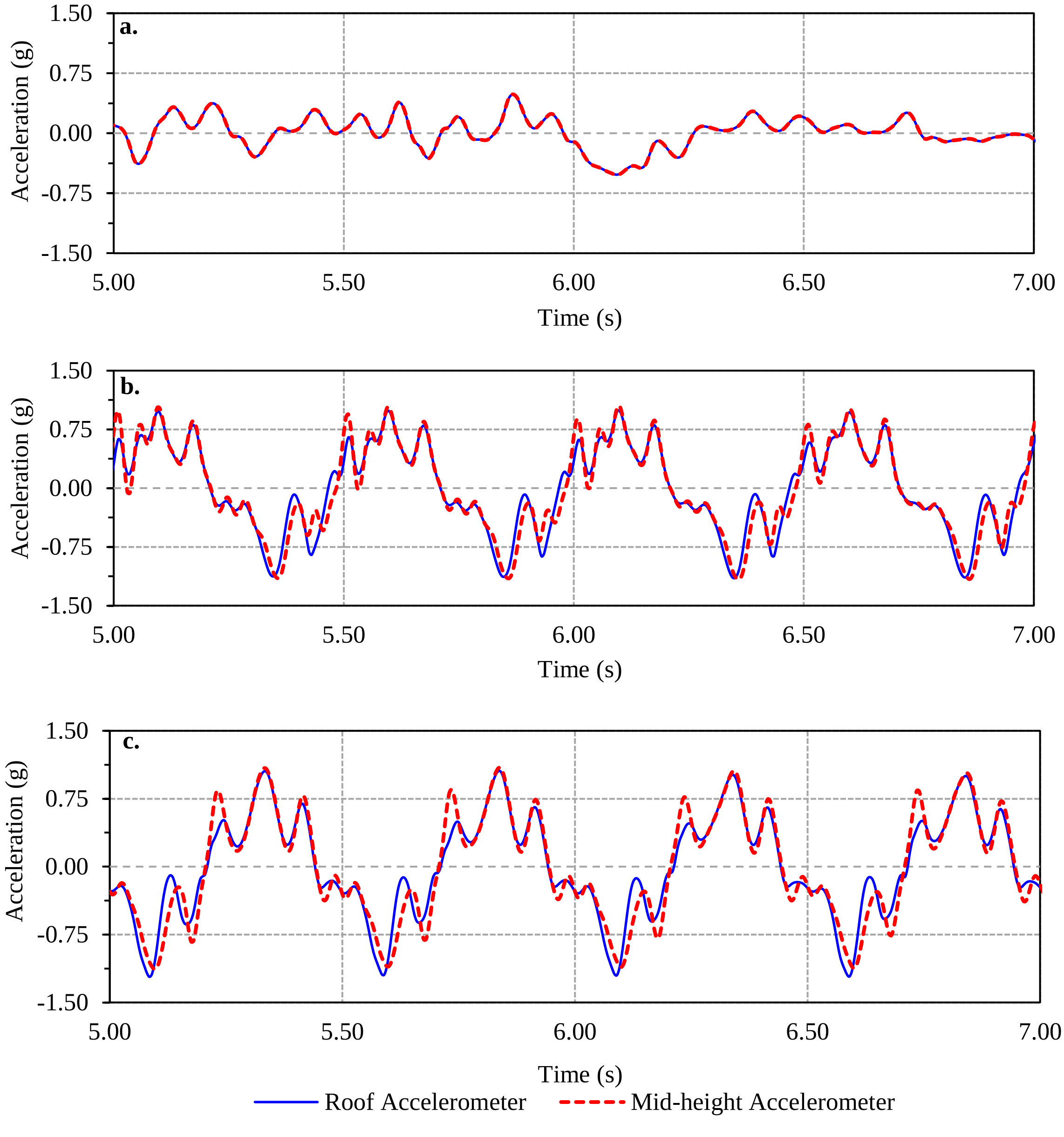

Figure 4.15. Acceleration time histories obtained at mid-height and roof level; (a) GMD-3, (b) GMD-5 and (c) GMD-6.

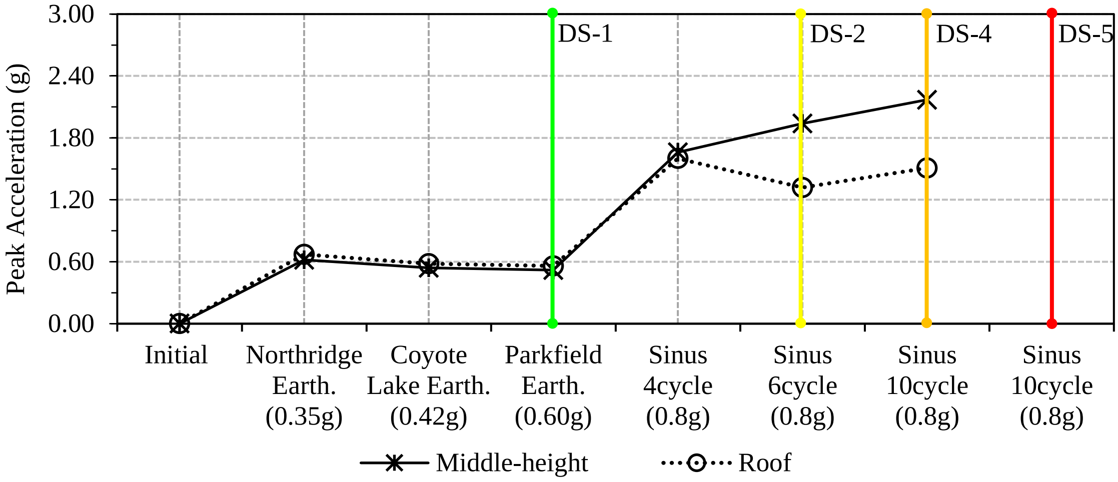

Figure 4.16. The discrepancy between the peak accelerations during the ST tests.

5. VISUAL SIMULATION – BLENDER + BCB

5.1. General Description

Bullet Constraint Builder (BCB) is a simulation add-on tool that is based on the Discrete Element Method (DEM) in a broader term. It enables the simulation of collapse scenarios using the freely available software Bullet Physics engine and Blender. The software package is made up of three program modules that work in harmony. Each software unit is released under an open-source license, allowing third-party programmers to use and alter the source code [86]. This collaborative effort enables continuing quality assurance cross-check and consistent software enhancements. The Components of the program include:

- ✓ Bullet Physics Engine [87]
- ✓ Blender [88]
- ✓ The BCB script [89]

5.1.1. Basics of DEM

DEM is a numerical approach for predicting the interaction of deformable and/or rigid objects that move independently. Objects travel along basic trajectories and paths, which are specified by Newton's motion theories. DEM could be used in any situation where a vast number of objects interact with one another and where frictional, electromagnetic, and cohesive forces, among other concepts, can be applied. The goal of the DEM approach is to simulate building collapse with a focus on the creation of a model automatically and the time of the simulation. DEM is used for a variety of things, from designing agricultural equipment that could handle bulk materials such as seeds and grains to studying the viscosity and geomechanics of gravel and sands in the soil processing sector, see figure 5.1 as depicted in [90, 91, 92]. DEMs are now commonly employed as algorithms in the reputed "Interactive Rigid Body Dynamics", see section 5.1.2. It permits easy interaction between the user and the simulation as well as the delivery of results in "real-time". Accuracy is significantly reduced since the most crucial factor in these situations is speed [93].

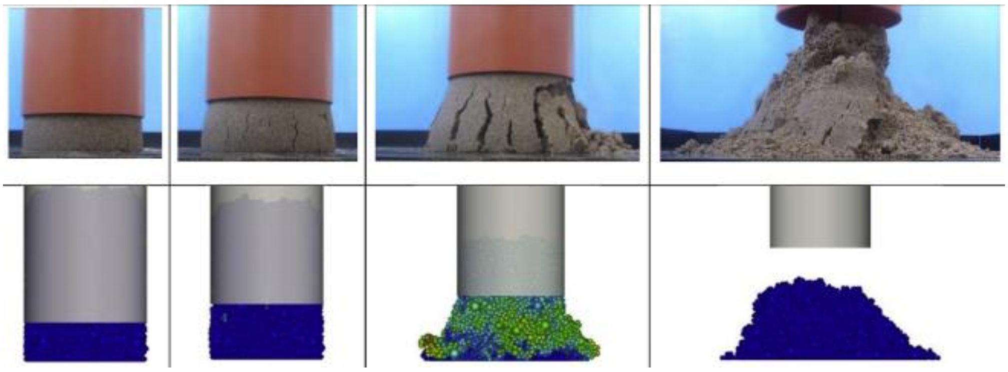

Figure 5.1. Analysis of bulk material flow using DEM [90].

The fundamental physics principles like mass and momentum conservation are the basis of DEM. As a result, the numerical algorithms use the fundamental tenets of conventional mechanics, particularly Newton's motion equations. The forces acting on a particle are calculated using Newton's 2nd rule of motion which states that the applied force equals the rate at which a body's momentum changes over time.

$$F = m\frac{dv}{dt} = \frac{d(mv)}{dt} \tag{5.1}$$

$$m_i\frac{dvi}{dt} = \sum_j \left(F_{ij}^n + F_{ij}^t\right) + m_i g \tag{5.2}$$

$$I_i = \frac{dw_i}{dt} = \sum_j \left(r_i * F_{ij}^t\right) \tag{5.3}$$

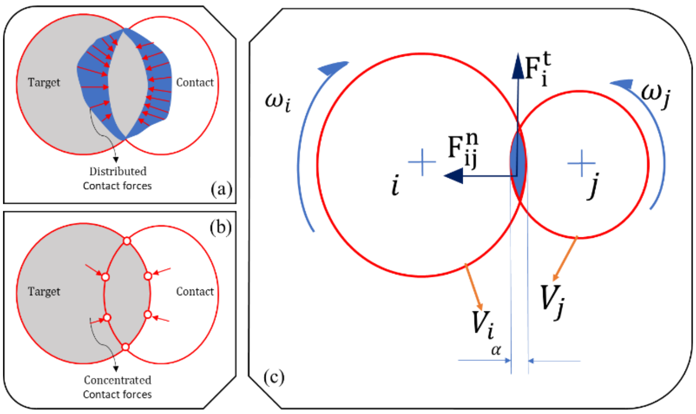

Figure 5.2. Mechanism of the contact and collisions between objects; (a) Distributed contact forces, (b) Concentrated contact forces and (c) The collision penetration - α and Momentum conservation mechanism

Where r_i, m_i, I_i, v_i, and ω_i are the radius, mass, moment of inertia, translational velocity, and angular velocity of the corresponding particle I, respectively. The sum of force acting on each particle is made up of potential forces (like gravity) and external, discrete forces make up the total of forces acting on each particle. It is subdivided into a normal ($\boldsymbol{F_{ijn}}$) and tangent ($\boldsymbol{F_{ijt}}$) component to the contact surface [94]. The algorithm's main goal is to estimate forces of contact and collisions amongst the elements after the discretization of a physical problem and the application of initial conditions (such as velocities or gravitation). The elements/particles' acceleration vectors and trajectories are updated when the force equilibrium becomes more imbalanced. The DEM simulation is carried out in incremental calculation cycles, otherwise known as "loops," that span a predetermined time period known as time step Δt. Different solution processes are calculated and repeated in each time step till the normal termination is achieved. The first step looks for prospective object collisions that are in close proximity. Several methods, such as cell or sorting algorithms, can be used for this job [95]. Once an overlap between two objects is recognized, the second procedure computes the tangential and normal forces based on the overlap magnitude. The third determines the objects' total net force, as well as their direction, new velocity, and acceleration. The third aspect computes displacement and rotation at the conclusion of each time step. The cycle then begins again for the following time step, and so on, till the simulation is complete. This procedure is depicted schematically in Figure 5.3.

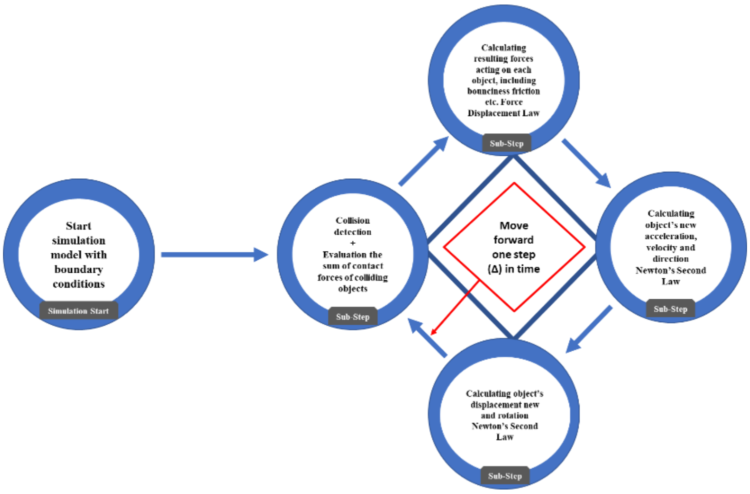

Figure 5.3. A typical calculation cycle of DEM [86].

5.1.2. Interactive Rigid Body Dynamics

There exist a variety of models and methods for handling contact in DEM. The supposed Linear Spring-Dashpot Model, which considers the effects of dissipative and elasticity, is one of the first models [5]. More complicated models are presented in [11] and [12]. Those models, on the other hand, are applicable to "soft sphere" scenarios in which spheres with different characteristics such as compliance, adhesion, and plasticity effects, along with others are used to depict discrete elements. Only rigid bodies are considered in the employed upgraded version of the DEM, commonly known as Rigid Body Dynamics (RBD), which simplifies the calculation by eliminating the need to define interior stresses and strains. Furthermore, with the friction between bodies being exempted, dissipative mechanisms such as plasticity are also ignored.

The most visible difference between RBD and traditional DEM is the prevention of colliding bodies from penetration in RBD, whereas, forces in the standard spring-dashpot model are calculated progressively in dependency on minor penetrations. In the used approach contact forces and velocity changes take place instantly, with no penetration [13]. The main benefit of this approach is its computational efficiency, which greatly reduces the computational costs of contact management [14]. Hence, the phrase Rigid Body Dynamics would be a more precise description of the method used.

The motion's governing equations are recreated as a Linear Complementary Problem, and the contact forces are exploited as constraint conditions in a time-stepping model creation [8, 15]. The Projected Gauss-Seidel algorithm [31] is subsequently used to solve the model iteratively. It employs an implicit time-stepping technique that permits for bigger time steps and consequently a speedier calculation than traditional DEM methods. Explicit time integration techniques are commonly used by the DEM, which considerably escalates the number of cycles and hence the computational expenses.

5.1.3. The Benefits and Drawbacks in Terms of Collapse Simulations

When compared to continuum techniques, where an extremely complicated material behaviour is estimated for each element, the underlying RBD simulation approach has significant advantages. Since only rigid bodies are addressed, and these bodies relate primarily using Newton's equations, the numerical exertion to define and analyze the overall problem is reduced significantly. As a result, the RBD is a highly rapid method in general, and it can even be utilized in "real-time" settings.

Furthermore, a large number of structural features are averaged in simplified engineering formulas and the geometry is merely approximated crudely. Consequently, the time it takes to develop an executable simulation model is much reduced. These benefits come with the drawback that continuous deformations cannot be estimated within bodies and can only be viewed as a relative change in distance between them. This, along with a coarsely discretized structure, results in an approach with lower accuracy. The failure to pay attention to structural elements could, of course, be viewed as negative. Although the governing equations apply the core physics of structural dynamic behaviour, they only apply to discrete objects. They are not applicable to the continuum, that serves as the beginning point in collapse situations. Bakeer [5] has documented various noteworthy and successful efforts to use RBD and variants of the approach to model and simulate the collapse of masonry structures.

Considering brickwork structures have a grid of uniform blocks and failure occurs predominantly on the mortar joining bricks, the RBD is an excellent choice. Mortar properties can be incorporated into sophisticated force models. In general, the same is true for reinforced concrete structures, where the distinctive connection between numerical and structural elements is lost. All techniques of this type, however, have one commonality: modifications must be applied in the method's primary algorithm. In the case of the utilized application, no change was made to the physics engine instead exploited the existing potentials offered by the algorithm. Hence the prospect of restrictions between dissolved objects after a specific threshold is surpassed is considered. They are employed alongside a physical understanding of the thresholds.

5.1.4. Bullet Physics Engine

Physics Engine is the software code (could be commercial or open-source) used for the implementation of DEM and RBD. It is responsible for solving the discrete-time model stated above. It was created for the purpose of simulating physical and mechanical processes that occur in real life in order to provide realistic game experiences. Physics engines use a combination of techniques to mimic sophisticated physical processes in games, including rigid bodies (such as rocks and dirt particles), soft bodies (such as clothing), fluids (such as water), and their interactions. As a result, physics engines are capable of simulating realistic particles [96]. It is also utilised in movie production to create extraordinary visual effects and almost realistic animations that are physics-based. Its application has also been deployed in robotics simulations such as NASA's tensegrity robotics simulator [97] or BBZ medical technologies' robotic surgical simulation [98].

Real-time and high-precision physics engines are the two most common types. Factors such as the license type, features available, platforms supported, and performance and accuracy during runtime distinguish the two types. Scientists and computer-animated movies typically employ high-precision physics engines, which demand greater computing power to calculate very fine physics. Real-time physics engines, such as those seen in video games and other forms of interactive computing, rely on simplified computations and lower precision to compute in time for the game to reply at a reasonable rate.

There exist several real-time physics engines such as Bullet [87], PhysX [99], Box2D, PhysicsJS, Open Dynamics Engine [100], BeamNG, Havok, and True Axis [101] among others. Examples of high-precision (otherwise known as offline) physics engines are Icarus and VisSim. The term “Offline” means that the simulation results are decoupled from user interaction. The high-precision physics engines bear the drawback of high time consumption and decoupled simulation results from user interaction. However, they provide extremely accurate results. The interactive physics engines, on the other hand, are inspired by situations that need only satisfactory realistic outcomes in lieu of real-time solutions [93, 102]. The concept "interactive" suggests it is furnished with the instant provision of simulation results and continuous user interactions.

The interactive Bullet Physics engine [87] which is one of the most widely used physics simulations today is employed in this study. The Bullet is a non-proprietary real-time physics engine that simulates soft and rigid body dynamics as well as the detection of a collision. It was created by Erwin Couman for Sony's PlayStation in [103].

5.1.5. Blender Software

Blender is a freely available powerful 3D modelling software through which continuous user interactions are achieved. It is linked to the physics engine and permits the creation of a model as well as the simulation visualization. It was initially a Dutch Animation Studio NeoGeo-owned proprietary program in 1995. Game logic, real-time physics simulation, advanced texture mapping, video editing, path tracing rendering, sculpting, animation tools, and other features have all been added to this software as a result of active and consistent advancement. A rising number of programmers, in addition to a growing number of users, contribute to Blender's functionality on a regular basis. Blender is a strong tool for the exploitation of simulation results, allowing interactive "walkthroughs" in environments with lighting, textures, and realistic shading. It also includes capabilities for cavity identification and tracing of the victim in the event of a collapse scenario. Custom extensions can be used via a python-based script language program interface.

The creation of Blender 2.47 and newer versions are bullet physics engine incorporated, hence it permits us to kill two birds with a stone. The Bullet features can be controlled directly in the modelling area, and their functionality can be accessed from the main toolbar. Rigid bodies can have one of two qualities in this environment: passive or static. Collisions and gravity have a dynamic effect on the position of active objects, whereas the position of passive items is fixed. A scene can have a huge number of objects that are either independent or connected by basic constraints. The physical simulation is instantly displayed in the program's viewport, and objects in the scene can be interactively grasped and moved around with the pointer, affecting the other objects dynamically.

5.1.6. BCB

As previously stated RBD was originally developed to simulate material with separately moving objects. Rigid bodies, on the other hand, must first be joined to each other in order to depict members of a building structure. Because no material behaviour is considered within the rigid bodies, the connection between components must be formed between them by constraints to describe the material's strength characteristics in a broader context. The BCB add-on extends Blender's Bullet physics features effectively. It combines discrete rigid bodies with sophisticated constraint arrangements that allow complicated collapse simulations by taking into account the mechanical properties of the materials that comprise the components.

The BCB's fundamental principles are as follows:

- Description of the appropriate degrees of freedom for each element pair using multiple constraints, see Section 5.1.6.1.
- Precise placement of constraint, see Section 5.1.6.2.

➢ Admissible forces calculations based on the building element's physical structural characteristics, see Section 5.1.6.3.

5.1.6.1. Multiple Constraints

Constraints connect two rigid bodies and are allowed to dissolve at a certain point known as “breaking threshold". This value is general by default in the Bullet physics engine, which implies that as soon as the magnitude of one of the force components F_i or moment components M_i exceeds the specified threshold the constraint is removed. At each iterative computation step, the bullet solver assesses each force component (F_i or M_i) independently but does not distinguish between forces, moments, their orientations, or their combined effects. When any of the evaluated components exceeds the defined breaking point, the constraint is automatically deactivated and the connection is severed. This is a critical limitation for representing the actual behaviour of the structure because various loading conditions might cause the material to behave differently depending on the direction and kind of applied load.

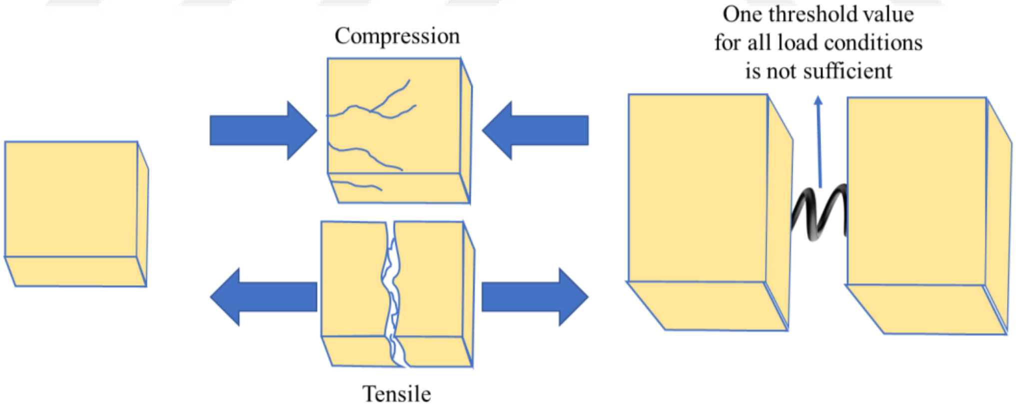

Figure 5.4. Illustration to justify the need for multiple constraints

With the help of a simple concrete element, Figure 5.4. illustrates the necessity for numerous constraints. Concrete has a strong compressive stress resistance but a poor tensile strength. Assuming that the strength within a concrete body is represented by a single constraint, with the breaking threshold specified by its compressive strength f_c, the element will not fail until this stress magnitude is met – even in tensile stress states. This is why multiple restrictions must be applied to each connection, even if the same degree of freedom is covered. The BCB add-ons [89] proposed 23 new connection types (presented in appendix 3). They can be as simple as a point or single fixed constraint or as complex as a combination of generic and spring constraints. Some of the several types of connections are depicted in Figure 5.5.

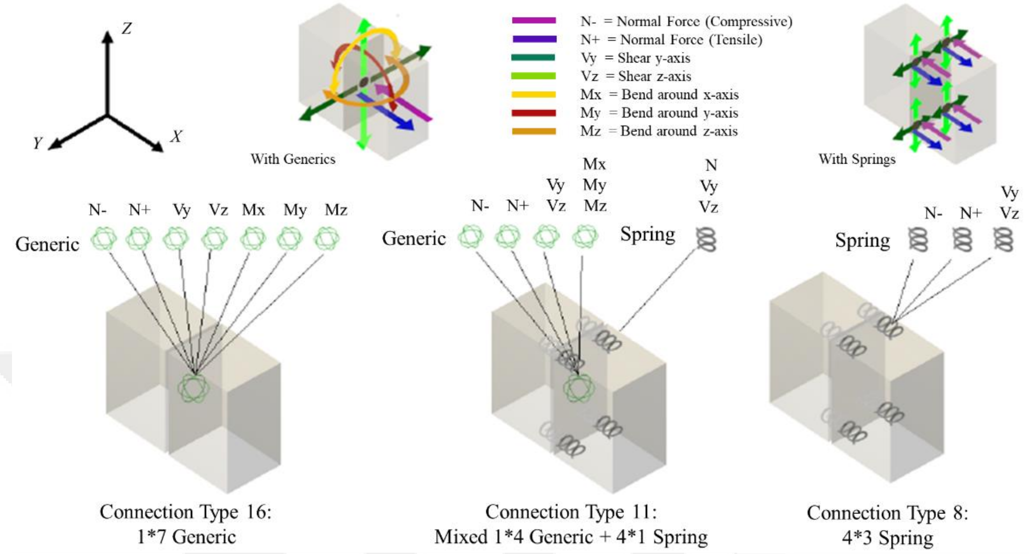

Figure 5.5. Connection types in BCB [86].

➢ Generic constraints

The generic constraint type allows you to constrain one DOF while leaving the other six unconstrained. After that, an individual breaking threshold based on strength calculations is used to secure the restricted DOF. Figure 5.6. shows an example of a generic constraint arrangement. Generic constraints are effective tools for determining when a structure may fail. When the threshold of one of the relevant constraints is exceeded, the BCB monitors the state of the generic constraints during the simulation process and dissolves the other constraints of the connection under consideration.

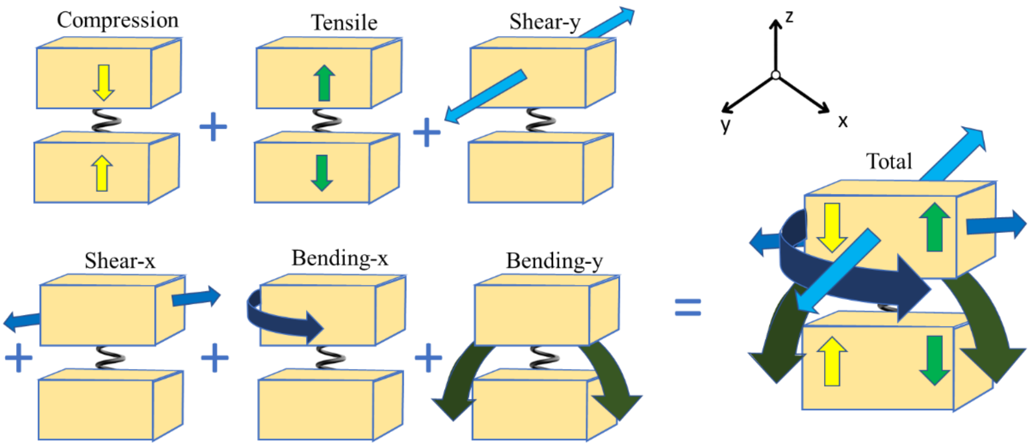

Figure 5.6. The constraint structure of connection type 15

- Springs

The development of BCB was originally intended for compound materials specifically reinforced concrete (RC). Generally, the failure of concrete occurs at relatively low stress compared to that of rebar, and even after concrete failure, the entire structure might still be functional due to the presence of the rebar. This implies that the connection does not completely dissolve until the failure of the rebar, which is characterized by considerable deformation due to its ductile nature. This same concept could be extended to masonry which has extremely high compression strength but fails at a very low tensile stress. The integration of springs in addition to generic constraints to the BCB connection types makes the simulation of these types of scenarios feasible. The springs can effectively recreate the ductility of the masonry by allowing irreversible and reversible deformation amongst rigid components. The spring connection also dissolves and the rigid bodies detach but contrary to force/moment thresholds, it occurs only after a particular deformation threshold is exceeded. Stiffness, low linear and angular thresholds at the plastic state of the spring, and linear and angular higher thresholds at the dissolves of the spring are some of the characteristics that characterize the spring attributes.

5.1.6.2. Precise Placement of Constraint

The BCB inserts the constraints in the contact region of the bounding box of two rigid bodies that are in proximity. A bounding box is a geometrical description of a rigid body that is used to detect contact. Close lying constraints can be aggregated by specifying a cluster radius, and all constraints within the specified radius will be adjusted to the cluster's centre point, as seen in Figure 5.7. If the connection is not stiff but creates a pivoting joint, this process plays an important role. The BCB script automatically estimates the contact area size, which is subsequently used to evaluate the various constraints' breaking thresholds.

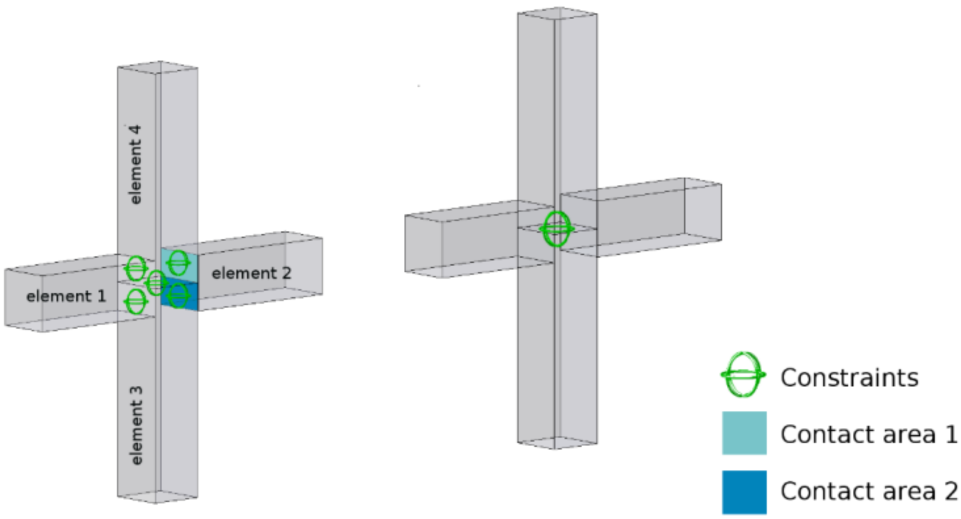

Figure 5.7. Detection of contact area and constraint placement [86].

5.1.6.3. Admissible Forces Calculation

As stated in Section 5.1.6.1 (Springs), BCB was specifically intended for RC hence the general formulation assumptions are towards RC but to a greater extent applicable to masonry structures. The assumptions are formulated to deal with complicated behaviour within the simplified RBD framework and for constraint thresholds determination and regulation. The assumption goes thus:

- The permissible forces that cause the entire cross-section to fail may be approximated using simple engineering formulas.
- Cross-sectional failure due to a certain stress condition such as tensile stresses results in an immediate and total loss of the cross-section’s ability to transmit subsequent loads (such as shear) in different orientations.
- The rebar's integrity is unaffected by the concrete matrix failure, and its ability to resist tensile forces is uncompromised.

The instant one permissible strength is surpassed, all generic connections are removed. In the course of the monitoring, pass springs restore the lost tie between rigid bodies and offer the residual tensile strength that was not achieved before the connection removal. Due to the obvious general approach, which is based on the assumptions described above, additional amount load-carrying abilities, which might have emerged in reality, cannot be addressed.

5.1.7. Fracture Modifier

The DEM technique is being developed with the goal of solving the simulation challenge in "real-time" and within a short period of time. Despite the fact that the RBD technique with much-decreased computing time is used, the simulations in the current Blender version fall well short of this goal. Baking (real simulation time) of the masonry model subjected to Northridge EQ with over 625 simulation frames, for example, lasted 13,620 secs (almost four hours). Substantially discretized models with their constraints' setups, clutter Blender scenes to the point that they are complicated and time-consuming to manage. The existing object management performance of Blender decreases rapidly as the number of objects in the scene increases. The scene in this context refers to the Blenders model space while Cameras, lamps, constraints, and rigid bodies, just to mention a few are examples of objects in Blender. Hence the development of a custom-made modified Blender version titled - Fracture Modifier (FM).

A significant and marvellous speed enhancement can be attained when the model is exported to FM for analysis. The same masonry model analysis that lasted for 13,620 secs in standard Blender, took just 347 secs with the FM under the same condition – an approximately 3900% speed increase.

Object management approaches that are not compatible with the dependency graph of Blender's internal storage management are utilized by the FM. Figure 5.8 shows a comparison between the FM method with the typical Blender approach. Constraint objects are introduced to the model space during the "SB1" construction stage in the conventional technique. The constraint configuration is submitted to the bullet solver for numerical evaluation at simulation step "SB2". However, the location of each rigid body must be modified at each animation frame, resulting in a high number of operations while the real computational effort required to solve the simulation is limited. The FM simulation approach, on the other hand, avoids having a high number of objects in the model space by combining all components as mesh islands into a single object container at step "FM1". Furthermore, the constraint configuration is only processed by the bullet solver at step "FM2" and is not deposited in the model space. Hence the super increased speed. The FM is not a proper Blender version, however, it is available through the GraphicAll [89] site as a one-of-a-kind bespoke Blender build. The speeds of the standard Blender and the FM are compared in Appendix 7.

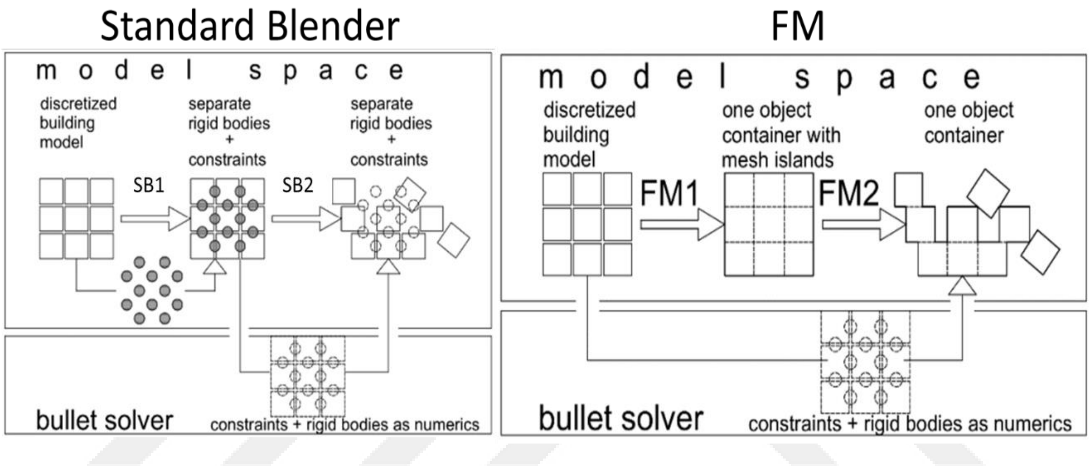

Figure 5.8. The Basic simulation approach in standard blender versus FM [86].

5.1.8. Relative Displacements Visualization

The DEM implementation described here is unable to visualise the internal forces' magnitude. The reason is that Blender's Python API allows add-ons like the BCB to link directly to core Blender functions and data. However, there is no way to directly access the forces that the Bullet engine analyses during simulations. Nonetheless, the displacements of neighbouring rigid bodies generated by these forces may be observed, indicating where high-strain zones are located. A deformation visualizer v1.10 python script was integrated into Blender to visually generate elements displacements relative to the elements' start frame positions. The script was written and developed by Kai Kostack. Rigid bodies having a relatively small displacement compared to their surrounding bodies are coloured blue, whereas bodies with large relative displacements are coloured red.

5.2. Modelling of the Masonry Structure

The structure was modelled using mesh cubes and rigidity was enabled during the preprocessing of the model. However, BCB uses a "convex hull" as a standard collision shape for all elements which does not allow for concave shapes like the notch presented in the base. Hence, the base was split into blocks so that every sub-element is convex and can easily be discretized. This topology modification was necessary to avoid problems with the shape collision. Also scaling of objects (Ctrl+A) was applied since Boolean operations in the preprocessing stage work better when the scaling is unity. The ground motion was added as a “.csv” file in the preprocessing stage. To reduce the computational time the FM version of the blender was used for the simulation [86, 89, 104].

5.3. Selection of Values and Parameters

5.3.1. Compression and Tensile Strength

The compression property of masonry was selected as 10MPa as suggested by [86]. Tensile strength is assumed to be 10% of compression strength, as recommended in the literature [86]. However, because of the use of numerous EQ data that were not addressed in the simulation, the tensile strength is assumed to be 0.1. The depiction of the cracks before the application of the 10-cycles sine function confirms this drastic reduction.

5.3.2. Shear

According to several studies [1, 105, 106, 107, 108], the shear strength of masonry ranges from 0.01 to 0.65 MPa, but some researchers proposed a greater value of up to 0.5MPa [99]. However, for this research, an experimental mathematical expression was used.

╠→ $ss_t + abs\ (h_{tm} - z) * f_g$

╠→ ShearStrength + absolute(TotalModelHeight-z) *GradientFactor

Where ss_t represents the typical shear strength, h_{tm} represents total model height, z represents the height at the point being considered and f_g represents the gradient factor. Based on prior successful simulations [109], GradientFactor is estimated to be 0.1. It introduces an artificial strength gradient based on z (global coordinates) to reflect the higher friction (described in section 5.3.5.) caused by the pressure that the solver has difficulty recreating accurately.

5.3.3. Bend

As per CSA S304.1-04 “Design Of Masonry Structures” [110], the minimum bend strength should be 0.2, however, based on experimental results, some studies have indicated a number that is less than that. As a result, the bending strength is estimated to be between 0 and 0.54 Mpa. Because the bending strength was already lessened before the application of the 10-cycle sine wave, 0.1 was utilized for this investigation.

5.3.4. Density

Masonry has a density that ranges from 1660 and 2400 kg/m^3. The density of 1800 kg/m^3 was employed in this study.

5.3.5. Coefficient of Friction

The Coefficient of Friction (CoF) of masonry is between 0.2 and 0.7, according to numerous sources [55, 111, 112]. Although other scholars proposed larger values like 0.96 [113] and 1.3 [114]. High-value CoF comes with Masonry Walls pre-set in BCB analysis, especially 5. Even when under a heavy weight, bricks near the bottom of a building are tempted to slip. Tralli *et al* [115] also advocated for a thorough examination of a rigid-body collision in the context of frictional sliding. He also points out that when the grooves are exactly aligned, as is the case with the model, the static coefficient of friction between the block and the foundation is more than 1.3. Smoljanović *et al* [116] also describe sliding and bounding the block away from the base. This was seen in all of the analyses performed with CoFs of 0.75 and below. Lipscombe and Pellegrino [114] also advised using a high CoF, pointing out that a CoF value less than 0.5 causes sliding, which can be a major source of failure. Furthermore, according to Kai Kostach (the software's author), the high CoF in the pre-set is a desperate attempt to compensate for the aforementioned undesirable behaviours. It is also assumed that this is a numerical issue for the solver/method (i.e., the add-on tool and its working principle). However, one must note that these bricks are not clean flat bricks in the actual world, but have jagged mortar added to them when broken, which obviously affects friction. In general, friction is thought to be a minor component in collapse simulations since the structure is mostly kept together by constraints rather than friction. Nonetheless, it has a discernible effect on the form of a loose debris heap but only a negligible impact on the collapse dynamics itself. A paper titled – “Interactive Simulation of Rigid Body Dynamics in Computer Graphics” [117] describes the bullet engine algorithms in depth. In addition, a CoF of 5 was employed in the simulation test for the University of Auckland [109]. As a result, the usage of high CoF (specifically 5) is justified.

5.3.6. Time Step and Solver Iteration

Time step refers to the number of steps per second whilst the solver iteration is the number of constraint solver iterations per step. The actual structural deformation is significantly dependent on the timestep chosen. Generally, higher numbers are more accurate, but also slower and more unstable. Hence selection of optimum value is of utmost importance. Consequently, a parametric analysis was carried out to get the optimal value (see appendix 1 and 2). A time step of 200 and solver iteration value of 347 was used in this research. The comprehensive parameters and corresponding values are presented in Table 5.1.

Table 5.1. Values used for analysis

Parameter	**Unit**	**Value**
Discretization Size	*m*	0.3
Connection Type	-	15
Compressive	N/mm^2	10
Tensile	N/mm^2	0.1
Shear	N/mm^2	0.1 + abs (1.85-z) * 0.1
Bend	N/mm^2	0.1
Density	Kg/m^3	1800
Coefficient of Friction	-	5
Time Step	-	200
Solver Iteration	-	347

Since BCB was designed for concrete structure the add-on tool was designed with Formula Assistant which permits the selection of structural element types and then automatically calculates the required parameters based on the imputed values. It should be noted that it is only applicable for reinforced concrete elements, and not applicable to other materials such as masonry, woods, etc. The imputed values are listed below:

f_c Yield strength of concrete (N/mm^2)

f_s Yield strength of reinforcement irons (N/mm^2).

h Height of element (mm). Leave it 0 to pass it through as a variable instead of a fixed number

w Width of element (mm). Leave it 0 to pass it through as a variable instead of a fixed number

c Concrete cover thickness above reinforcement (mm).

s Distance between stirrups (mm).

ds Diameter of steel stirrup bar (mm).

dl Diameter of steel longitudinal bar (mm).

n Number of longitudinal steel bars

5.4. Analysis and Results

The collapse simulation of the masonry model corresponds with experimental in most aspects. The first point of collapse at the lower part of the northeast section perfectly harmonizes with the experimental result, see Figure 5.9. As observed in the experimental campaign, Figure 5.9 depicted a nearly horizontal crack on the eastern side as well as the step-like diagonal crack and slightly inclined cracks at the lower part of the southern part. The detachment of the RC slab from the Eastern side of the masonry was also illustrated in Figure 5.11. The horizontal division at the lower part of the eastern wall was also confirmed.

As stated in section 4.5.1, torsional movement of the model was observed and the simulation also perfectly depicted this motion. Figure 5.12 illustrate the comparisons between the model at 2.56 secs, 3 secs and 4 secs. The use of gridline and ruler was further used to reinforce the authenticity of this finding. The direction and pattern of debris formation are presented in Figures 5.13 and 5.14.

The calculated result closely matched the experimental result. The debris formation, on the other hand, does not match completely. This might be related to the simulation's incapability of including the initials. Nonetheless, the models give important information on crack propagation and collapse progress, which might be utilized as a guide for retrofitting. The perspective and orthogonal views of the collapse progress are presented in Tables 5.2 to 5.9. The views were taken at 2.56secs (point of crack initiation), 3secs, 4secs, 5secs, 6secs, 7secs, and 8.36secs (end of ground motion). However, the analysis was continued for up to 10secs to ensure accurate debris formation. The visual relative displacement of the model is illustrated in Table 5.10.

Figure 5.9. Comparison between experimental and visual simulation-1

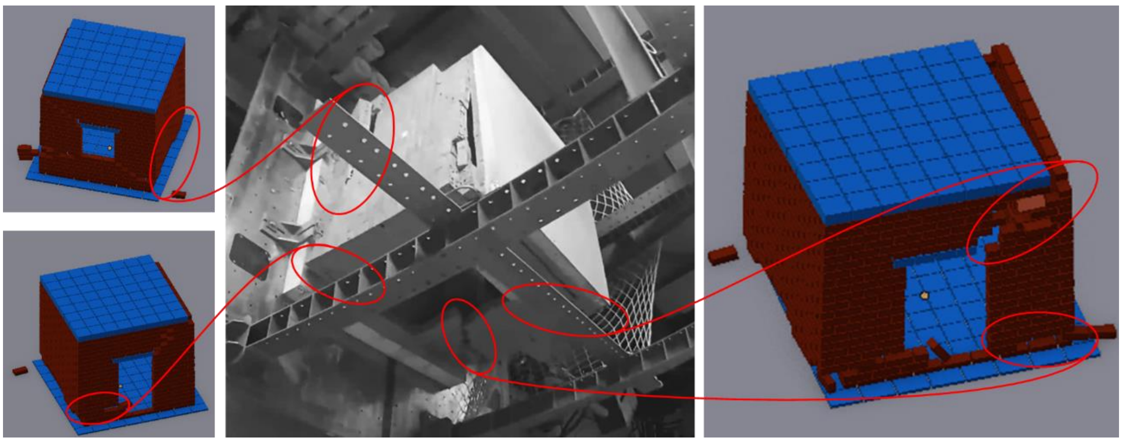

Figure 5.10. Comparison between experimental and visual simulation-2

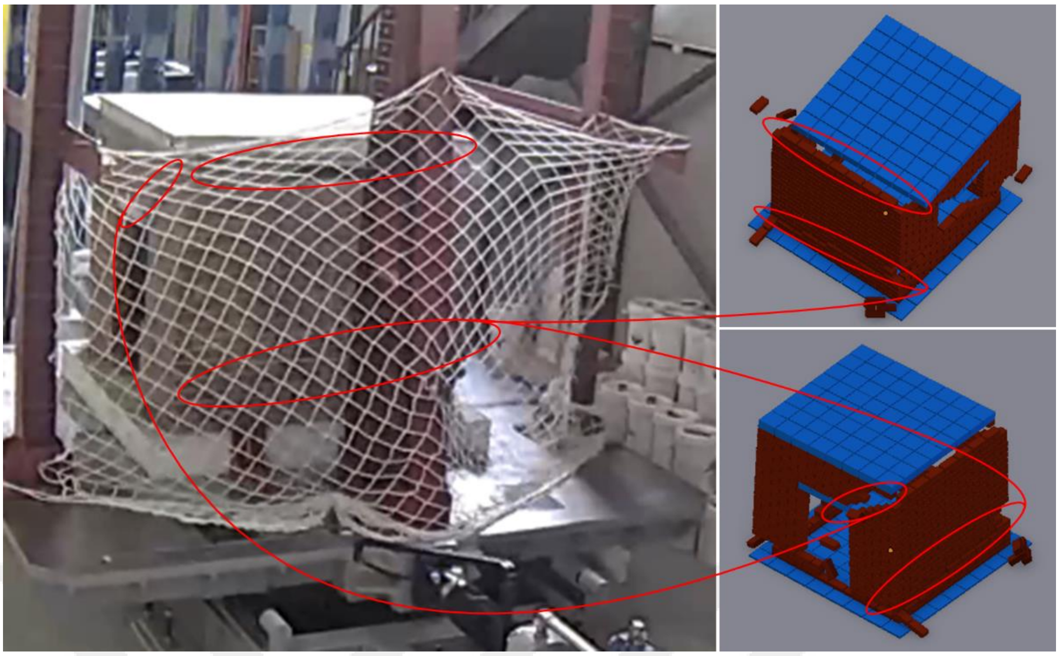

Figure 5.11. Comparison between experimental and visual simulation-3

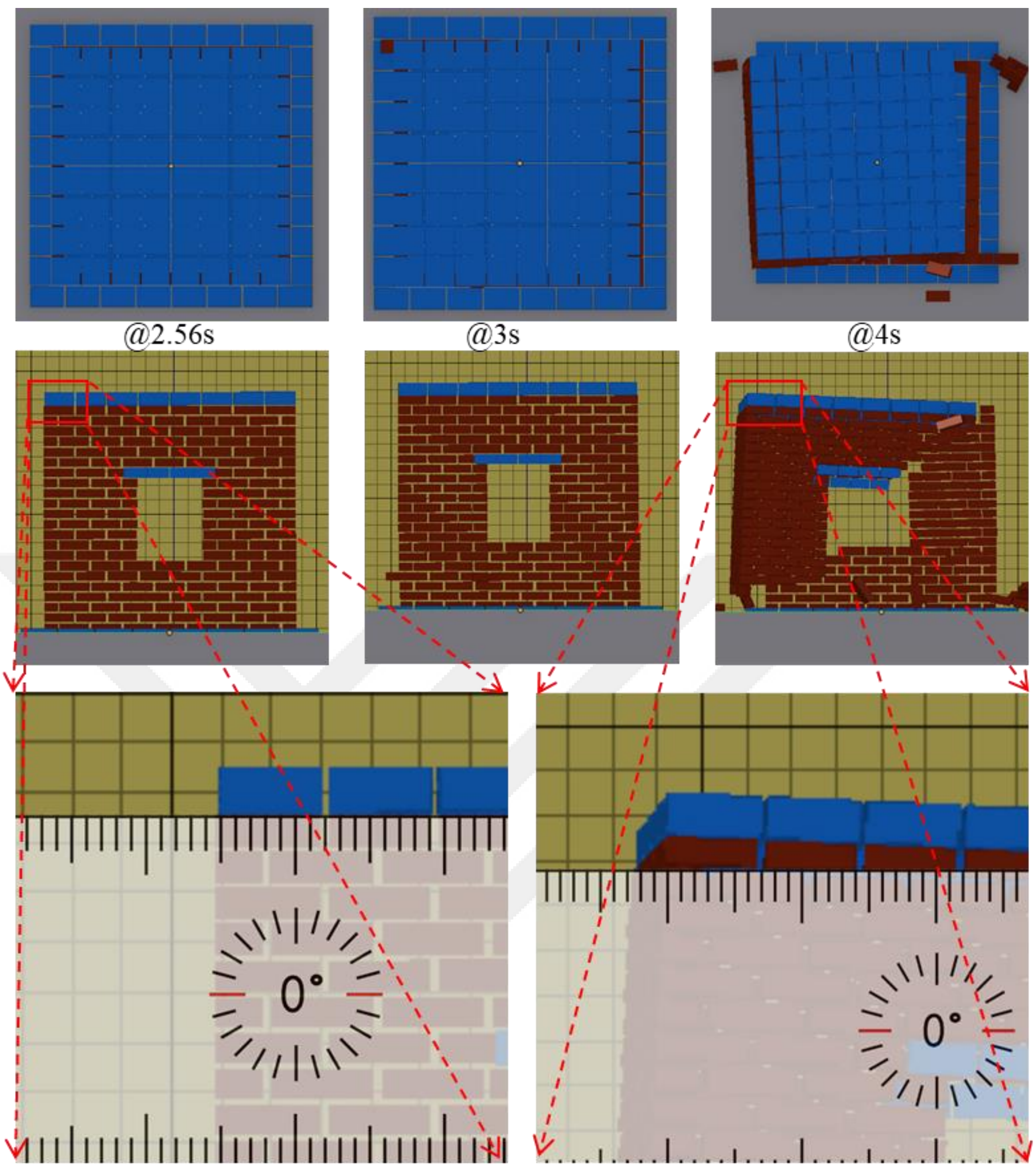

Figure 5.12. Torsional movement clarification

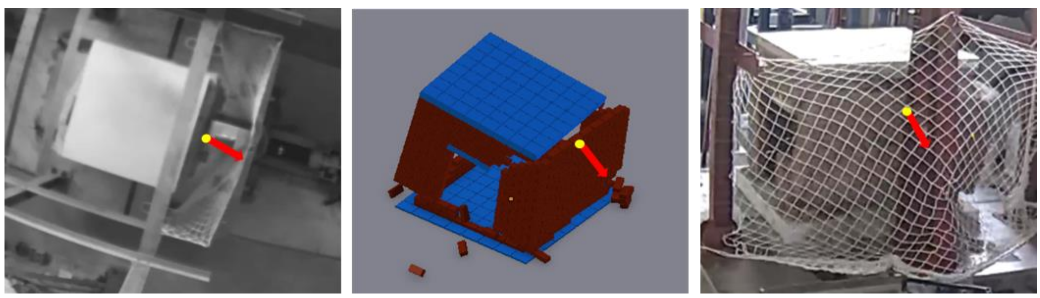

Figure 5.13. The direction of debris accumulation

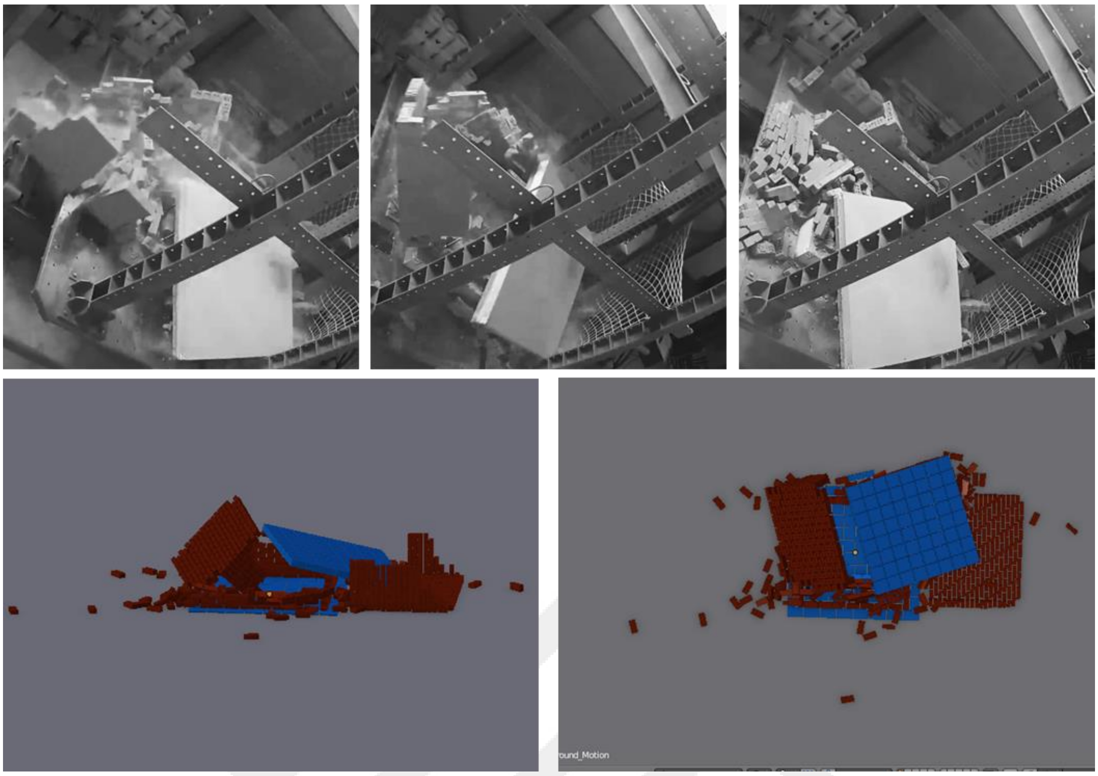

Figure 5.14. The pattern of debris formation

Table 5.2. Perspective and orthogonal views of the model at 2.56 seconds (Crack Initiation point)

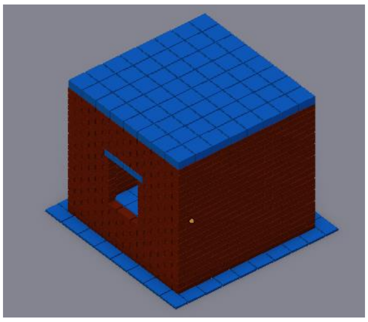	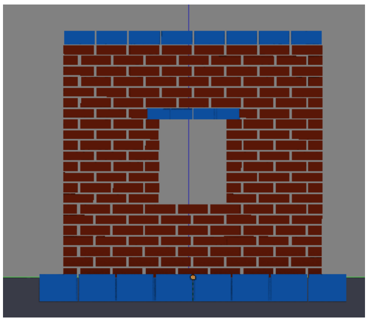	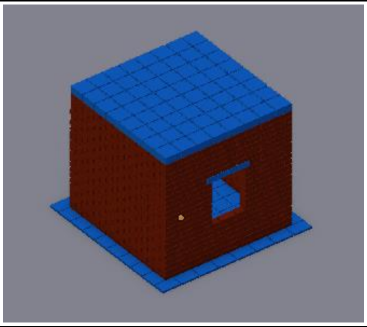
North-West (perspective)	**North**	**North-East (perspective)**
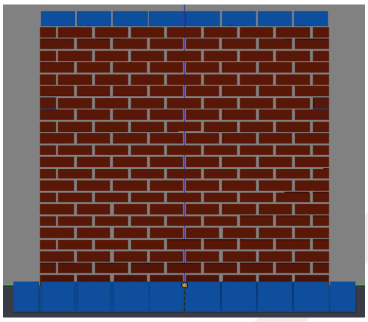	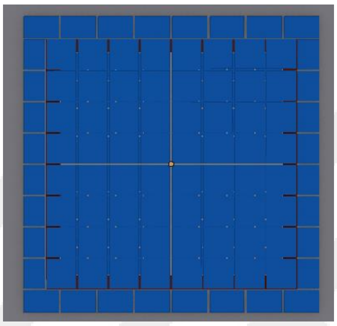	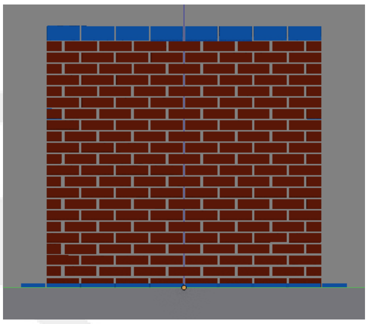
West	**Top**	**East**
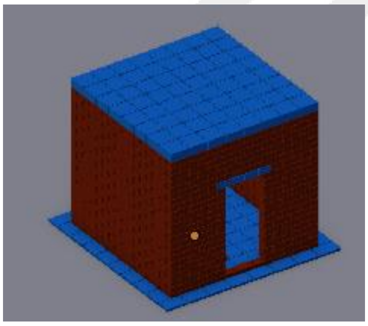	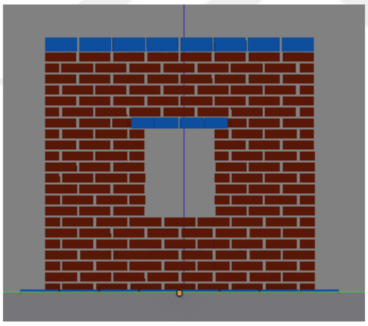	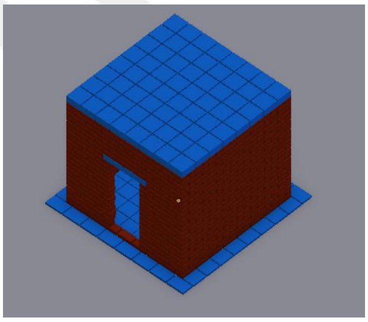
South-West (perspective)	**South**	**South-East (perspective)**

Table 5.3. perspective and orthogonal views of the model at 3 seconds

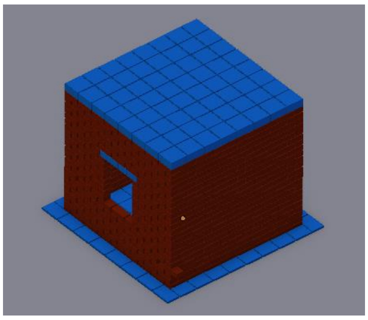	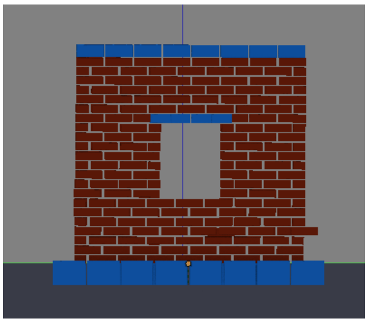	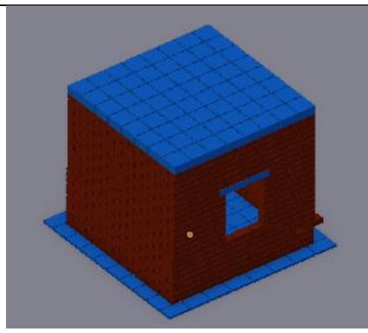
North-West (perspective)	**North**	**North-East (perspective)**
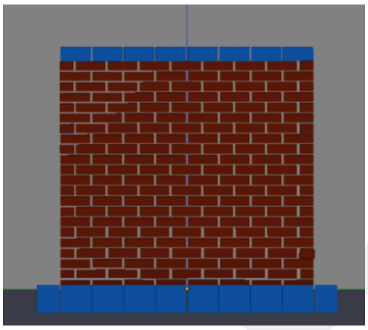	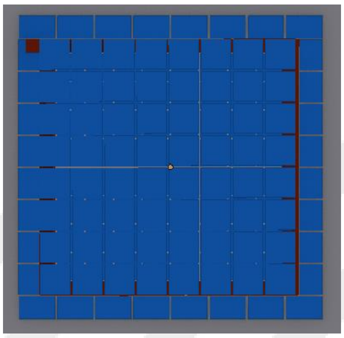	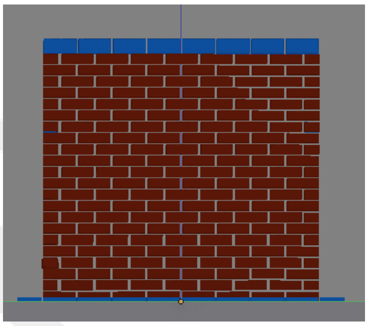
West	**Top**	**East**
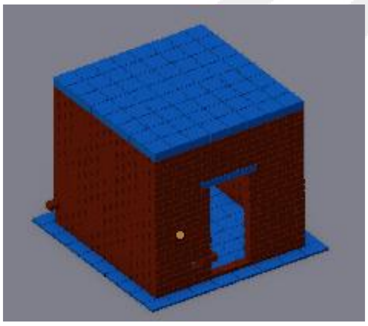	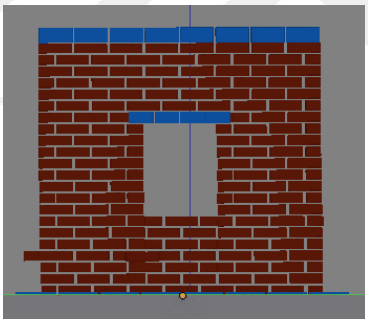	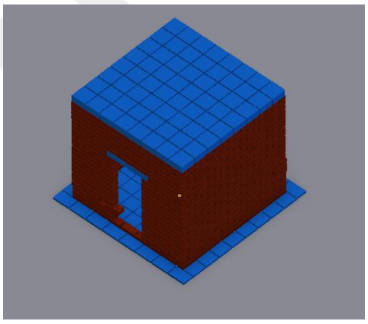
South-West (perspective)	**South**	**South-East (perspective)**

Table 5.4. Perspective and orthogonal views of the model at 4 seconds

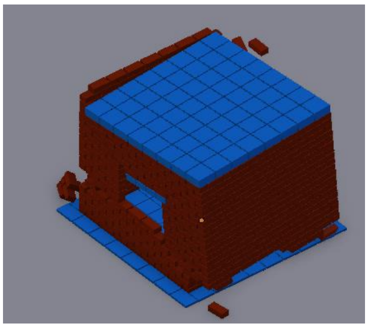	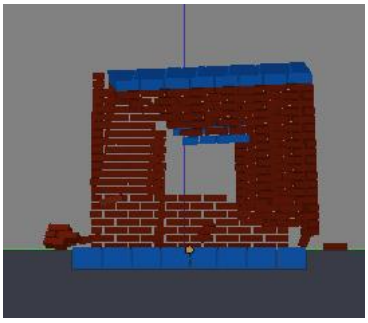	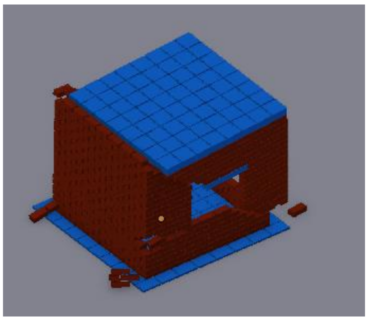
North-West (perspective)	**North**	**North-East (perspective)**
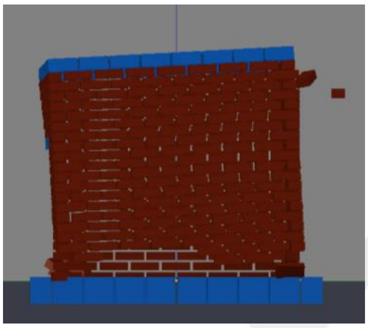	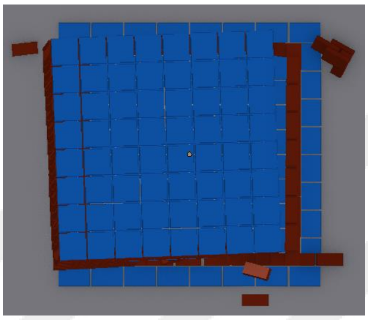	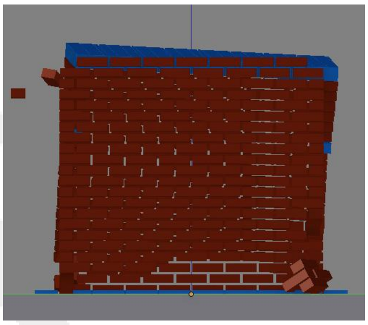
West	**Top**	**East**
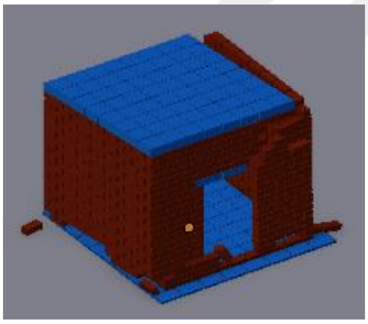	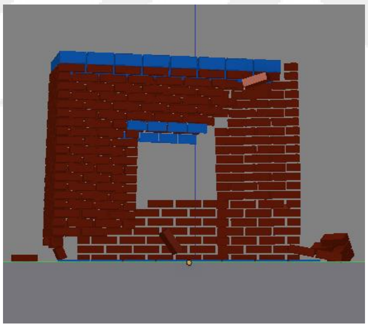	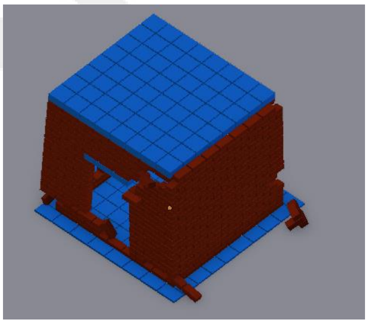
South-West (perspective)	**South**	**South-East (perspective)**

Table 5.5. Perspective and orthogonal views of the model at 5 seconds

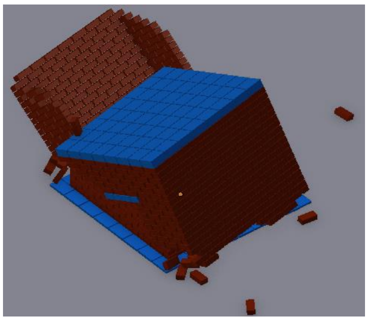	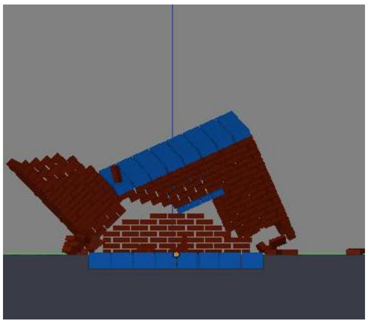	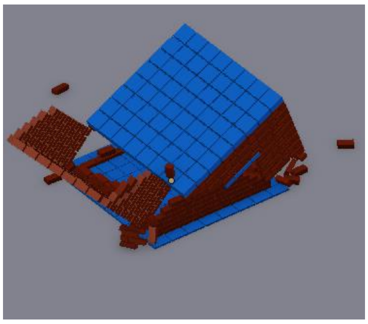
North-West (perspective)	**North**	**North-East (perspective)**
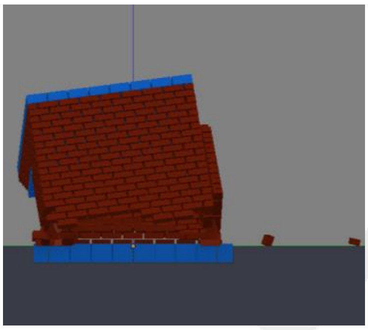	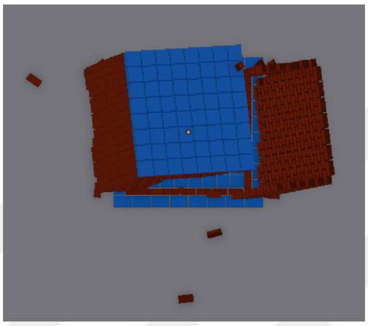	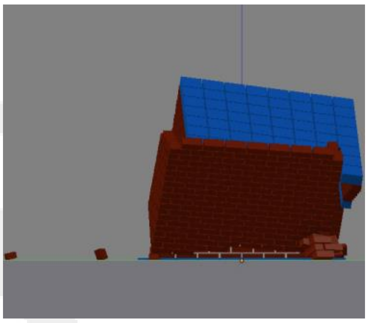
West	**Top**	**East**
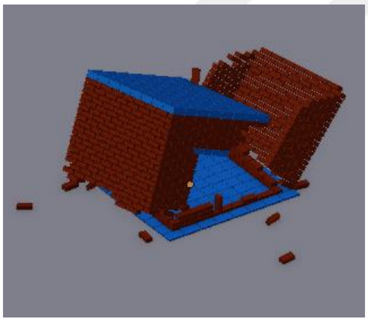	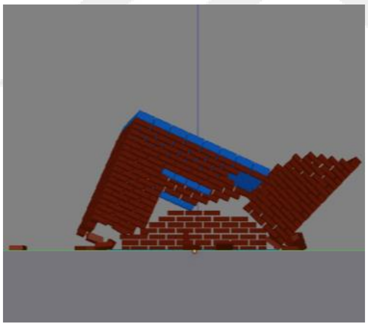	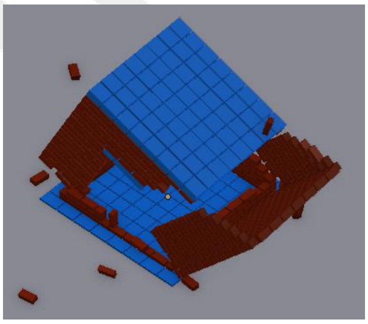
South-West (perspective)	**South**	**South-East (perspective)**

Table 5.6. Perspective and orthogonal views of the model at 6 seconds

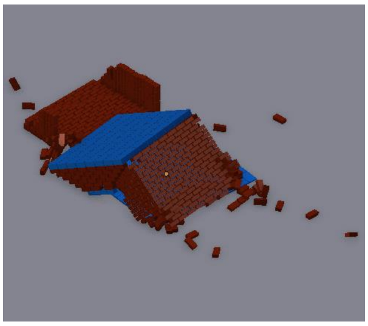	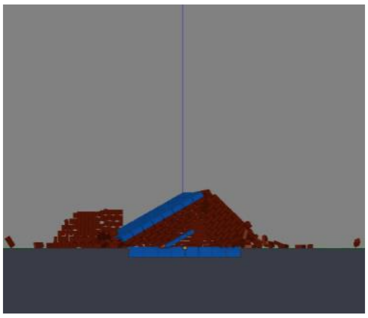	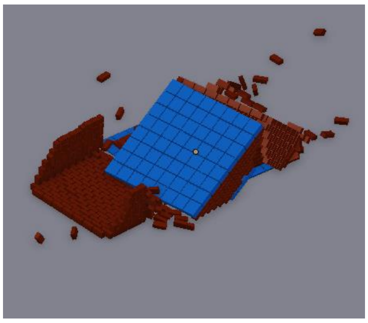
North-West (perspective)	**North**	**North-East (perspective)**
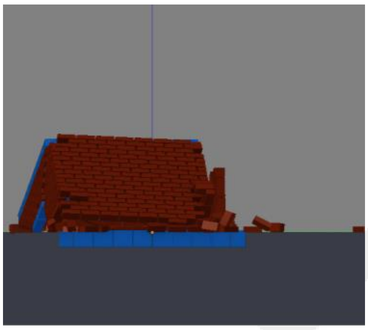	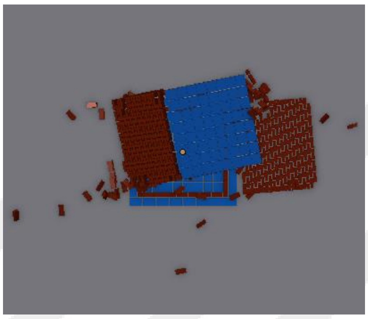	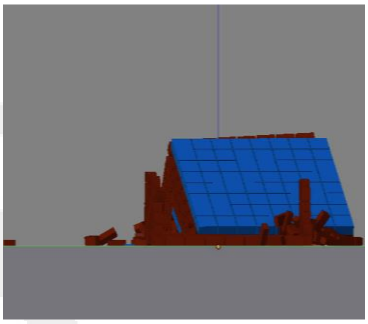
West	**Top**	**East**
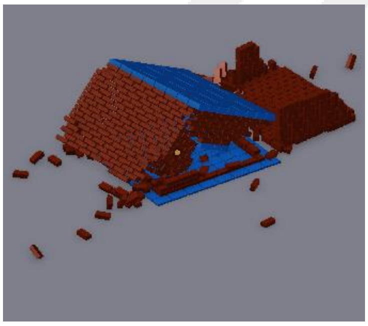	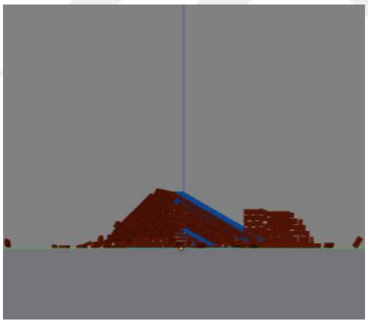	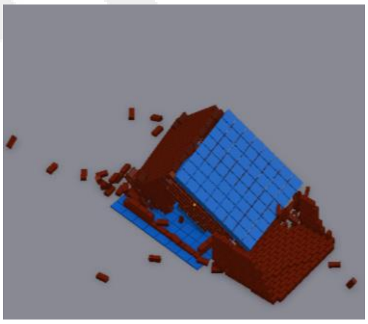
South-West (perspective)	**South**	**South-East (perspective)**

Table 5.7. Perspective and orthogonal views of the model at 7 seconds

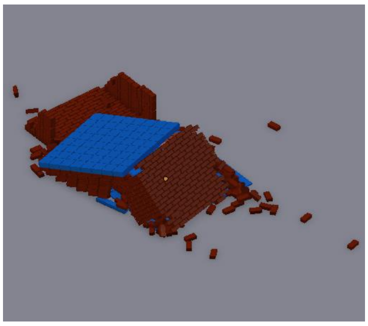	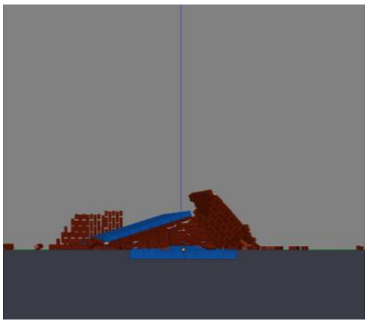	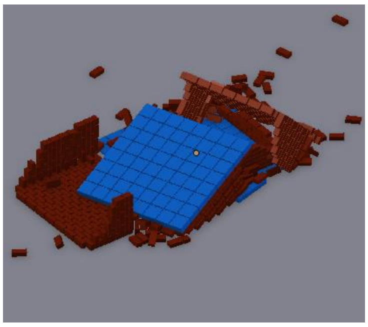
North-West (perspective)	**North**	**North-East (perspective)**
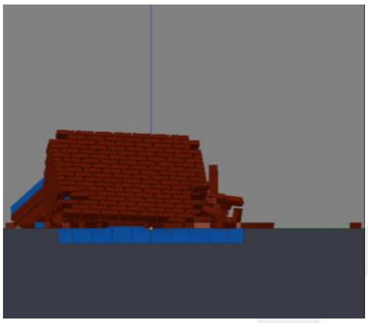	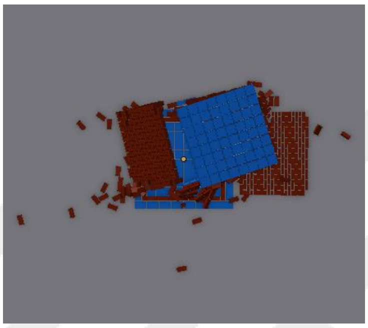	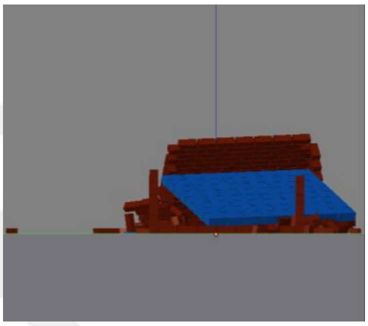
West	**Top**	**East**
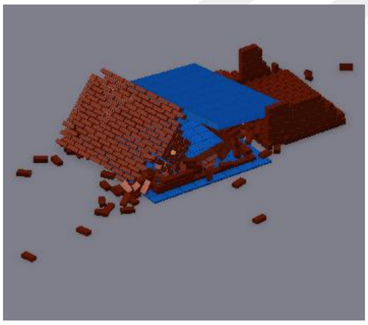	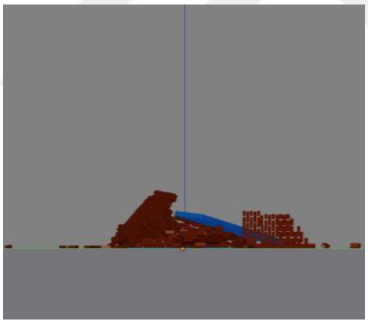	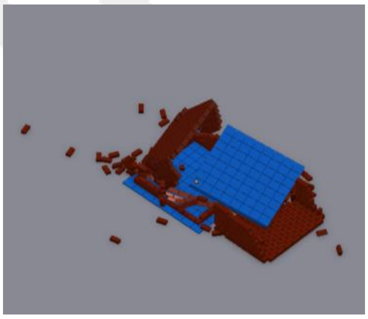
South-West (perspective)	**South**	**South-East (perspective)**

Table 5.8. Perspective and orthogonal views of the model at 8.36 seconds (Termination of ground motion)

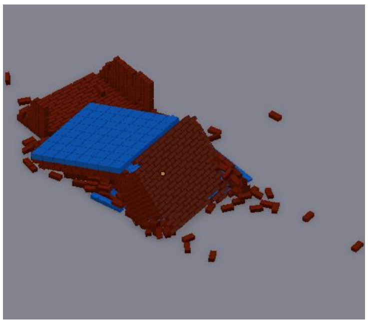	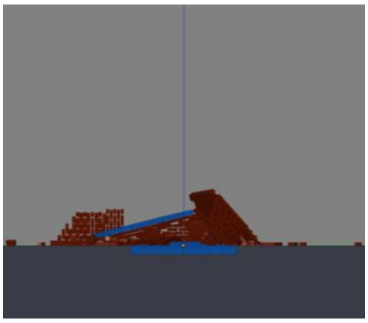	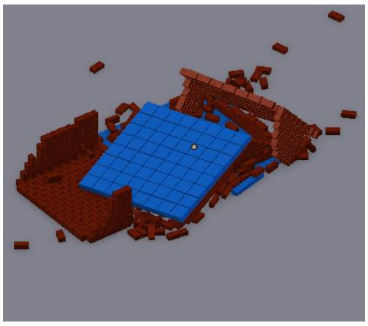
North-West (perspective)	**North**	**North-East (perspective)**
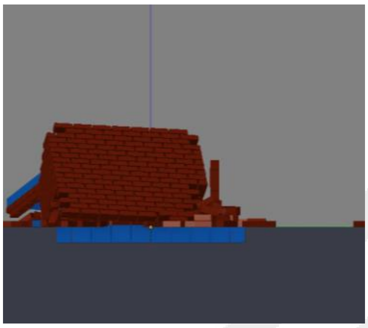	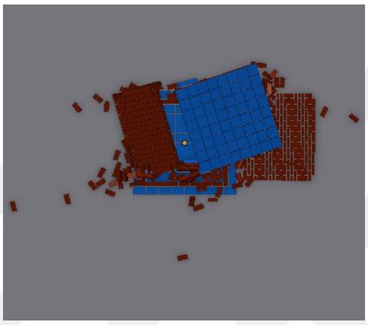	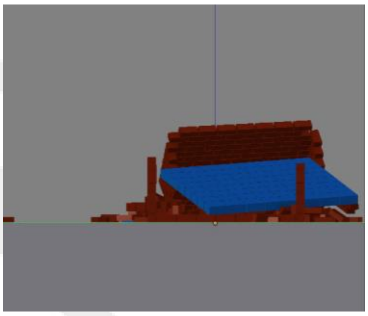
West	**Top**	**East**
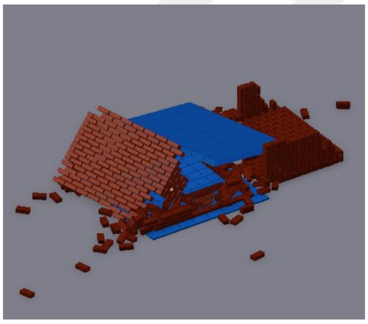	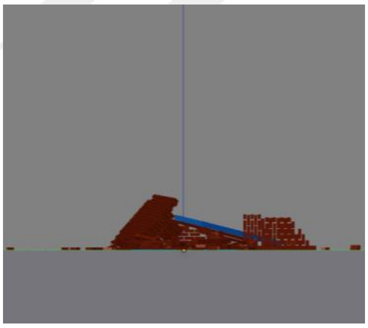	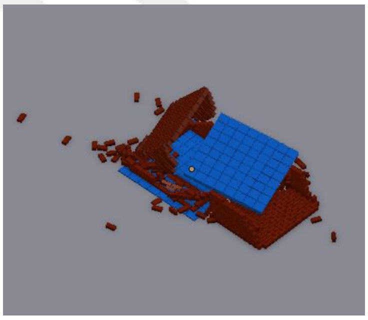
South-West (perspective)	**South**	**South-East (perspective)**

Table 5.9. Perspective and orthogonal views of the model at 10 seconds (Termination of analysis)

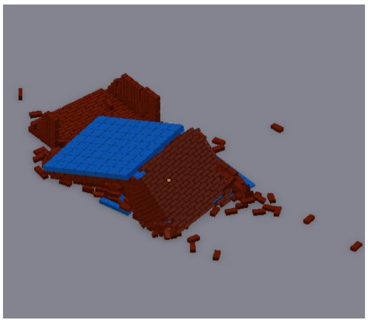	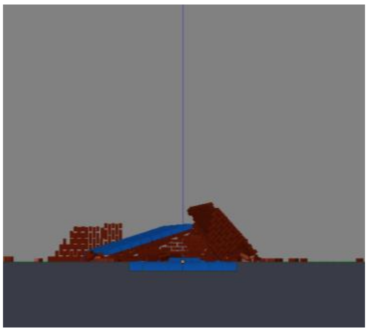	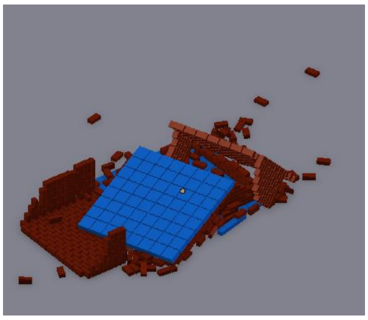
North-West (perspective)	**North**	**North-East (perspective)**
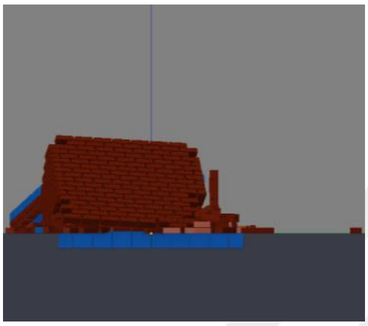	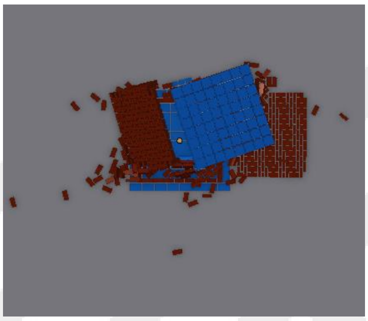	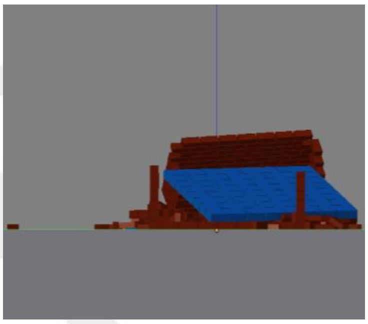
West	**Top**	**East**
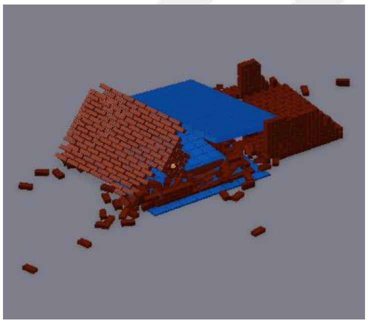	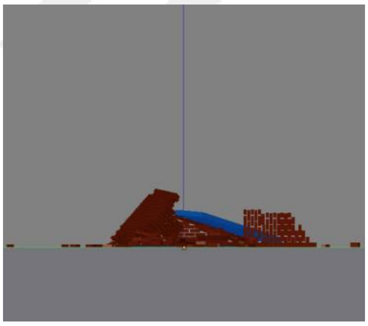	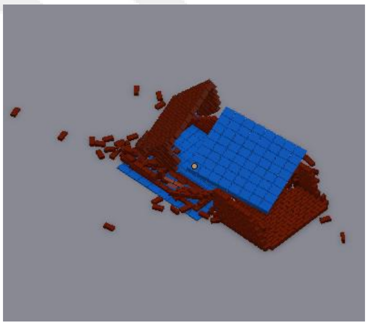
South-West (perspective)	**South**	**South-East (perspective)**

Table 5.10 Relative displacement views of the model at 2.56 seconds (Crack Initiation point).

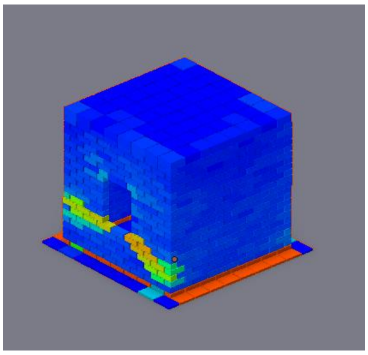	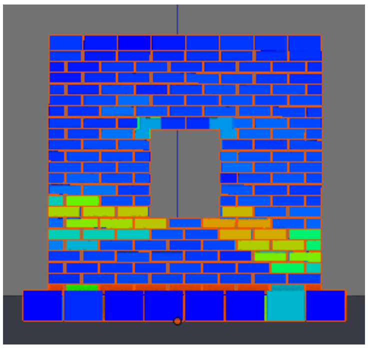	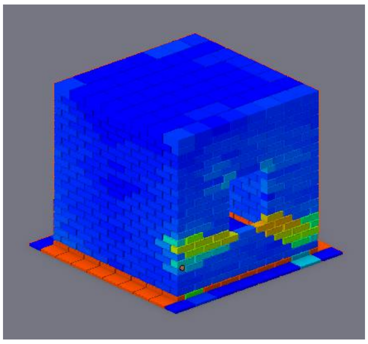
North-West (perspective)	**North**	**North-East (perspective)**
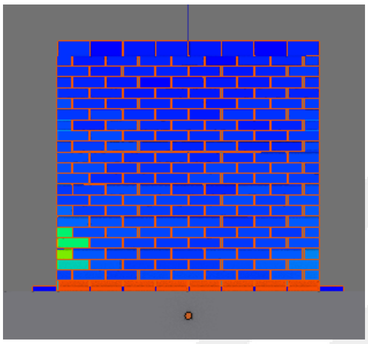	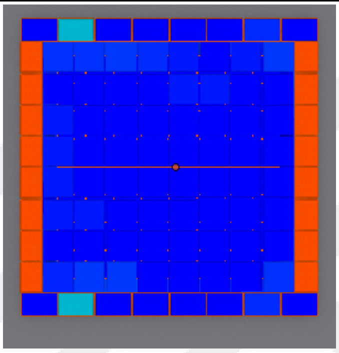	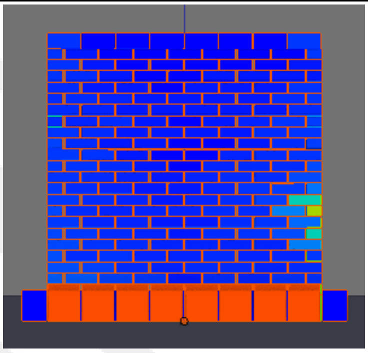
West	**Top**	**East**
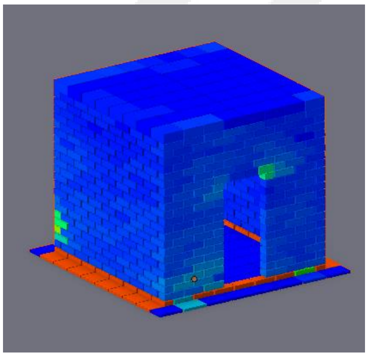	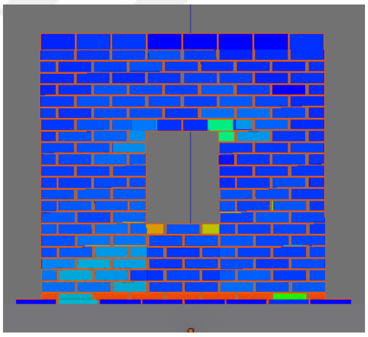	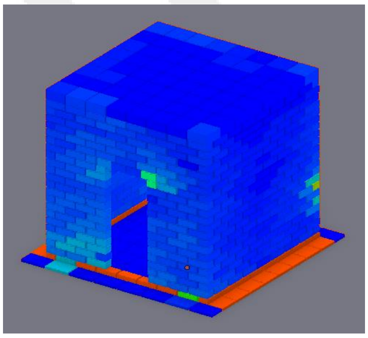
South-West (perspective)	**South**	**South-East (perspective)**

6. CONCLUSION AND RECOMMENDATIONS

Conducted ST tests provide for an understanding of the dynamic properties of masonry buildings as well as the detection of damage and mode of failure. This work provides insight into the structural state of a masonry structure in ST tests under strong ground motion. The ST experiments conducted in this study demonstrated that gradual ground movements can be damaging to masonry structures. Seven ground movements were used in this study to test the seismic performance of a masonry model constructed with perforated engineering bricks under dynamic stress. As a consequence of these seismic applications, the structure was damaged as anticipated and eventually collapsed. To evaluate the damage experimentally, ambient vibration experiments were done before and after every seismic application. The tests revealed the modal parameters for the model's undamaged and damaged states. The conclusions taken from the experimental research are presented in section 6.1. The numerical simulation was also carried out to replicate the collapse mode of the masonry model, discussed in section 6.2.

6.1. Shaking Table Test Results

The application of Northridge and Coyote EQ to masonry produced no visible damage, although an insignificant reduction in frequencies was observed. The first visible fractures were observed after the application of Parkfield EQ. This damage was classified as G-1D. Existing microcracks were substantially widened and many new ones were produced on all exterior surfaces during testing with four- and six-cycles sine waves. Most of the fractures were almost horizontal at this point and were produced by the sliding movement of the two topmost bricks just below the RC slab. The model was subsequently subjected to GMD-6 10-cycles sine function twice. The initial application triggered the existing fractures in the upper half of the walls to expand. Step-shear-sliding fractures were also spotted at the first two bricklayers slightly above the foundation level and around the support over openings. The damage at this stage was classified as G-4D. Hence the second application of the 10-cycles sine function was anticipated (which was the actual case) to produce G-5D. The structure collapsed due to an increase in out-of-plane deformations in the model. As a result, the model's static stability diminished. Simultaneously, the breadth of the staircase-shaped diagonal crack at the right top corner of the door expanded significantly, and the model eventually collapsed.

Many staircase-shaped diagonal and near-horizontal cracks were clearly discovered in the top and lower parts of the walls as a consequence of progressive dynamic tests. Following the application of the GMD-3 Parkfield Earthquake, where the first microcracks were spotted and the damage condition in the building was classed as G-1D. The GMD-5 six-cycle Sine Wave created shear-sliding fractures in the top portion of the walls with a corresponding G-2D structural damage. The structural damage associated with the G-5D type was caused by the second application of GMD-6 ten-cycles sine function. The measurement wasn’t possible at this point due to the collapse of the model.

Since the northern and southern walls had differing opening ratios, there were considerable discrepancies in the relative displacements collected at the roof's corners. These discrepancies depict the presence of torsional movement along the Z axis at the slab level of the model. This also had an effect on the walls' in-plane rigidity. The differences were estimated as follows: 56.88% for the GMD-3, 73.97% for the GMD-5 and 79.37% for the GMD-6. The opening areas for the southern wall were $0.45m^2$ and $0.25m^2$ for the northern wall.

6.2. Blender Simulation

The primary goal of a collapse simulation is to show the expected damage pattern and/or debris generation. However, it may be used to further study the implications of a building collapse due to EQ. This approach is primarily intended to visually simulate the impact of the EQ on the building. This approach enables the re-creation of historical EQs as well as the prediction of the disastrous repercussions of future EQs. The structural behaviour can be visualized prior to seismic movements using the techniques presented in this research. A realistic and effective simulation in which the half-scale masonry structure is subjected to progressive seismic action until collapse was carried out. Although the debris formation differs, the damage pattern appears to be a perfect fit. Hence this technique might aid engineers in the decision-making process for strengthening and retrofitting. This technique could also be extended to explosion analysis for examination of various risk/threat scenarios (although not discussed within the scope of this study). Visualize probable cracks inside the structure.

To take complete advantage of the simplified software for structural application, important parameters such as Elasticity modulus, Poisson ratio, Shell object etc. should be incorporated. Also, the python script for relative displacement visualization should be updated to permit the extraction of displacement values which will also be extended to the extraction of force and stress values.

7. REFERENCES

1. Lourenco, P. B., Computational Strategies for Masonry Structures, PhD Thesis, Delft: Delft University Press, 1996.

2. Britannica, T., Editors of Encyclopaedia, "Masonry," 2017.

3. Hrvoje, S., Nikolina, Ž. and Željana, N., Overview of the methods for the modelling of historical masonry structures, Gradevinar, (2013) 603-618.

4. Heyman, J., The Stone Skeleton - Structural Engineering of Masonry Architecture, Cambridge University Press, Cambridge, 1995.

5. Bakeer, T., Collapse Analysis Of Masonry Structures Under Earthquake Actions, PhD thesis, TU Dresden, Dresden, 2009.

6. Oliveira, D. V. C., Experimental and numerical analysis of blocky masonry structures under cyclic loading, PhD Thesis, Universidade do Minho, Minho, 2003.

7. Roca, P., Gonzálcz, J., Dilate E. and Lourenço, P.B., Experimental And Numerical Issues In The Modelling Of The Mechanical Behaviour Of Masonry, Structural Analysis Of Historical Constructions Il, (1998) 58-91.

8. Reilinger, R., Toksoz, N., McClusky S. and Barka, A., 1999 Izmit, Turkey Earthquake Was No Surprise, GSA Today, vol. 10, 1 (2000) 1-6.

9. Noort, J. V., Computational Modelling of Masonry Structures, MSc Thesis, Delft University Press, Delft, 2012.

10. Aşıkoğlu, A., Vasconcelos, G., Lourenço, P. B., and Pantò, B., Pushover analysis of unreinforced irregular masonry buildings: Lessons from different modeling approaches, Engineering Structures, 218, 10830 (2020) .

11. Smith, N., "The seven ages of materials," 9 September 2019. [Online]. Available: https://eandt.theiet.org/content/articles/2019/09/the-seven-ages-of-materials/.

12. Billington, D. P., Shirley-Smith H. and Billington, P. N., Bridge, https://www.britannica.com/technology/bridge-engineering 27 March 2022.

13. Lourenço, P. B., "Computations of historical masonry constructions," Progress in Structural Engineering and Materials, 4, 3 (2002) 301 - 319.

14. Admin, Syrian Beehive Houses, EarthArchitecture.org17 September 2021.

15. Economidou, V., Cycladic Settlements In The Early Bronze Age And Their Aegean Context, PhD Thesis, University College London, London,1993.

16. Croci, G. A., The conservation and structural restoration of architectural heritage, WITPress- Advances in Architecture, Rome, 1998.

17. Musgrove, J., A Hıstory Of Archıtecture, Butterworths, London, 1987.

18. Warren, K., The Roman Aqueduct Of Segovia: Bringing Water To The City, https://www.worldwidewriter.co.uk/exploring-roman-aqueduct-of-segovia.html 28 march 2022.

19. Filliâtre, P., 5 Facts About The Pont Du Gard To Impress Your Friends, https://www.france.fr/en/occitanie-south-of-france/list/5-facts-about-the-pont-du-gard-to-impress-your-friends 28 March 2022.

20. Drysdale, R. G., Ahmad, H. A. and Lawrie, B. R., Masonry structures-Behaviour and Design., Prentice-Hall Inc., Englewood Cliffs, New Jersey 1994.

21. History.com Editors, Parthenon, A&E Television Networks, https://www.history.com/topics/ancient-greece/parthenon 28 March 2022.

22. Dendrinos, D. S., On the Lions Gate at Mycenae: Its Geometry and Roots, Mathematics in archeological artifacts and structures, (2017).

23. Drysdale, R., A. Hamıd and L. Baker, Masonry Structures Behaviour and Design, (3rd edition), The Masonry Society, Boulder, Colorado, 2008.

24. Martinelli, P. and Filippou, F. C., Simulation of the shaking table test of a seven-story shear wall building, Earthquake Engineering & Structural Dynamics, 38, 5, (2009) 587– 607.

25. Saranik, M., Lenoir, D., and Jézéquel, L., "Shaking table test and numerical damage behaviour analysis of a steel portal frame with bolted connections," Computers & Structures, 112-113, 4 (2012) 327–341.

26. González, Caballero A., Fehling, E. and Kieker, J., ESECMaSE - Enhanced Safety and Efficient Construction of Masonry Structures in Europe, European joint research project on the shear load-bearing behavior of masonry components, Masonry Journal of Technology and Architecture, 9,5 (2005) 238-243.

27. Li, S., Wu C. and Kong, F., Shaking Table Model Test and Seismic Performance Analysis of a High-Rise RC Shear Wall Structure, Shock and Vibration, (2019) 1-17.

28. Carydis, P. and Mouzakis, Static and Dynamic Shear Test on Structural Members - Technical Report D7 of the Collective Research Project ESECMaSE, National Technical University of Athens, Laboratory for Earthquake Engineering, Athens, 2007.

29. Lin, Y., Leng, W., Yang, G., Li, L. and Yang, J., Seismic response of embankment slopes with different reinforcing measures in shaking table tests, Natural Hazards, 76, 2 (2015) 791-810.

30. Chen, G., Wang, Z., Zuo, X., Du, X. and Gao, A. H., Shaking table test on the seismic failure characteristics of a subway station structure on liquefiable ground, Earthquake Engineering & Structural Dynamics, 42,10 (2013) 1489–1507.

31. Srilatha, N., Latha, G. M. and Puttappa, C. G., Effect of frequency on seismic response of reinforced soil slopes in shaking table tests, Geotextiles and Geomembranes, 36, 1 (2013) 27–32.

32. Liu, W., Qin, C., Liu, Y., He W. and Yang, Q., Shaking table tests on earthquake response characterization of a complex museum isolated structure in high intensity area, Shock and Vibration, (2016) 1-23.

33. Lu, X., Zou, Y., Lu, W. and Zhao, B., Shaking table model test on Shanghai world financial center tower, Earthquake Engineering & Structural Dynamics, 36,4 (2007) 439–457.

34. Lignos, D. G., Chung, Y., Nagae, T. and Nakashima, M., Numerical and experimental evaluation of seismic capacity of high-rise steel buildings subjected to long duration earthquakes, Computers & Structures, 89,11-12 (2011) 959–967.

35. Graziotti, F., Tomassetti, U., Kallioras, S., Penna A. and Magenes, A. G., Shaking table test on a full scale URM cavity wall building, Bulletin of Earthquake Engineering, 15,12 (2017) 5329–5364.

36. Morris, H. M. and Albert H. A., Vitruvius: The Ten Books of Architecture (English Translated), Harvard University Press, Cambridge, 1914.

37. Bhanushree, The Eads Bridge that received the assent from an elephant, https://historychunks.com/index.php/2021/12/01/the-eads-bridge-that-received-the-assent-from-an-elephant/ 27 March 2022.

38. Hooke, R., A Description of Helioscopes and Some Other Instruments, Printed by T.R. for John Martyn - Provided by ETH-Bibliothek Zürich, Rar 4339, London, 1676.

39. Rogermong, The Enigma of Robert Hooke, https://quantumfrontiers.com /2015/08/31/the-enigma-of-robert-hooke/ 28 December 2021.

40. Garrison, E., Advancements in Arch Analysıs and Desıgn Durıng the Age of Enlıghtenment, MSc Thesis, Kansas State Unıversıty, Manhattan, Kansas, 2016.

41. Poleni, G., Memorie istoriche della gran cupola del tempio vaticano, e de'danni di essa, e de'ristoramenti loro, divise in libri cinque, Stamperia del Seminario, Padova, 1748.

42. Heyman, J., "Couplet’s engineering memoirs 1726-33," History and Technology, 1, (1976) 21-44.

43. Coulomb, C. A., "Essai sur une application des regles des maximis et minimis à quelques problémes de statique relativs a l’arquitecture," in Mémoires de mathematique et de physique présentés à l’académie royal des sciences per divers savants et lus dans ses assemblées, France, Royal Academy, 1773, 343–382.

44. Fajfar, P., A non-linear analysis method for performance-based seismic design, Earthquake Spectra, 16,3 (2000) 573–592.

45. Molins, C. and Roca, P., Capacity of masonry arches and spatial frames, Journal of Structural Engineering, ASCE, 124, (1997) 653-663.

46. Belmouden, Y. and Lestuzzi, P., An equivalent frame model for seismic analysis of masonry and reinforced concrete buildings, Construction and Building Materials, 23, (2009) 40-53.

47. Sima, J. F., Roca, P. and Molins, C., Nonlinear response of masonry wall structure subjected to cyclic and dynamic loading, Engineering Structures, 33, (2011) 1955-1965.

48. Cundall, P. A. and Hart, R. D., Numerical modelling of discontinua, First US Conference on Discrete Element Methods, Colorado, 1989.

49. Cundall, P. A., A computer model for simulating progressive large scale movements in blocky rock systems, International Symposium on Rock Fracture (ISRM), Nancy, France, 1971.

50. Dolatshahi, K. M. and Aref, A. J., Computational, Analytical, and Experimental Modeling of Masonry Structures, MCEER Thrust Area 2, Sustainable and Resilient Buildings, New York, 2015.

51. Massart, T. J., Multi-scale modeling of damage in masonry structures, PHd Thesis, Technische Universiteit Eindhoven, Eindhoven, 2003.

52. Bustamante, A. O., Seismic Assessment of Ancient Masonry Structures by Rigid Blocks Limit Analysis, PhD Thesis, University of Minho, Department of Civil Engineering, Guimarães, 2003.

53. Seyedrezai, S., Modeling of Arching Unreinforced Masonry Walls Subjected to Blast Loadings, MSc Thesis, McMaster University, Ontario, 2011.

54. ORR, A., Damage and Vulnerability Analysis of Debris Slide Impacts to Buildings through Analytical Methods, MSs. Thesis, University of Twente, Twente, 2019.

55. Fıta, J. L., Besuıevsky, G. and Patow, G., Earthquake Simulation on Ancient Masonry Buildings, Journal on Computing and Cultural Heritage, 13, 2 (2020) 1-18.

56. Furukawa, A., Spence, R., Ohta, Y. and So, E., Analytical study on vulnerability functions for casualty estimation in the collapse of adobe buildings induced by earthquake, Bulletin of Earthquake Engineering, 8 (2010) 451–479.

57. Köseoğlu, G. Ç., Investıgatıon Of A Damaged Hıstorıcal Mosque Wıth Fınıte Element Analysıs, Msc Thesis, Mıddle East Technıcal Unıversıty, Ankara, 2011.

58. Beattie, G., Joint Fracture in Reinforced and Unreinforced Masonry under Quasi-Static and Dynamic Loading, PhD Thesis, University Of Liverpool, Liverpool, 2003.

59. County Surveyors Society (Great Britain), The assessment and design of unreinforced masonry vehicle parapets: County Surveyors' Society guidance note., Preston: Lancashire County Council, Surveyor's Department, 1995.

60. BS 6779-4:1999, Highway Parapets for Bridges and Other Structures - Part 4: Specification for Parapets of Reinforced and Unreinforced Masonry Construction, British Standards Institution, 1999.

61. ASTM C 270, Standard Specification for Mortar for Unit Masonry, Subcommittee C12.03 on Specifications for Mortars, West Conshohocken: ASTM International, 2010.

62. Shakya, J., Brick masonry – Types, Tools, materials required and Procedure, Civil Concept, https://www.civilconcept.com/brick-masonry/?v=c86ee0d9d7ed 10 May 2022.

63. Grünthal, G., European Macroseismic Scale 1998, Luxembourg, 1998.

64. Lee, W. Concrete Plastıcıty: Macro And Mıcro Approaches, Concrete Plastıcıty: Macro and Mıcro Approaches, Advances in Engineering Plasticity and its Applications, 1993, 27-34.

65. Belytschko, T. and Bazant, Z. P., Strain-softening materials and finite element solutions, ASME Symposium on Constitutive Equations: Macro, Micro and Computational Aspects, New Orleans, 1984.

66. Hordijk, D. A., Local approach to fatigue of concrete, PhD Thesis, Delft University of Technology, Delft, 1991.

67. Van der Pluijm, R., Out-of-plane bending of masonry - behaviour and strength, PhD Thesis, Eindhoven University of Technology, Eindhoven, The Netherlands, 1999.

68. Vasconcelos, G. F., Experimental investigations on the mechanics of stone masonry: Characterization of granites and behavior of ancient masonry shear walls, PhD Thesis, University of Minho, Guimarães, Portugal, 2005.

69. Coulomb, C. A., Remarque sur la rupture des corps - Mémoires presentés par ivers savants à l' Académie, 1776.

70. Griffith, A. A, The Phenomena of Rupture and Flow in Solids, Philosophical Transactions of the Royal Society of London, A,221 (1921) 163-198.

71. Eberhardt, E., Stead, D. and Stimpson, B., Quantifying Progressive Pre-Peak Brittle Fracture Damage in Rock during Uniaxial Compression, International Journal of Rock Mechanics and Mining Sciences, 36,6 (1999) 361-380.

72. Hillerborg, A., Modéer,M. and Petersson P. E., Analysis of crack formation and crack growth in concrete by means of fracture mechanics and finite elements, Cement and Concrete Research, 6, (1976) 773-782.

73. Page, A. W., The Bıaxıal Compressıve Strength Of Brıck Masonry, Proceedings Of The Institution Of Civil Engineers, 1981.

74. Nelissen, L. J. M., Biaxial Testing Of Normal Concrete, Heron, 18,1 (1972) 7-80.

75. Dhanasekar, M., Page, A. W. and Kleeman, P. W., The Faılure Of Brıck Masonry Under Bıaxıal Stresses, Proceedings Of The Institution Of Civil Engineers, 79, 2 (1985) 295-313.

76. Schwer, L. E., Laboratory Tests for Characterizing Geomaterials, Proceedings of the FEA Information News for the World-wide Engineering Community, 2001.

77. Turkish Earthquake Code: Specifications for Building Design Under Earthquake Effects, Ankara, 2019.

78. Pacific Earthquake Engineering Research Center, PEER Strong Ground Motion Databases, https://peer.berkeley.edu/peer-strong-ground-motion-databases September 2021.

79. Chellappa, S. and Dubey, R. N., Performance Evaluation of a Reinforced Masonry Model and an Unreinforced Masonry Model Using a Shake Table Testing Facility, Journal of Performance of Constructed Facilities, 32,1 (2017).

80. Ganz, H. R., Masonry walls subjected to normal and shear forces, PhD Thesis, ETH Zurich Research Collection, Zurich, 1985.

81. Calvi, G. M., A Dısplacement-Based Approach For Vulnerabılıty Evaluatıon Of Classes Of Buıldıngs, Journal of Earthquake Engineering, 03,03, (1999) 411-438.

82. Graziotti, F., Penna, A. and Magenes, G. A comprehensive in situ and laboratory testing programme supporting seismic risk analysis of URM buildings subjected to induced earthquakes, Bulletin of Earthquake Engineering, 17,4 (2019) 4575–4599.

83. Tomassetti, U., Correia, A. A., Candeias, P. X., Graziotti, F. and Costa, A. C., Two-way bending out-of-plane collapse of a full-scale URM building tested on a shake table, Bulletin of Earthquake Engineering, 17,3 (2019) 2165–2198.

84. Bothara, J. K., Dhakal, R. P. and Mander, J. B., Seismic performance of an unreinforced masonry building: An experimental investigation, Earthquake Engineering and Structural Dynamics, 39, 1 (2010) 45-68.

85. Ghezelbash, A., Beyer, K., Dolatshahi, K. M. and Yekrangnia, M., Shake table test of a masonry building retrofitted with shotcrete. 219, Engineering Structures, 219,110912 (2020).

86. Kai, K. and Oliver, W., "Final release of the Blender and Bullet physics engine based on fast on-site assessment tool," INACHUS, 2017.

87. Couman, E., GitHub, https://github.com/- bulletphysics/bullet3 23 June 2021.

88. T. B. institute, Blender, https://www.blender.org-/download/. 07 June 2021.

89. LUAS, GitHub, https://github.com/KaiKostack-/bullet-constraints-builder. 23 June 2021.

90. Roessler, T. and Katterfeld, A., DEM parameter calibration of cohesive bulk materials using a simple angle of repose test, Particuology, 45, (2019) 105-115.

91. Hustrulid, A. I. and Graham, G. W. M., Engineering analysis of transfer points using discrete element analysis, Geomechanics Research Center, Colorado School of Mines, Colorado, 1996.

92. Clearly, P. W., Discrete Element Modeling of Industrial Granular Flow Applications, Task - Quarterly Scientific Bulletin of Academic Computer Centre, 2,3 (1998) 385-416.

93. Bender, J., Erleben, K., Trinkle, J. and Coumans, E., Interactive Simulation of Rigid Body Dynamics in Computer Graphics, Computer Graphics Forum, 33,1 (2014).

94. Chen, P., Quantitative Study of Granular Flow, Mixing and Segregation Using the Discrete Element Method (DEM), Northwestern University Evanstión Illinois, Illinois, 2008.

95. Mirinavičius, A., Markauskas, D. and Kačianauskas, R., Computational Performance of Contact Search During DEM Simulation of Hopper Filling, 10th International Conference of Modern Buildings Materials, Structures and Techniques, Vilnius, Lithuania, 2010.

96. He, H., Zheng, J., Sun, Q. and Li, Z., Simulation of Realistic Particles with Bullet Physics Engine, E3S Web of Conferences 92, Glasgow, 2019.

97. National Aeronautics and Space Administration, Autonomous Systems-NASA Tensegrity Robotics Toolkit (NTRT) v1 (ARC-17093-1), https://software.nasa.gov/software/ARC-17093-1 06 May 2022.

98. BBZ, LEO training system for robotic surgery, https://www.bbzsrl.com/index.php/materialis/leo-3/ 25 May 2022.

99. Wikipedia, the free encyclopedia, PhysX, https://en.wikipedia.org/wiki/PhysX. 25 February 2022.

100. Russell, L. S. Open Dynamics Engine, http://www.ode.org/. 25 February 2022.

101. True Axis Pty Ltd, True Axis Physics SDK, https://trueaxis.com/physics/index.html 25 February 2022.

102. Hummel, J., Wolff, R., Stein, T., Gerndt, A. and Kuhlen, T. An Evaluation of Open Source Physics Engines for Use in Virtual Reality Assembly Simulations, Lecture Notes in Computer Science, Springer-Verlag Berlin Heidelberg, 7432 (2012) 346–357.

103. Wikipedia, the free encyclopedia, Bullet (software), Wikipedia®, https://en.wikipedia.org/wiki/Bullet_(software) 28 November 2021.

104. Martin, F., Kai, K., JT, N., Dennis, F. and V. Jens, "Fracture Modifier for Blender 2.79x, http://kaikostack.com/fracture 27 June 2021.

105. Antonio, B., Giulio, C. and Marco, C., Determination of Shear Strength of Masonry Panels Through Different Tests, International Journal of Architectural Heritage, 9,8 (2015) 913-927.

106. Liu, G., Shi, C. and Bin, J., The Shear Strength Of Unreınforced Masonry Wall, 11th Internatıonal Brickblock Masonry Conference, Shanghaı, Chına., 1997.

107. Tomazevic, M., Shear resistance of masonry walls and Eurocode 6: shear versus tensile strength of masonry, Materials and Structures (2009) 42, (2009) 889–907.

108. Enea, M., Erion, L., Marco, C., Antonio, B., Ylber, M. and Aleksandra, Z. Physical-Mechanical Properties of Stone Masonry of Gjirokastër, Albania, Materials- MPDI, 14, 5 (2021) 1127.

109. Earthquake / Masonry Building Collapse Simulation - WIP | BCB | INACHUS. [Film]. Kostack Studio, New Zealand, 2015.

110. Laird, D. A., Drysdale, R. G., Stubbs, D. W. and Sturgeon, G. R., The New CSA S304.1-04 - Desıgn Of Masonry Structures, 10th Canadian Masonry Symposium, Banff, Alberta, June 2005.

111. Doğan, O. and Odacıoğlu, O. G., An Experimental Study To Determine Sliding Shear Strength And Internal Friction Coefficient Of Clay Brick Wall In A Masonry Building, International Journal of Engineering Research and Development, 11,2 (2019) 670-676.

112. Nazir, S. and Dhanasekar, M., Modelling the failure of thin layered mortar joints in masonry, Engineering Structures, 49 (2013) 615-627.

113. Ferretti, F., Ferracuti, B., Mazzotti, C. and Savoia, M., Destructive and minor destructive tests on masonry buildings: Experimental results and comparison between shear failure criteria, Elsevier - Construction and Building Materials, 199 (2019) 12-29.

114. Lipscombe, P. R. and Pellegrino, S., Free Rockıng Of Prısmatıc Blocks, J. Eng. Mech., 119, 7 (1993) 1387-1410.

115. Tralli, A., Alessandri, C. and Milani, G., Computational Methods for Masonry Vaults: A Review of Recent Results., The Open Civil Engineering Journal. 8, (2014) 272-287.

116. Smoljanović, H., Zivaljic, N. and Nikolić, Ž., Overview of the methods for the modelling of historical masonry structures, Građevinar, 65,7 (2013) 603-618.

117. Bender, J., Erleben, K., Trinkle, J. and Coumans, E., Interactive Simulation of Rigid Body Dynamics in Computer, Computer Graphics Forum, 33,1 (2013).

8. APPENDICES

A parametric analysis, otherwise known as a sensitivity analysis, is the investigation of the effect of various geometric or physical characteristics, or both, on the solution of a problem. Hence, these appendices contain some interesting results and additional details that will provide greater insight to the interested reader. The following sections demonstrate the impact of various settings.

Appendix 1 Solver Iteration Influence

Appendix 2 Time Step Influence

Appendix 3 Connection Types

Appendix 4 Connection Type Influence

Appendix 5 Shear Value Influence

Appendix 6 Discretization Influence

Appendix 7 Fracture Modifier, why?

Appendix 1. Solver Iteration Influence

	Time of Crack Initialization		@ 4 secs	@ 6 secs	@ 8.35 secs	@ 10 secs
300	2.8	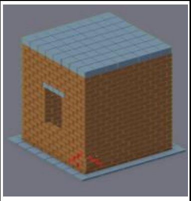	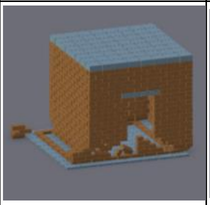	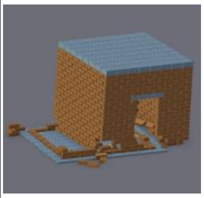	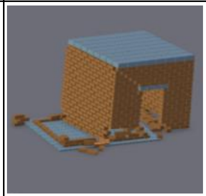	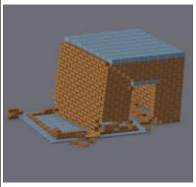
340	2.56	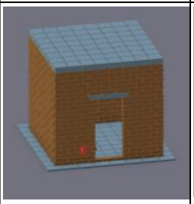	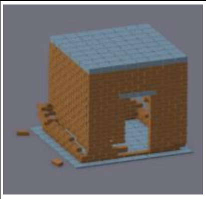		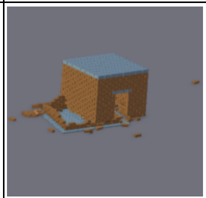	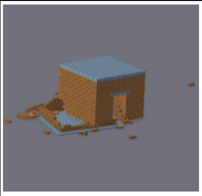
345	2.6	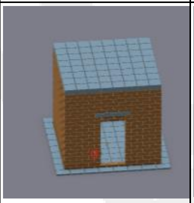	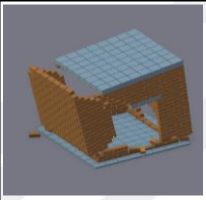		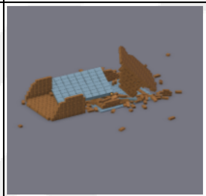	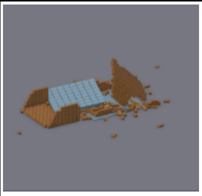
346	2.6	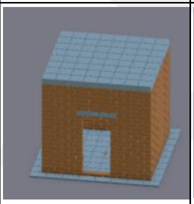	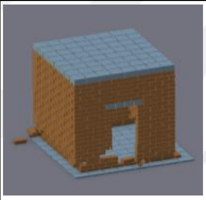	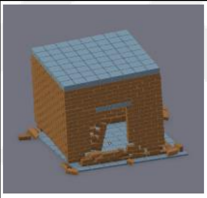	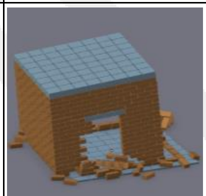	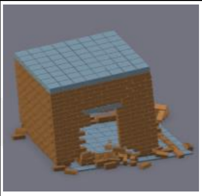
348	2.6	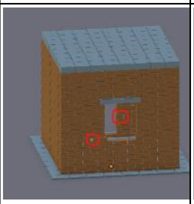	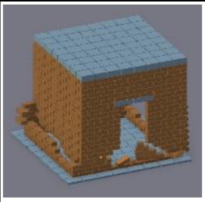	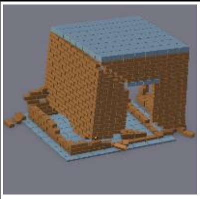	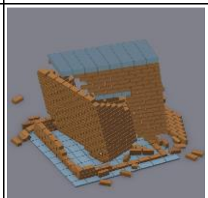	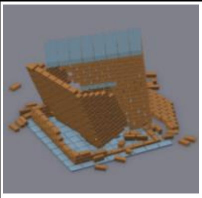
350	2.08	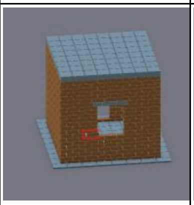	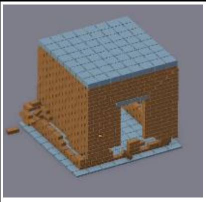	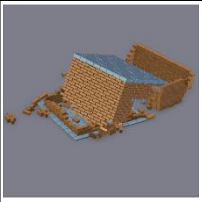	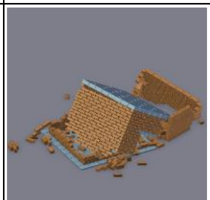	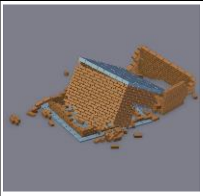
352	2.52	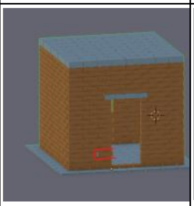	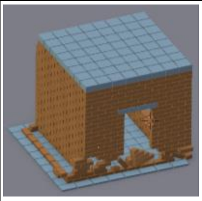		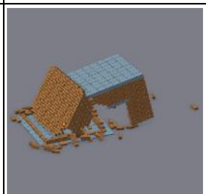	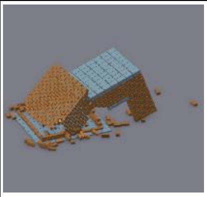

Appendix 1. continued

	Time of Crack Initialization		@ 4 secs	@ 6 secs	@ 8.35 secs	@ 10 secs
355	62.5	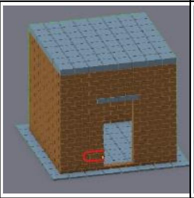	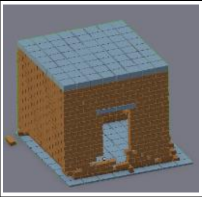	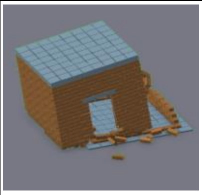	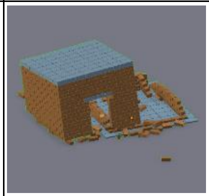	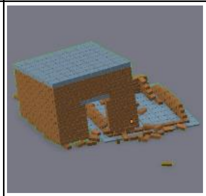
360	63	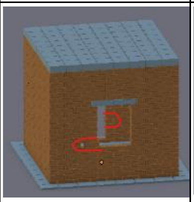	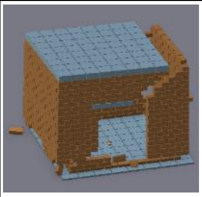	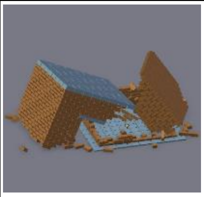	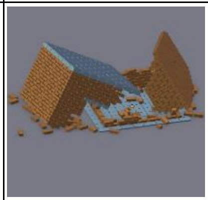	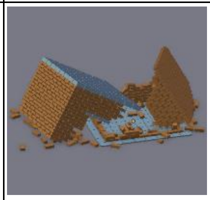
400	51.5	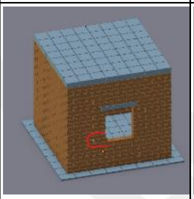	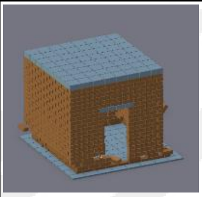	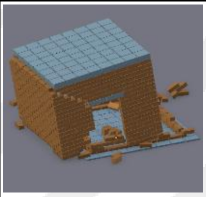	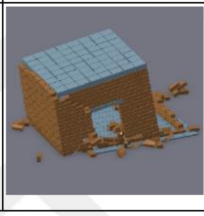	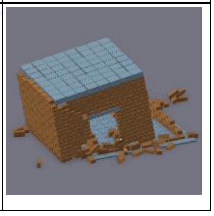

Appendix 2. Time Step Influence

	Time of Crack Initialization		@ 4 secs	@ 6 secs	@ 8.35 secs	@ 10 secs
100	2.04	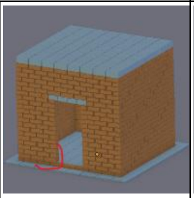	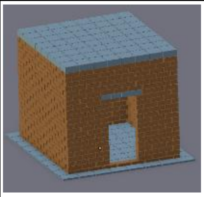	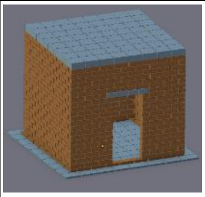	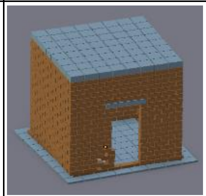	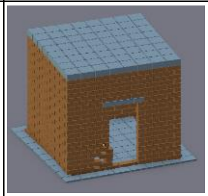
150	-	No visible physical damage was observed	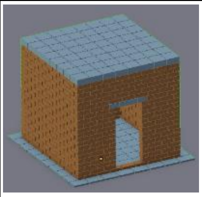	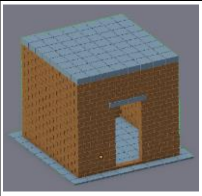	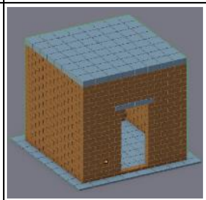	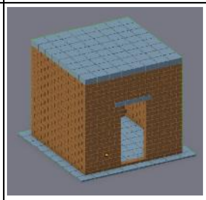
180	3.02	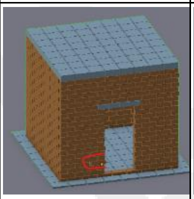	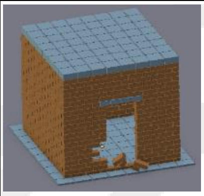	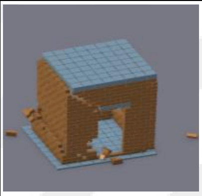	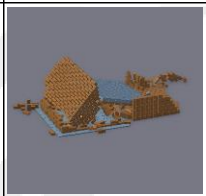	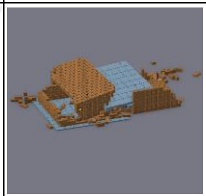
190	3.22	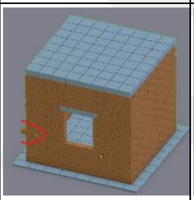	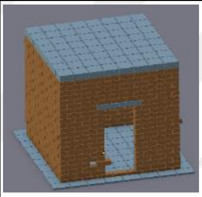		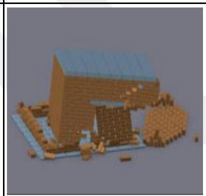	
210	2.08	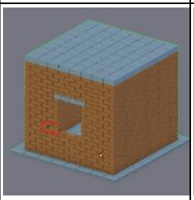	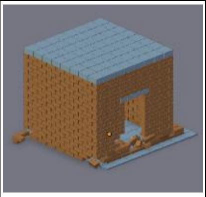		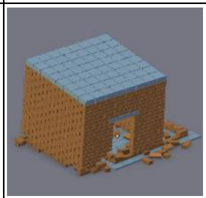	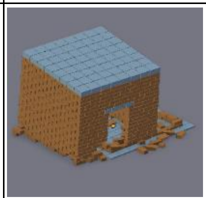
220	2.36	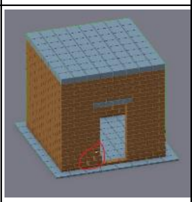	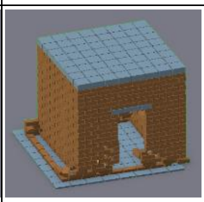	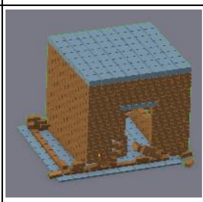	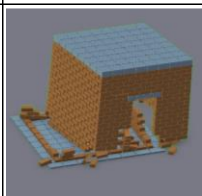	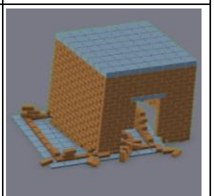
250	2.04	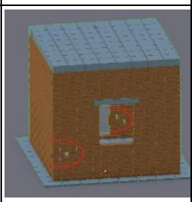	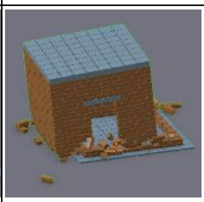	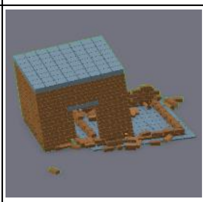	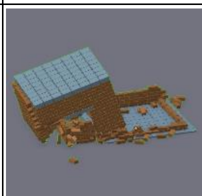	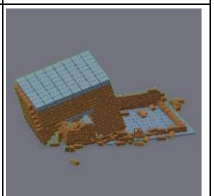

Appendix 2. continued

	Time of Crack Initialization		@ 4 secs	@ 6 secs	@ 8.35 secs	@ 10 secs
300	1.8	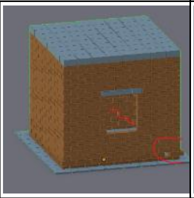	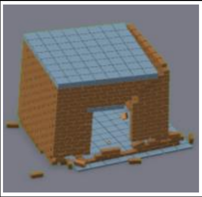	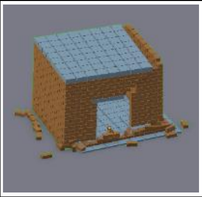	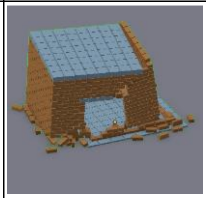	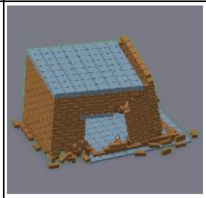
400	1.04	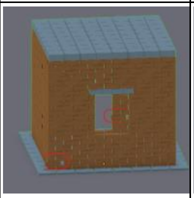	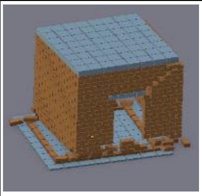	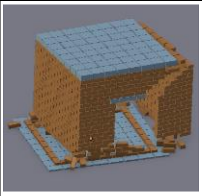	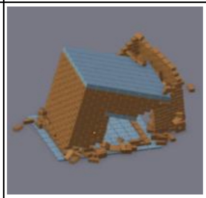	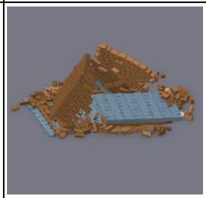
500	0.84	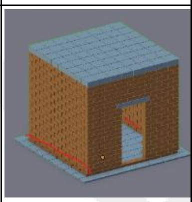	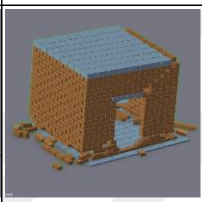	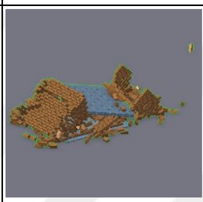	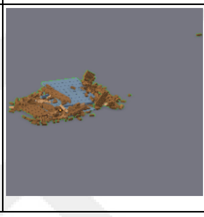	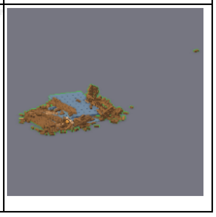

Appendix 3. Connection Types

CT ID	Name in BCB interface	Constraint Count	Short Description
0	PASSIVE	0	Passive (all other connection types will have priorityover it)
1	1x FIXED	1	Linear omni-directional + bending breaking threshold
2	1x POINT	1	Linear omni-directional breaking threshold
3	1x POINT + 1x FIXED	2	Linear omni-directional and bending breaking thresholds
4	2x GENERIC	2	Compressive and tensile breaking thresholds
5	3x GENERIC	3	Compressive, tensile + shearing and bending breaking thresholds
6	4x GENERIC	4	Compressive, tensile, shearing and bending breakingthresholds
7	3x SPRING	3	Linear omni-directional breaking threshold withplastic deformability
8	4x SPRING	4	Linear omni-directional breaking threshold withplastic deformability
9	1x FIXED + 3x SPRING	4	Linear omni-directional + bending breaking thresholdwith plastic deformability
10	1x FIXED + 4x SPRING	5	Linear omni-directional + bending breaking thresholdwith plastic deformability
11	4x GENERIC + 3x SPRING	7	Compressive, tensile, shearing and bending breakingthresholds with plastic deformability
12	4x GENERIC + 4x SPRING	8	Compressive, tensile, shearing and bending breakingthresholds with plastic deformability
13	3 x 3x SPRING	9	Compressive, tensile and shearing breaking thresholds with plastic deformability
14	3 x 4x SPRING	12	Compressive, tensile and shearing breaking thresholds with plastic deformability
15	6x GENERIC	6	Compressive, tensile, shearing XY and bending XYbreaking thresholds
16	7x GENERIC	7	Compressive, tensile, shearing XY and bending XYand torsion breaking thresholds
17	6x GENERIC + 3x SPRING	9	Compressive, tensile, shearing XY and bending XYbreaking thresholds with plastic deformability
18	7x GENERIC + 3x SPRING	10	Compressive, tensile, shearing XY and bending XYand torsion breaking thresholds with plastic deformability

Appendix 3. Continued

19	1x FIXED + 1x SPRING	2	Linear omni-directional + bending breaking threshold with plastic deformability
20	1x PNT + 1x FXD + 1x SPR	3	Linear omni-directional and bending breaking thresholds with plastic deformability
21	4x GENERIC + 1x SPRING	5	Compressive, tensile, shearing and bending breakingthresholds with plastic deformability
22	6x GENERIC + 1x SPRING	7	Compressive, tensile, shearing XY and bending XYbreaking thresholds with plastic deformability
23	7x GENERIC + 1x SPRING	8	Compressive, tensile, shearing XY and bending XYand torsion breaking thresholds with plastic deformability

Appendix 4. Connection Type Influence

	Time of Crack Initialization		@ 4 secs	@ 6 secs	@ 8.35 secs	@ 10 secs
4	1.28	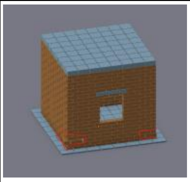	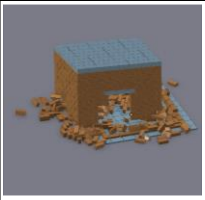	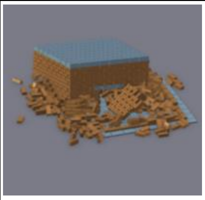	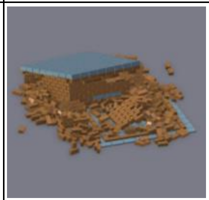	
5	1.32	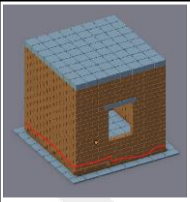	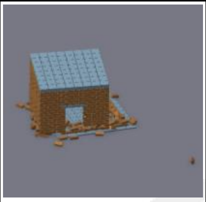	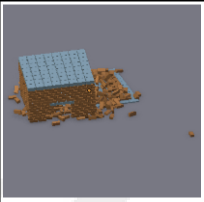	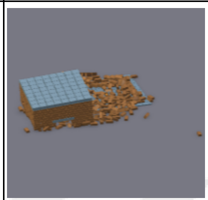	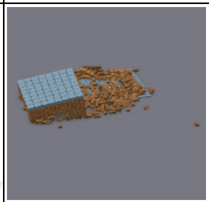
6	2.84	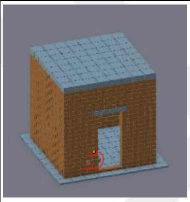	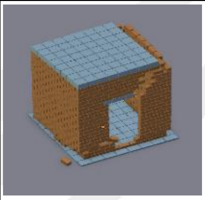	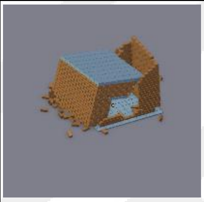	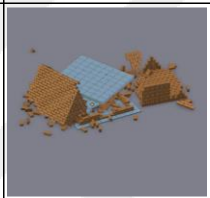	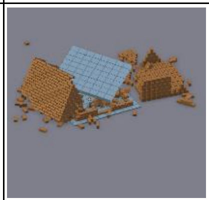
12	2.92	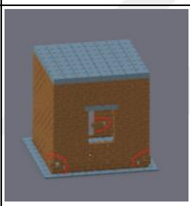	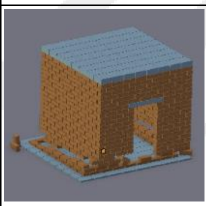	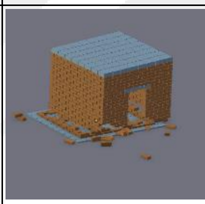	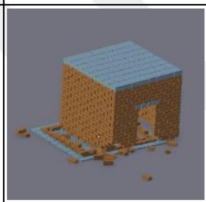	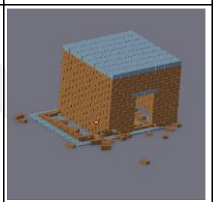
13	1.72	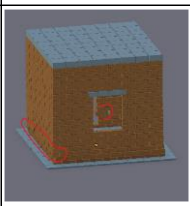	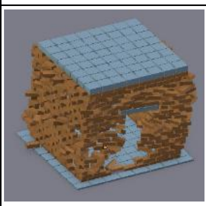	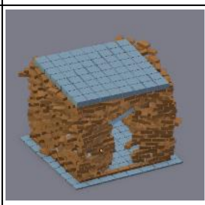	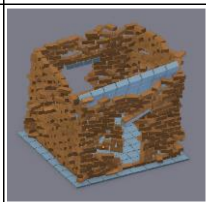	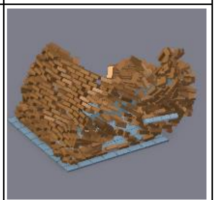
16	3.04	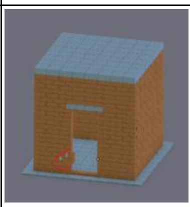	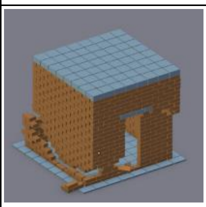	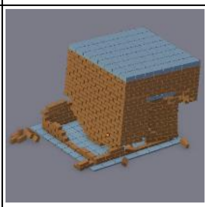	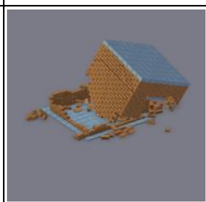	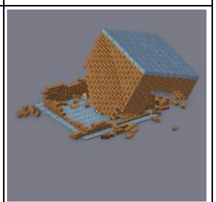
17	3.12	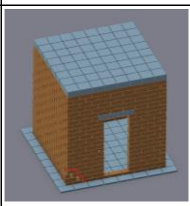	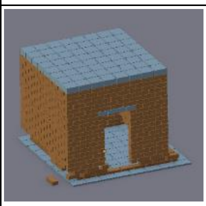	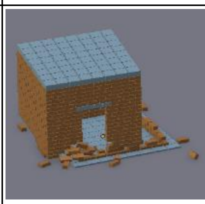	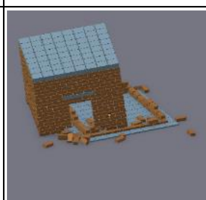	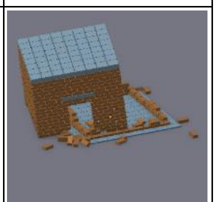

Appendix 5. Influence of Mathematical Expression and GradientFactor on Shear Value

	Time of Crack Initialization		@ 4 secs	@ 6 secs	@ 8.35 secs	@ 10 secs
Without Formula	1.24	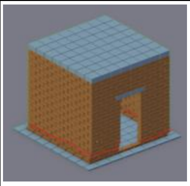	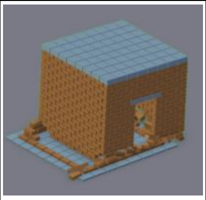			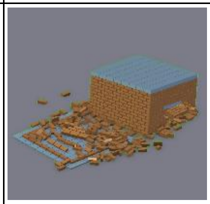
0.02	1.68	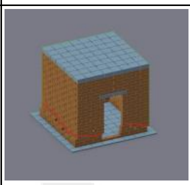	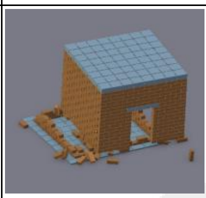	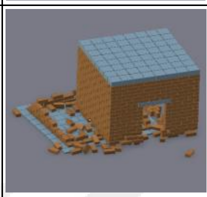	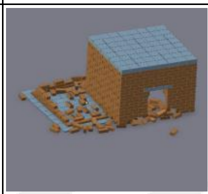	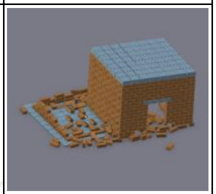
0.04	2	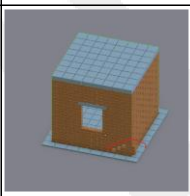	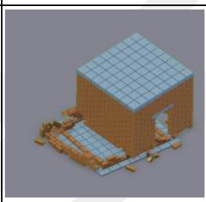	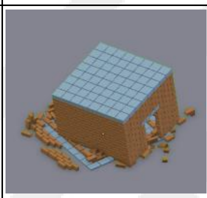	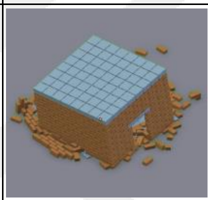	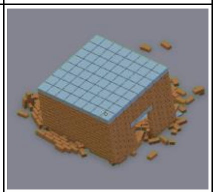
0.06	2.04	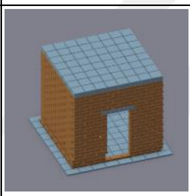	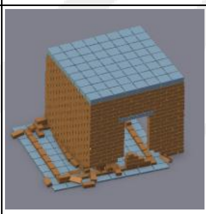	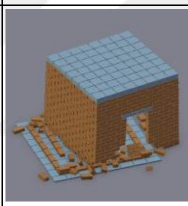	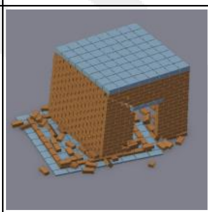	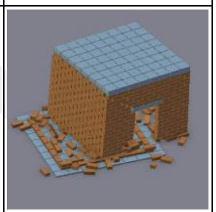
0.08	2.72	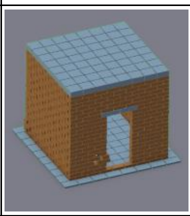	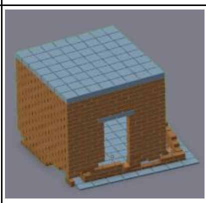	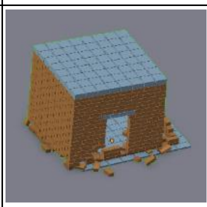	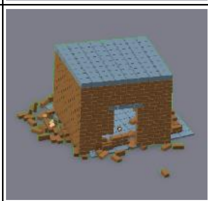	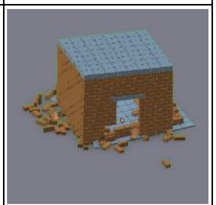
0.2	-	No visible physical damage was observed	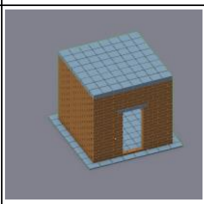	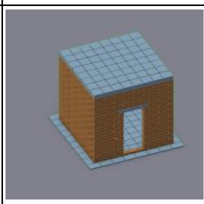	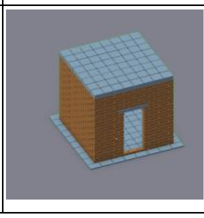	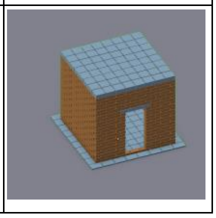

Appendix 6. Discretization Influence

	Time (secs)	Time of Crack Initialization		@ 4 secs	@ 6 secs	@ 8.35 secs	@ 10 secs
3.0	726.82	2.52	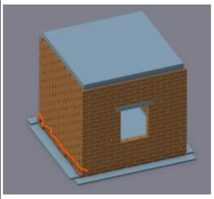	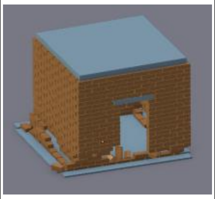	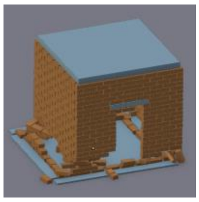	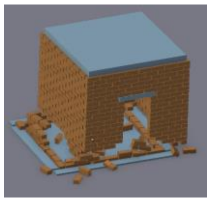	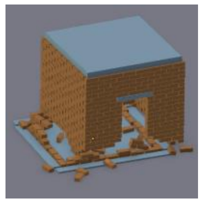
2.5	822.98	2.48	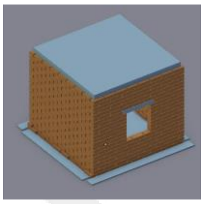	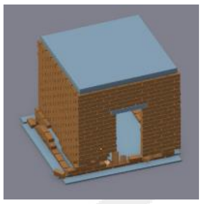	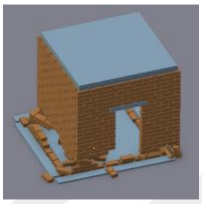		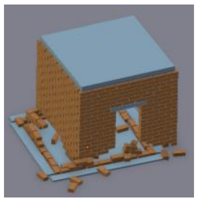
2.0	879.65	2.32	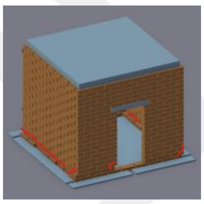	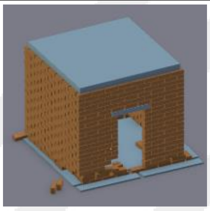	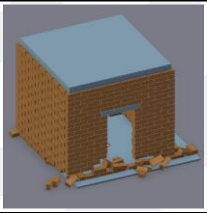	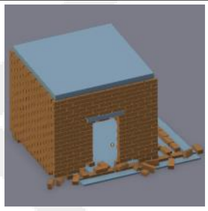	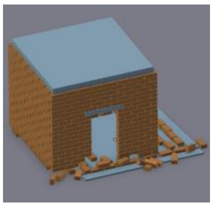
1.5	912.54	2.64	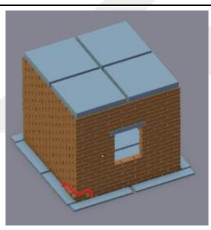	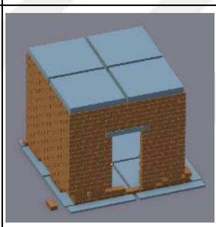	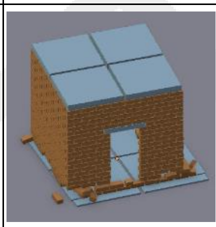	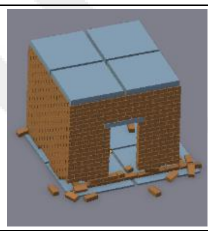	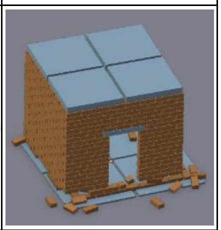
1.0	934.8	2.82	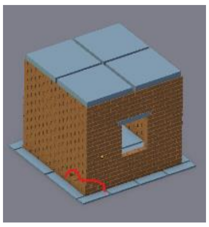	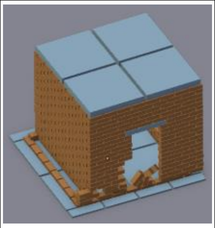	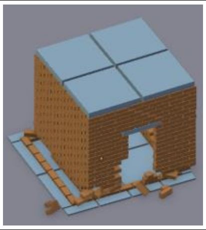	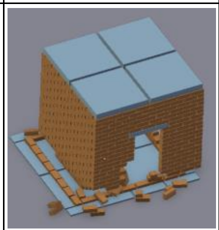	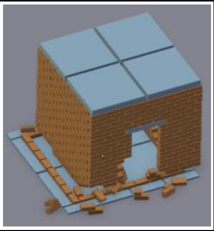
0.5	992.07	2.32	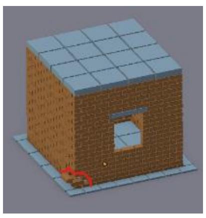	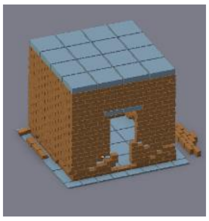	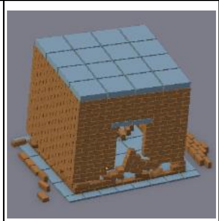	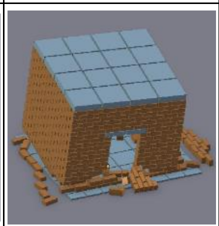	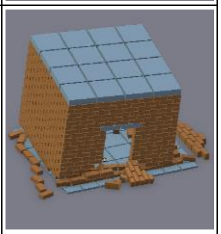
0.2	1687.07	4.48	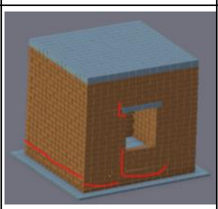	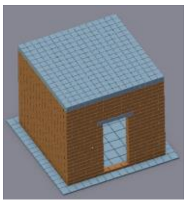	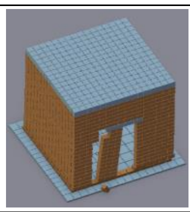	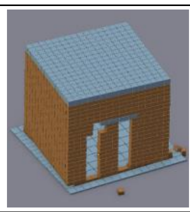	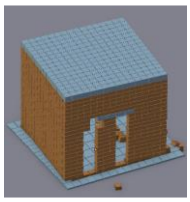

Appendix 7. Fracture Modifier, Why?

The table below presents the analysis time utilizing standard blender and FM under various discretization values

Discretization	Standard Blender	FM
3.5	850	655
3	1052.25	726.82
2.5	1857.25	822.98
2	2932.5	879.65
1.5	4412.17	912.54
1	5989.54	934.8
0.5	7697.33	992.07
0.3	8462	1284
0.2	9637	1687.07

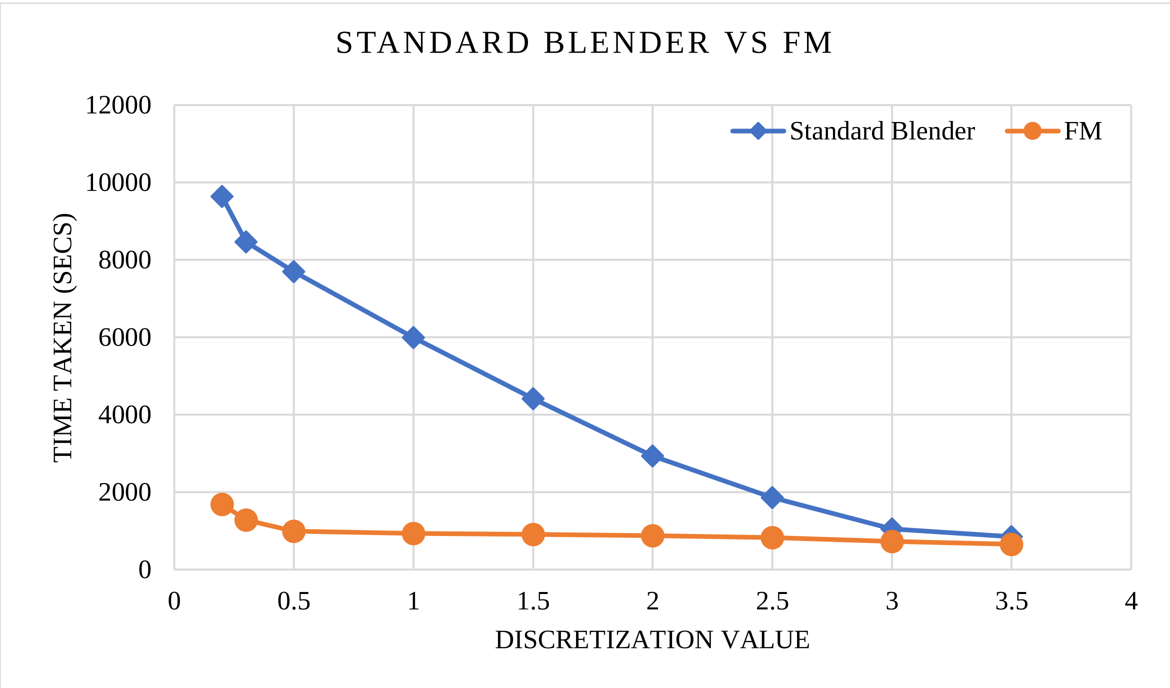

RESUME

He attained his First School Leaving Certificate in 2003. He attended Muslim College, Oworoshonki where he completed his junior and senior high school education in 2006 and 2009 respectively. He then enrolled for a two-year national diploma in Civil Engineering at Yaba College of Technology and graduated in 2012. Afterwards, he did a year internship before proceeding to the Federal University of Technology, Minna. He earned a Bachelor of Engineering Degree in Civil Engineering in 2017 with the thesis titled "Partial Replacement of Cement with Guinea Corn Husk Ash in the Production of Sandcrete Blocks". In 2018 he won the Turkiye Scholarship which presented him with the opportunity to study Master of Science in civil engineering at the prestigious Karadeniz Technical University. He did a year of the Turkish language course and resumes for the MSc program in 2019. Ridwan speaks English, Yoruba and Turkish. Ridwan is currently enrolled in the program with the hope to round up in July 2022.